

BRITTLE DEFORMATION AND CATACLASIS
ON THE SOUTHWEST FLANK OF THE
LLANO UPLIFT, MASON COUNTY, TEXAS

A Thesis

by

JOHN MARK SCHMITTLE

Submitted to the Graduate College of
Texas A&M University
in partial fulfillment of the requirements for the degree of

MASTER OF SCIENCE

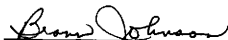
August 1987

Major Subject: Geology

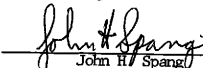
BRITTLE DEFORMATION AND CATACLASIS
ON THE SOUTHWEST FLANK OF THE
LLANO UPLIFT, MASON COUNTY, TEXAS

A Thesis
by
JOHN MARK SCHMITTLE

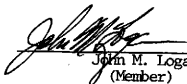
Approved as to style and content by:



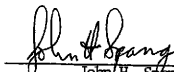
Brian Johnson
(Chairman of Committee)



John H. Spang
(Member)



John M. Logan
(Member)



John H. Spang
(Head of Department)

August 1987

ABSTRACT

Brittle Deformation and Cataclasis

on the Southwest Flank of the

Llano Uplift, Mason County, Texas

John Mark Schmittle, B.S., Allegheny College

Chairman of Advisory Committee: Dr. Brann Johnson

The Lower Comanche Creek on the southwest flank of the Llano Uplift was investigated to more clearly define the brittle deformation of the Lower Paleozoic rocks. Brittle deformation in this area occurred on the macroscopic, mesoscopic and microscopic scales.

Macroscopic deformation is manifest by northeast-trending large-displacement (up to 100 m) normal faults. These normal faults are characterized by linear, segmented sections formed in a zig-zag pattern.

Mesoscopic deformation is manifest by the ubiquitous occurrence of small faults (deformation bands) within the Lower Paleozoic sandstones and calcite-cemented quartz sandstones. These small faults are distinguished by thin (typically <0.5 mm), light-colored, resistant ridges on weathered outcrop surfaces. They form by cataclastic deformation and exhibit an extreme comminution of the host rock grains within the gouge zone. The gouge zone thickness increases slightly with displacement and increasing host rock grain size. The small faults develop into anastomosing, braided zones. They also roughly parallel the large-displacement faults.

Brittle deformation on the microscopic scale is manifest primarily

by intragranular extension microfractures that form in preferred orientations between grain contacts, typically at angles of 20 to 40 degrees with the small faults. The linear density of microfractures decreases rapidly away from the small fault gouge zone attaining a relatively constant non-zero value in the host rock. Healed microfractures are detected by linear trails of fluid or bubble inclusions that transect grains between grain contacts. Microfractures, particularly healed microfractures, are pervasively distributed within the detrital grains of the Lower Paleozoic sandstones. Preferred orientations of microfractures are indicative of local and perhaps regional stress control and may be used to determine paleostress orientations.

A chronology of deformation consists of four overlapping phases: 1) pore reduction/pressure solution, 2) grain microfracturing and comminution, 3) localization and fracture concentration, and 4) subsequent or simultaneous displacement along the localized gouge zone. During all phases, solution/precipitation mechanisms promote healing and cementation of the microfractures and resultant gouge zones.

ACKNOWLEDGEMENTS

Numerous people have provided support, encouragement and guidance during the preparation of this thesis and my gratitude and appreciation is extended to them.

First, I would like to thank Brann Johnson, chairman of my advisory committee, for his continual support, encouragement and advice throughout the course of this research. His editorial and often thought provoking comments considerably improved the final form of this thesis. My thanks is also extended to committee members John Logan and John Spang whose suggestions and critical comments also improved the text.

I would like to thank my friends at the Department of Geology and Center for Tectonophysics, especially Ted, Ned, Molly, Dave, Erol, Dave and Myrna, with whom interaction both in and out of the classroom made my years at A&M an enjoyable and rewarding experience. I am indebted to two good friends, Reif Hedgcoxe and Joe Becker, for their support, thought provoking discussions and collective encouragement throughout the past few years.

Appreciation is extended to the ranchers in the study area south of Mason, Texas who allowed me access to their land and even a cabin to stay in during part of the field work.

I am indebted to Rick Bost who provided the necessary motivation at critical times during the past few months. His friendship and encouragement are greatly appreciated. I would also like to thank my friends at ERM-Southwest for their encouragement, understanding and support.

Special thanks to my parents and family for the opportunity and means to explore, encouragement during all phases of this work, and the love and support that only a family can provide.

Most of all, I would like to thank my wife, Lori, for continually providing a stable base from which to work, understanding during the early writing period, and the love and encouragement, especially during the past few months, necessary to complete this thesis. Her patience is unsurpassable.

TABLE OF CONTENTS

	Page
ABSTRACT	iii
ACKNOWLEDGEMENTS	v
TABLE OF CONTENTS	vii
LIST OF FIGURES	ix
LIST OF TABLES	xii
LIST OF PLATES	xiv
CHAPTER I: INTRODUCTION	1
Background and Previous Geologic Studies	4
Background	4
Previous Work	9
Previous Work in the Llano Uplift	12
Regional Structural Geology	14
The Study Area	17
Methods of Investigation	19
CHAPTER II: STRATIGRAPHY	22
Precambrian Units	22
Riley Formation	25
Hickory Sandstone	25
Cap Mountain Limestone	28
Lion Mountain Sandstone	29
Wilberns Formation	30
Welge Sandstone	30
Morgan Creek Limestone	31
Point Peak Member	31
CHAPTER III: FIELD OBSERVATIONS	32
Macroscopic Structures	32
Large Fault Morphology	33
Main Faults	36
Minor Faults	39
Strike Rosettes	41

TABLE OF CONTENTS (continued)

	Page
Mesoscopic Structures	44
Deformation Bands	45
Morphology of Deformation Bands	47
Orientations	56
Displacement Characteristics	65
Fractures	71
CHAPTER IV: MICROSCOPIC OBSERVATIONS	72
Deformation Band Characteristics	73
Grain Size Reductions	80
Grain Deformation	83
Microfracture Orientation and Density	90
Microfracture Length	102
Grain Boundary Index	102
CementingMaterialObservations.....	104
CHAPTER V: DISCUSSION	112
Deformation Bands and Large-Displacement Faults.....	112
Basement Fault Control	114
Parameters Controlling Deformation Band Development.	116
Microfractures	118
Bubble Lineations	123
Chronology of Deformation	126
CHAPTER VI: SUMMARY AND CONCLUSIONS	130
REFERENCES	136
VITA	141

LIST OF FIGURES

Figure	Page
1. Location of the Llano Uplift and Mason County in Central Texas (a) and the Lower Comanche Creek Study area in south-central Mason County (b)	3
2. Deformation bands (small faults) in the weathered Hickory Sandstone manifest as curvilinear, intersecting resistant ridges of extremely comminuted host rock grains	5
3. Sequential development of a zone of deformation bands from a single band (3a) to a zone of anastomosing bands (3b and 3c) to ultimately a slip surface (3d).....	7
4. Zone of deformation bands (Fig. 3c) developed in the Lower Hickory Sandstone in the Lower Comanche Creek area, Mason County, Texas.....	8
5. Major Pennsylvanian tectonic features of Texas; Llano Uplift is stippled; Mason County is located on the southwest flank of the uplift.....	15
6. Main faults in the Mason area (Southwest flank of the Llano Uplift).....	18
7. Generalized Precambrian and Paleozoic stratigraphic section of the Llano Uplift.....	23
8. Large-displacement, macroscopic faults in the Lower Comanche Creek area.....	34
9. Three minor faults formed in the Middle Hickory Sandstone on the northwest side of Bare Hill.....	40
10. Strike rosettes constructed for the large-displacement and minor faults in three areas of the Lower Comanche Creek area.....	42
11. Single deformation bands manifest as raised-relief, slightly sinuous, intersecting ridges on weathered outcrop surfaces in the Lower Hickory Sandstone.....	46
12. Small zone of deformation bands acting as a barrier to fluid movement as illustrated by the presence of orange-brown hematitic-stained and light-gray host rock on opposite sides of the zone	48
13. Zones of deformation bands consisting of multiple, closely associated deformation bands.....	50

LIST OF FIGURES (continued)

Figure	Page
14. Intersecting sets of deformation bands typically with an acute angle <60 degrees.....	51
15. Gouge-zone thickness as a function of displacement for 81 single deformation bands in the Middle Hickory Sandstone.	53
16. Deformation bands in the Lower Hickory Sandstone traversing coarse and fine-grained beds.....	55
17. Deformation band thickness as a function of mean grain size for 6 hand samples.....	57
18. Scatter (18a), contour(18b), and rose (18c) diagrams illustrating preferred orientations of deformation bands in Area 1.....	60
19. Scatter (19a), contour (19b), and rose (19c) diagrams illustrating preferred orientations of deformation bands in Area 2.....	61
20. Scatter (20a), contour (20b), and rose (20c) diagrams illustrating preferred orientations of deformation bands in Area 3.....	63
21. Scatter diagrams of deformation band orientations measured around the south and north ends of Bare Hill.....	64
22. Displacement associated with small faults manifest by: (a) offset bedding markers in cross-sectional view and (b) offset deformation bands in bedding plane (horizontal) view.....	66
23. Slip vectors (black dots) manifest as slickensides on exposed deformation band surfaces at the south end of Bare Hill.....	68
24. Deformation bands displaying reverse-slip displacements in the Middle Hickory Sandstone.....	69
25. Normal drag formed as a result of normal-displacement along closely spaced deformation bands.....	70
26. Typical deformation band in Hickory Sandstone thin section characterized by a thin gouge zone of fractured and highly comminuted grains.....	75

LIST OF FIGURES (continued)

Figure	Page
27. Large, microfractured grain in the gouge zone producing numerous fragments that have rotated, translated and become incorporated into the gouge material.....	76
28. Elongated grain fragments produced by a concentration of microfractures in a quartz grain adjacent to a gouge zone.....	78
29. Thin zone immediately adjacent to a deformation band characterized by a reduction in pore space, an increase in concavo-convex (CC) and long (LC) contacts and by intragranular microfractures (MF).....	79
30. Histograms of grain size for traverses within and at 2 mm and 4 mm away from the gouge zone.....	81
31. Mean grain size for the Hickory and Welge Sandstones and Cap Mountain Limestone as a function of distance from the center of the gouge zone.....	82
32. Intragranular microfractures connecting grain contacts in the Hickory Sandstone.....	84
33. Type-1 microfractures in the Welge Sandstone that connect point contacts.....	85
34. Healed Type-1 microfractures manifest as linear trails of fluid or bubble inclusions that traverse the grains between contact points.....	87
35. Offsetting bubble lineations at nearly right angles in Hickory Sandstone sample Crh 202T.....	88
36. Type-2 wedge-shaped microfracture that partially penetrates the grain.....	89
37. Type-3 microfractures manifest as a dense array of microfractures within a single grain that result in full or partial pulverization of the grain	91
38. Intragranular movements resulting in translation and rotation of grain fragments and producing irregularly-shaped, but distinguishable grain boundaries.....	92
39. Mosaic extinction pattern manifest in a single grain by small crystallographic re-orientations due to rigid-body translation and rotation of the grain fragments.....	93

LIST OF FIGURES (continued)

Figure	Page
40. Microfracture map (a) and strike rosettes for Hickory Sandstone sample Crh 202T.....	95
41. Microfracture map (a) and strike rosette for Hickory Sandstone sample Crh 202S.....	96
42. Microfracture map (a) and strike rosettes for Cap Mountain Limestone sample Crc 184BT.....	97
43. Microfracture map (a) and strike rosettes for Welge Sandstone sample Cwv 209A.....	98
44. Histograms of microfracture length.....	103
45. Grain boundary index as a function of distance from the gouge zone.....	105
46. Deformation of concentric-layered hematite ooid into a multi-pointed star that appears to have "flowed" into the interstices between grains.....	107
47. Scaly quartz overgrowths surrounding and optically continuous with a rounded quartz grain.....	108
48. Euhedral-shaped quartz overgrowths that have grown into the pore spaces between grains.....	109

LIST OF TABLES

Table	Page
1. Summary of grain size/deformation band width measurements.....	58
2. Host rock characteristics.....	74
3. Microfracture linear density.....	99

LIST OF PLATES

Plate (Found in Pocket)

1. Geologic map of the Lower Comanche Creek area, Mason County, Texas.

CHAPTER I

INTRODUCTION

Brittle deformation in a shallow crustal environment creates areas of localized discontinuities (for example, faults and fractures) in the rock mass. Many of these discontinuities involve a deformation mechanism known as cataclastic flow. Cataclastic flow, or cataclasis, is the response of a rock mass to deformation, resulting primarily in intergranular movements including rigid-body rotation and/or translation of the material. This process occurs on scales ranging from large rock masses to the microscopic level.

A particular structural element formed by cataclastic deformation, and a subset of faulting, is the deformation band. A deformation band, as described by previous workers, is essentially a small fault that exhibits an extreme comminution of host rock grains within a narrow gouge zone. The largest offsets are typically less than 10cm. Although deformation bands exhibit small offsets relative to large-scale faults, their role in the faulting process is significant as evidenced by their ubiquitous occurrence in porous sandstones deformed under shallow crustal conditions. However, the initiation and development of the deformation bands and their relationship to other structural elements are not well understood.

Several investigators (Aydin, 1977, Jamison, 1979; Young, 1982; Dyer, 1983; Heald, 1956; Pittman, 1981; Blenkinsop and Rutter, 1986)

This manuscript follows the style of the Geological Society of America Bulletin.

have addressed the formation and development of deformation bands. These studies described and compared the physical appearance of deformation bands in different lithologies and textures and in different tectonic environments. The noted differences between the morphologies of the deformation bands, such as gouge zone width and displacement along bands, were largely attributed to the porosity of the host rock as a controlling parameter of deformation band development (Jamison, 1979; Young, 1982). However, based on field observations during this study, it appears that other textural and compositional parameters such as grain size and matrix material also may be important in the development of these structures. In addition, some of these studies were conducted on rocks deformed under various different tectonic conditions. Comparisons are inherently more difficult given multiple variables, such as the local and regional stress conditions (e.g., P , T , $\dot{\epsilon}$), in addition to lithologic differences.

This investigation strives to eliminate variations due to different tectonic conditions by studying deformation bands produced in lithologically and textually different rock types deformed in the same tectonic setting, specifically a normal faulted environment. This study of deformation bands in relation to other structural elements additionally provides information on the regional and local deformation fields.

The Llano Uplift in Central Texas (Fig. 1) was chosen as the geologic setting because it exhibits the desired attributes for this type of study. Deformation bands are usually most prominent in high

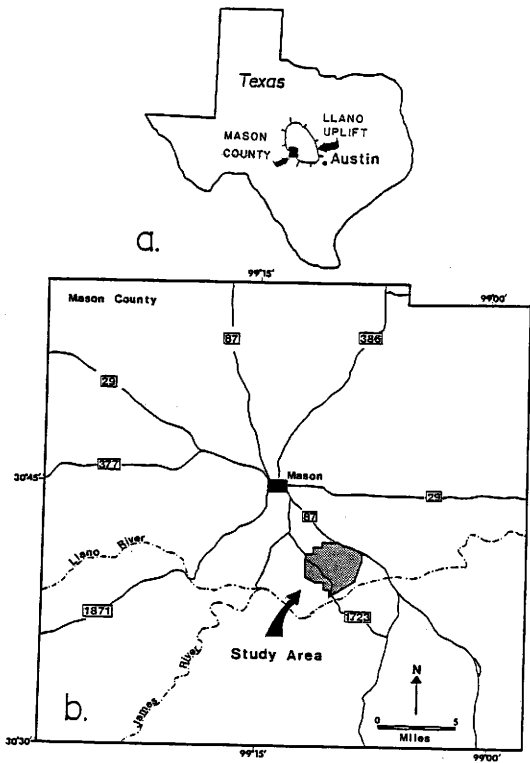


Figure 1. Location of the Llano Uplift and Mason County in Central Texas (a) and the Lower Comanche Creek Study area in south-central Mason County (b).

porosity quartzose sandstones. In the Llano region, they are well developed in the Cambrian Hickory Sandstone Member of the Riley Formation and the Welge Sandstone Member of the Wilberns Formation. Deformation bands are also found in the lower quartzose beds of the Cambrian Cap Mountain Limestone Member of the Riley Formation. These three members are well exposed throughout the Llano Uplift area.

The principal objectives of this research are: (1) to describe and characterize the brittle deformation with an emphasis on the small faults and cataclasis associated with faulting on the macro-, meso-, and microscopic scales, (2) to assess the role of specific lithologic and textural parameters (grain size, cement, composition, and porosity) on deformation band characteristics, and (3) to investigate the relationship between the deformation band as a structural element and its significance in the Llano region, especially relative to large-scale faults and/or the nature of the deformation field.

The remainder of this chapter provides necessary background information and a survey of relevant geologic studies on deformation bands and cataclasis. The location and general structural geology of the study area are described, and the methods of investigation are outlined.

Background and Previous Geologic Studies

Background. As seen in outcrops, deformation bands are usually characterized as whitish-colored, straight to sinuous bands of highly comminuted host rock grains. On weathered surfaces, the deformation bands are often in raised relief (Fig. 2). In three dimensions, the



Figure 2. Deformation bands (small faults) in the weathered Hickory Sandstone manifest as curvilinear, intersecting, resistant ridges of extremely comminuted host rock grains. Pencil for scale is 15 cm long; Ruler is 30 cm.

sinuous deformation bands are manifest as curvilinear surfaces, and the gouge zone is commonly a few millimeters in width. The comminution of grains in the gouge zone results in significant decreases in porosity and permeability within the zone (Aydin, 1977; Jamison, 1979; Young, 1982; Pittman, 1981). The low permeability of the gouge zones, in turn, reduces the rock mass permeability normal to these zones.

Offsets along individual deformation bands typically vary from a few millimeters to a few centimeters. With larger offsets, zones or networks of deformation bands form by the coalescence and interaction of single bands approximately parallel to the original band (Fig. 3) (Aydin, 1977). A zone of anastomosing bands, as formed in the Lower Hickory Sandstone, is shown in Figure 4. Aydin (1977) and Jamison (1979) have suggested that the addition of single deformation bands to a zone of deformation bands is the result of strain-hardening of the individual gouge zone with increasing displacement. Although deformation bands form along discrete planar regions in the host rock (that is, they are localized and not pervasive), and typically display small offsets, they can be the primary manifestation of the cataclastic deformation of the host rock (Jamison, 1979).

Unlike most faults that show a discrete surface of displacement discontinuity with movement, deformation bands usually display no apparent slip surface within the zone of comminuted grains where there has been a loss of cohesion. The small displacements are accommodated by distributed shear deformation within the gouge zone. A discrete slip surface is usually found adjacent to an anastomosing zone of deformation bands (Aydin, 1977). Also, unlike discrete faults that

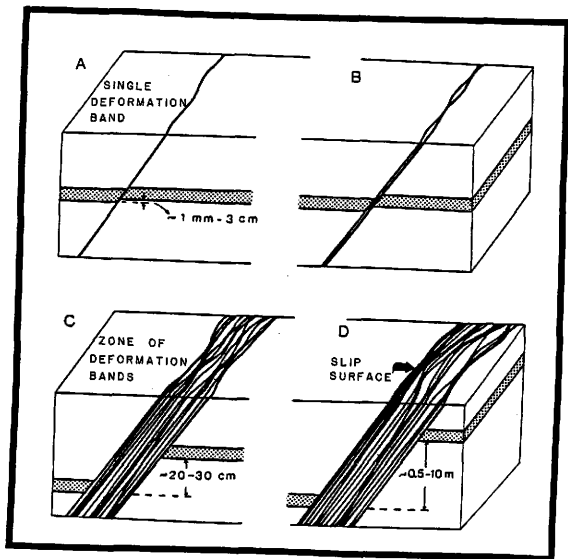


Figure 3. Sequential development of a zone of deformation bands from a single band (3a) to a zone of anastomosing bands (3b and 3c) to ultimately a slip surface (3d). Single bands form adjacent to and anastomose with other bands to form a braided zone. Slip surface develops along one edge of the zone and accommodates up to tens of meters of displacement. Sequence inferred by Aydin (1977).

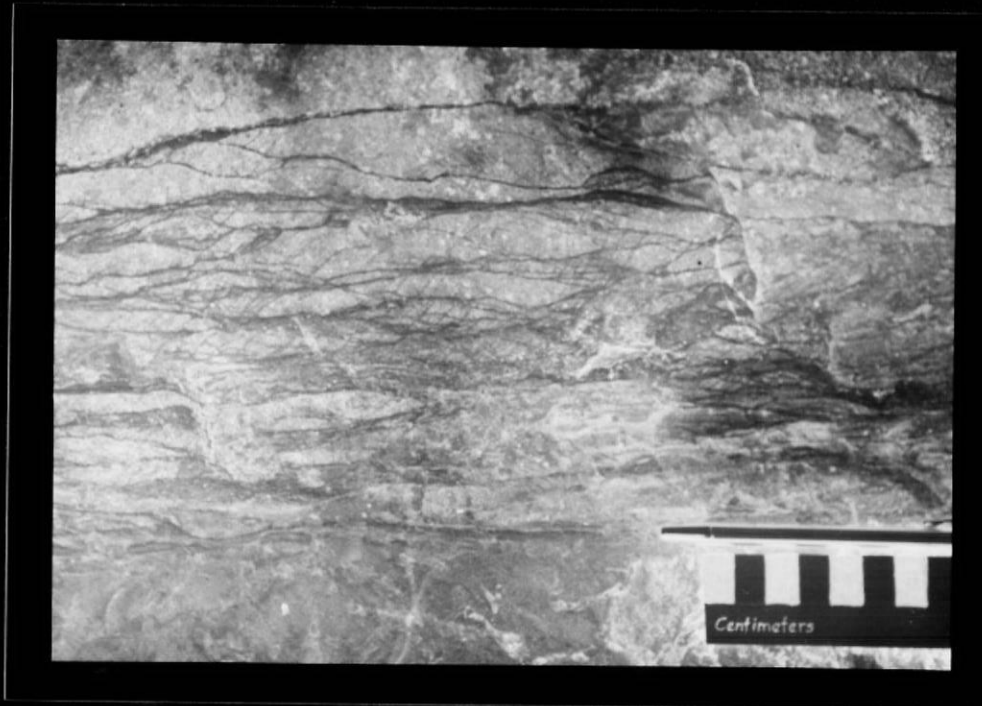


Figure 4. Zone of deformation bands (Fig. 3c) developed in the Lower Hickory Sandstone in the Lower Comanche Creek area, Mason County, Texas.

commonly show a strain softening with displacement, deformation bands are inferred to strain-harden with increased deformation (Aydin, 1977; Jamison, 1979).

Previous Work Studies of deformation bands have been conducted in various locations. Heald (1956) identified deformation bands in the Simpson Sandstone in the Arbuckle Mountains in Oklahoma and in the St. Peter Sandstone in Arkansas and Missouri. He noted that the white stringers in these sandstones that previously were called veins were the result of grain breakage and, consequently, he termed them granulation seams. The granulation seams are synonymous with deformation bands.

Engelder (1974) studied four fault zones and identified small faults or deformation bands that he termed shear fractures. The shear fractures were defined as any fault with a displacement arbitrarily less than 10 cm. He noted that a correlation between displacement and shear fracture thickness was not established in the field. However, in experimentally deformed Coconino Sandstone, he noted a direct linear displacement/thickness relationship for the gouge zone.

Aydin (1977, 1978) and Aydin and Johnson (1978) studied the faulting within the Entrada and Navajo Sandstones in the San Rafael Desert in Utah. They classified three types of faults: deformation bands, zones of deformation bands, and slip surfaces where continued deformation caused a loss of cohesion and development of discrete fault planes. Aydin (1977) also recognized that deformation bands differ slightly in the two units with respect to weathering, thickness and displacement characteristics. The deformation bands are the primary

deformation features preceding the large-scale faulting.

Jamison (1979) studied the cataclastic deformation developed in the Wingate Sandstone in Colorado National Monument, west-central Colorado. Deformation bands were the dominant deformation feature with little or no deformation (including microfractures) occurring in the host rock between zones of deformation bands. He also noted that the appearance and density of the deformation bands changed character within the Wingate Sandstone in relation to compositional and textural variations.

Young (1982) examined deformation bands in sandstones from five separate areas in New Mexico, Wyoming, Utah and California to assess the effect of host-rock porosity. He concluded that with decreasing host-rock porosity: (1) the displacement across single deformation bands increases and (2) for a given unit of displacement, the number of single bands in a zone of deformation bands decreases. He also found that the sandstones were not pervasively deformed, and the microscopic deformation was limited to the area immediately adjacent to the deformation bands.

Dyer (1983) found that deformation bands formed colinear with zoned joints in the Moab Member of the Entrada Sandstone in Arches National Park, Utah. The deformation bands, having the typical raised relief character when weathered, frequently began (or ended) at the termination of open extensional joints and possessed the same orientation as the joints. Dyer inferred that the cataclastic deformation bands resulted from shear displacement along the previously formed extensional joint, and that there potentially is a genetic relationship

between these two physically different features.

The effect of deformation bands on porosity and permeability in the quartz sandstone of the Ordovician Simpson Group in Oklahoma was investigated by Pittman (1981). In general, he found that an increase in the number of deformation bands in a given sample resulted in a lower bulk porosity and permeability.

More recently, Blenkinsop and Rutter (1986) investigated small fault zones within a quartzite in the Moine thrust zone using cathodoluminescence in a scanning electron microscope. They determined that although the quartzite was now well-cemented, at the time of deformation, it essentially behaved like a porous sandstone. They also identified a sequential development of the fault gouge zones and host rock that ranged from intact quartzite through a protobreccia stage to a breccia and ultrabreccia.

Friedman and Logan (1973) produced Luders' bands in experimentally deformed sandstone (effective confining pressures of 0 to 240 MPa, dry, triaxial compression, 10^{-4} per sec strain rate) and likened them to deformation bands formed in the Entrada Sandstone along Trachyte Mesa in Utah. The experimentally produced Luders' bands displayed extreme comminution of grains similar to that in deformation bands, and the shear displacements were on the order of one grain diameter or less. They also noted that the dihedral angle between the conjugate sets of Luders' bands is: (1) bisected by the maximum compressive stress direction, (2) larger than that produced by shear fractures, and (3) widened with increasing confining pressures.

Experimentally produced shear fractures (faults) that develop

gouge with sliding also have been likened to deformation bands (Jamison, 1979). However, according to Jamison (1979), the characteristics of the experimentally produced gouge zones differ from natural deformation bands in several ways: (1) gouge zones develop a discrete slip surface whereas deformation bands appear to lack a discrete slip plane, (2) gouge zones widen by increasing the thickness of the gouge material while deformation bands widen by the addition of single bands to form a zone, and (3) in thin section, the grains near the shear fracture gouge zone display microfractures rather than different extinction patterns as noted by Jamison in deformation bands in the Wingate Sandstone.

Other studies of the orientation and development of deformation bands include those of Reches (1978, 1983), Aydin and Reches (1982), and Aydin and Johnson (1983). The orthorhombic symmetry of deformation bands observed in the field by Aydin (1977) is explained using a theory of slip along the deformation bands to accommodate the three-dimensional strain of the host rock (Reches, 1978, 1983; Aydin and Reches, 1982). Aydin and Johnson (1983) constructed a constitutive model for the development of deformation bands based on a theory of inelastic deformation developed by Rudnicki and Rice (1975).

Previous Work in the Llano Uplift. Few studies of the Llano Uplift have concentrated on the structural geology of the Paleozoic section. The majority of work in this area has been from a stratigraphic viewpoint. In the early investigations, deformation bands were identified as sandstone dikes and recemented fractures but not studied in detail as a structural element.

Fritz (1954) briefly described the deformation bands in the Hickory and Welge Sandstones as "nearly vertical fractures which have been re-cemented with a relatively resistant siliceous material". Coughran (1959) and Peterson (1959) similarly referred to the deformation bands in the Hickory and Welge Sandstones as "sandstone dikes" formed by the percolation of silica-saturated water through fractures. Apparently, none of these earlier investigators recognized the deformation bands as small faults that involved cataclasis. Further, the development of these features in the Cap Mountain Limestone was not discussed.

Recent investigations of faults and associated structural elements on the southwestern flank of the Llano Uplift are those of Johnson (1983), Becker (1985), Becker and Johnson (1985), Johnson and Becker (1986), Hedgcocke and Johnson (1986) and Hedgcocke (1987). These studies have found that the large-displacement normal faults are steeply dipping, consist of interconnected segments resulting in a zig-zag fault trace and that deformation bands are present adjacent to segments of the faults within the Hickory and Welge Sandstones and Cap Mountain Limestone. Hedgcocke and Johnson (1986) and Hedgcocke (1987) found that deformation bands form in ordered networks with specific geometries. These networks, or zones of secondary faults, form in the intervening area between overlapping, en échelon, oblique slip deformation bands that step opposite to the sense of shear displacement. The secondary faults, therefore, form as a result of interaction between the two primary, bounding deformation bands of the network. Consequently, these networks are a mechanism by which displacement can be transferred

from one bounding deformation band or zone of deformation bands to an adjacent deformation band(s).

Regional Structural Geology

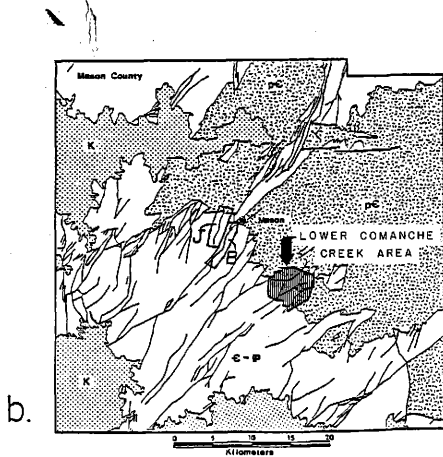
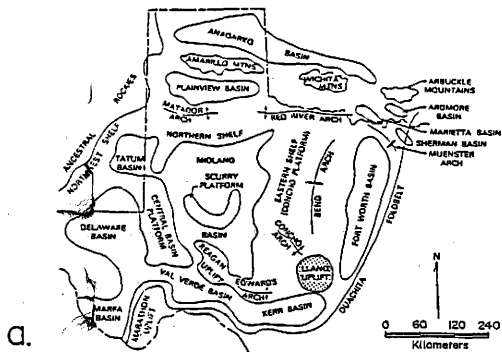
The Llano Uplift is located in Central Texas approximately 80 km northwest of Austin, Texas (Fig. 5a). Structurally, the Llano Uplift is a broad domal arch trending roughly northwest, although topographically, it is a basin surrounded by flat lying Cretaceous beds. Both Precambrian and Paleozoic rocks are exposed at the surface. In particular, Paleozoic rocks crop out near the periphery of the uplift surrounding the central core of Precambrian igneous and metamorphic rocks.

The Llano Uplift is located near the apex of the central Texas recess on the western edge of the Ouachita fold and thrust belt (Fig. 5a). The Carboniferous structural elements extending out from the Llano Uplift include the Fort Worth Basin to the northeast, the Kerr Basin to the south and southwest, and the Bend Arch, the Concho Arch and the Edwards Arch to the north, northwest, and west, respectively.

Northwest trending normal faults within the Paleozoic section formed during the Ouachita orogeny in early Pennsylvanian time as loading of the North American lithospheric plate produced extension in the upper section of the plate (Becker 1985). Normal faulting in the Llano region ended in late Pennsylvanian time as demonstrated by the presence of unfaulted Strawn beds of Morrow time (late Pennsylvanian) (Cheney and Goss, 1952).

The regional structural geology of Mason County (Fig. 5b, p. 16) on the southwest edge of the Llano Uplift illustrates the dominant

Figure 5. (a) Major Pennsylvanian tectonic features of Texas; Llano Uplift is stiped; Mason County is located on the southwest flank of the uplift. Modified from Wermund and Jenkins, 1970; (b) Generalized regional structural geology of Mason County, Texas. Lower Commanche Creek Area mapped in this study is indicated; B=Mason Fault Area mapped by Becker (1985); and J=Kothman Fault Area mapped by Johnson (1983). Modified from Barnes (1981).

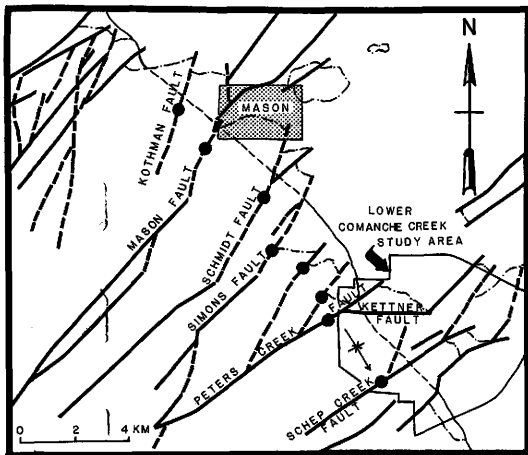


northeast-trending, large-displacement normal faults. East-west and north-south trending faults are also present. Becker (1985) noted several characteristics of the northeast trending faults west and south of Mason (Fig. 6): (1) there exists a northwest trending zone about 4-5 km wide where the trend of the large-displacement faults changes to a more northerly strike and splaying is more common, (2) the maximum throws along these faults occur predominantly within this zone, (3) throws along the faults rapidly decrease to the northeast and slowly decrease to the south relative to the maximum throw location and (4) a large open syncline is present within this zone that has an axial trace colinear with the location of the maximum throws along the faults.

Becker (1985) attributes these fault characteristics to lithologic differences and mechanical anisotropy of the basement rocks. The northwest trending zone is approximately coincident with the granitic-metamorphic contact in this area. Deformation of the metamorphic schist is apparently more pervasive whereas the granitic deformation is localized along a few, widely-spaced, large-displacement faults.

The Study Area

The Lower Comanche Creek area is located on the southwest flank of the Llano Uplift in south-central Mason County (Fig. 5b, p. 16). The area encompasses about 35 km² and lies roughly between U.S. Rt. 87 and Rt. 1723, approximately 10 km south of Mason, Texas. The large-displacement normal faults and the associated deformation bands exposed in this area are the structural elements studied in this report. The locations of three areas recently mapped by Johnson (1983), Becker



EXPLANATION







-  FAULT TRENDING MORE EAST-WEST THAN N35E
-  FAULT TRENDING MORE NORTH-SOUTH THAN N35E
-  LOCATION OF MAXIMUM FAULT THROW
-  SYNCLINE, SHOWING PLUNGE
-  PRECAMBRIAN-PALEOZOIC CONTACT
-  GRANITE-SCHIST CONTACT

Figure 6. Main faults in the Mason area (Southwest flank of the Llano Uplift). Dominant fault trend is northeasterly in Mason area, but more northerly trends and maximum fault throws occur within a northwest trending zone parallel to the granite-schist basement contact. Note the syncline in the western part of the Lower Comanche Creek area that has an axial plane colinear with this northwest trending zone of maximum fault throw. Modified from Becker (1985).

(1985) and Hedgcoxe (1987) to the northwest and south of the present study area are also shown in Fig. 5b.

Two previous studies on the Lower Comanche Creek area and surrounding areas are those by Fuller (1957) and Wilson (1957). Both mapped areas on aerial photo bases and, in part, overlapped the present study area. These earlier maps were constructed from a stratigraphic and sedimentologic viewpoint whereas this study mapped the area primarily from a structural viewpoint.

Methods of Investigation

The Lower Comanche Creek area has been mapped at a scale of 1:20,000 on an aerial photo base and transferred to a USGS topographic base map at the scale of 1:12,000. Mapping has concentrated on the large-displacement normal faults and the deformation bands present in the Hickory and Welge Sandstones and the Cap Mountain Limestone. Attitudes of deformation bands, faults, fractures, slickensides and bedding have been measured using a Brunton compass.

Strike rosettes of macroscopic faults have been constructed for three distinct areas within the Lower Comanche Creek area based on visual inspection of the large-displacement and minor fault orientations. In these rose diagrams, faults are normalized relative to fault length so that a long fault of a particular orientation (typically with larger offsets) is weighted more than a number of short faults (typically with smaller offsets) with a common orientation.

Orientations (poles) of deformation bands have been plotted and contoured on lower hemisphere, equal-area stereonet using the method

of Guzzetta (1966). Rose diagrams of deformation band trends have also been plotted. Using the map, three areas representing structural domains have been differentiated by the overall appearance of the large-displacement faults in order to analyze spatial variations of the deformation bands.

In order to assess the role of grain size on deformation band geometry and development, measurements of grain size and deformation band thickness have been performed on representative hand samples of each rock unit. A pocket micrometer capable of measuring to 0.05 mm (upper silt size range) has been utilized for the measurements. In each sample, the widths of single deformation bands have been measured, and descriptive statistics (e.g., mean and standard deviation) have been calculated. In addition, grain sizes for 150 to 300 randomly selected grains per sample have been measured in the same hand samples. The grain size obtained for the host rock using the pocket micrometer provides a comparative measurement of the actual grain size. Since each sample has been measured using the same technique, any discernable bias inherent in the method should be consistent between samples. In addition, grain sizes measured in thin sections of each unit correspond well to the field determined values using the pocket micrometer.

Host-rock porosity has been measured from selected samples of each unit that do not contain deformation bands. The interconnected pore volume has been measured using the water saturation method on prismatic blocks and cylindrical cores. The prismatic blocks have been used due to the difficulty in diamond coring the friable sandstones. The porosity has been measured twice to ensure precision. The difference

between the two porosity measurements usually does not exceed 2.0% of the measured porosity.

In order to characterize and compare the deformation of the three units at the microscopic level, thirty-three thin sections have been examined from samples containing deformation bands. Particular thin sections that contain a deformation band(s), often with known amounts of displacement, have been used for microstructural analysis of the Hickory and Welge Sandstones and Cap Mountain Limestone. Linear point count traverses have been made within the host rock to assess the host rock composition, grain size and porosity. In addition, linear traverses, have been made parallel to the deformation bands at 2 mm, 4 mm, and within and at the boundary of the gouge zone to determine microfracture length and linear density.

In order to better visualize the spatial distribution of the microscopic brittle deformation, microfracture maps have been constructed for four thin sections made from representative samples of the Hickory and Welge Sandstones, and Cap Mountain Limestone. Microfracture trends for 150 to 429 randomly selected microfractures in each thin section are illustrated on rose diagrams. The microfractures are plotted as a percentage of the total number measured and in 10 degree increments.

After describing the stratigraphy of the study area in Chapter II, the subsequent chapters present the results of each stage of this investigation, culminating in an overall discussion of the work. The final chapter gives a summary and conclusions.

CHAPTER II

STRATIGRAPHY

The stratigraphic units exposed in the Lower Comanche Creek area include Precambrian through Upper Cambrian rocks. Cambrian rocks were deposited on a Precambrian surface displaying up to a few hundred feet of relief (Cloud and Barnes, 1948). A basin existed to the south and southeast, and Cambrian strata generally thicken in these directions. The Precambrian rocks are primarily granites, gneisses and schists while sandstones, limestones and shales predominate the Cambrian units. Figure 7 shows a generalized Precambrian and Paleozoic stratigraphic section of the Llano Uplift. The exposed units are represented by the shaded areas and discussed subsequently.

Numerous stratigraphic studies of the Precambrian and Cambrian Moore Hollow Group rocks have been conducted (Bridge and others, 1947; Goolsby, 1957; Daugherty, 1960; Hooks, 1961; Wilson, 1962; Dekker, 1966; and Barnes and Bell, 1977). The following sections include a compilation of these works in addition to descriptions of the compositional and textural characteristics of the units observed during this investigation.

Precambrian Units

Precambrian rocks crop out in the northern and southeastern sections of the Lower Comanche Creek area (Plate 1, in pocket). Two units are identified in the area: the Packsaddle Schist and a younger-aged granite.

Figure 7. Generalized Precambrian and Paleozoic stratigraphic section of the Llano Uplift. Shaded Cambrian and Precambrian units were investigated during this study. Heavy horizontal lines represent major unconformities. Stratigraphic interpretation and thicknesses after Barnes (1981).

Era	System	Series	Group	Unit	Thickness	
P a l e o z o i c	Pennsylvanian	Canyon			233'	
		Strawn (Des Moines)		Strawn Fm.	—	
		Atoka		Smithwick Fm.	300'	
		Morrow		Marble Falls Ls	385'	
	Mississippian				Barnett Fm.	140'
					Chappel Ls	45'
	Devonian	Upper			Houy Fm.	—
		Middle			Zesch Fm.	—
					Bear Spring Fm.	—
					Stribling Fm.	11-20'
	Lower			Pillar Bluff Ls	—	
	Silurian				Starcke Ls	—
	Ordovician	Cincinnati			Burnam Ls	—
		Ozarkian	Ellenburger		Honeycut Fm.	0-680'
					German Fm.	425-490'
					Tonyard Fm.	525-680'
	Lower ?					
Cambrian	Upper	Moore Hollow	Riley Fm.	Sen Saba Mbr.	215-325'	
				Point Peak Mbr.	25-200'	
				Morgan Creek Ls. Mbr.	115-145'	
				Weige Sandstone Mbr.	20-25'	
				Lion Mt. Sandstone Mbr.	30-60'	
				Cap Mt. Limestone Mbr.	175-500'	
				Hickory Sandstone Mbr.	275-470'	
Upper & Middle						
PreCambrian				Younger Granite	—	
				Packsaddle Schist	~22,300'	

The Packsaddle Schist typically occurs as foliated bodies of quartz-feldspar-microcline schist and hornblende schist. In some areas, particularly in the southern section of the study area, it is gneissic. Marble and milky quartz veins are common, especially in the northern section along the Packsaddle-Hickory Sandstone contact. The Packsaddle Schist is commonly coarse-grained and weathers to dark pink and orange. In the northern section, it forms a gently rolling topography, whereas it weathers to well exposed, gneissic cliffs in the southern area along Comanche Creek.

The younger granite is primarily composed of a pink, coarse to medium-grained, homogenous, microcline-quartz-plagioclase granite with minor amounts of biotite. It outcrops in the southern section of the study area as a northwest-trending, elongated body that is terminated along its northern boundary by a northeast-trending fault. The younger granite is in contact with the Packsaddle Schist and the Hickory Sandstone on its eastern border. The granite is probably a late differentiate of the Town Mountain Granite (Barnes, 1981), and although not specifically named, is compositionally and texturally correlated with the Oatman Creek Granite (Wilson, 1957) found just north of the study area in similar, elongated bodies.

Riley Formation

Hickory Sandstone. The Hickory Sandstone comprises the basal member of the Riley Formation. Regionally over the Llano Uplift, its thickness ranges from about 126 m (415 feet) to a feather edge and averages about 110 m (360 feet) (Bridge and others, 1947). The varia-

tion in the thickness of the Hickory Sandstone is attributed to the irregular Precambrian surface on which it was deposited and the lateral gradation of the Hickory Sandstone to the Cap Mountain Limestone in the southeast. Within the study area, the Hickory Sandstone is estimated to be approximately 122 m (400 feet) thick (Wilson, 1957; Fuller, 1957; Bridge and others, 1947) although no complete section is present for accurate measurements.

The Hickory Sandstone can be divided into three units: the lower, middle and upper. Overall, it consists primarily of non-calcareous, quartz sandstone, light tan and brown to very dark red in color. The Hickory Sandstone is typically medium to coarse-grained, but silty and shaley beds are present. Wind-faceted, quartz pebbles are common at the base of the Hickory Sandstone indicating eolian processes. However, Barnes and Bell (1977) argue that the bedding characteristics, sorting, and the presence of *Cruziana* indicate that the Hickory Sandstone was primarily deposited in shallow water.

The lower unit of the Hickory Sandstone consists of light olive gray to reddish brown, alternating fine to coarse-grained, quartz sandstones about 27 m (90 feet) thick. At the contact with the Precambrian Packsaddle Schist, the Hickory Sandstone is commonly conglomeratic, containing large pebbles (up to 15 cm in diameter) of milky quartz and blocks of fragmented Packsaddle Schist. The sand grains are poorly to well-sorted. Cross-bedding is common throughout the Hickory Sandstone but is most prevalent in the lower unit. The lower unit is loosely cemented primarily by hematite occurring as thin coatings around grains. This results in a slightly friable, granular unit that

weathers to a very gentle slope that is commonly cultivated. Overgrowths of quartz are common (El-Jard, 1982). Measured porosities from this study of the lower unit range from 8.2 to 17.4%. El-Jard (1982) determined an average porosity of about 22% for the lower Hickory Sandstone using a mercury porosimeter on subsurface cores.

The middle unit of the Hickory Sandstone is about 40 m thick and consists primarily of light tan to olive-gray colored, alternating very fine to medium-grained, quartz sandstone. Greenish-gray shale interbeds, up to 10 cm thick, are present as well as flat pebble conglomerate beds near the upper part of the unit. The pebbles are often well aligned with the long axis nearly parallel to bedding or cross-bedding and are typically finer-grained than the host rock. Cross-bedding is common in the middle unit although not as common as in the lower unit. The middle unit is generally more indurated than the lower unit and cemented primarily by silica and hematite. Quartz overgrowths occur primarily as scaly envelopes along grain boundaries. Porosity measurements from the middle unit range from 28% in the fine-grained sandstones to 13% in the poorly sorted, coarse-grained sandstones. The resistive middle unit usually forms ledges and small hills.

The upper unit of the Hickory Sandstone consists of highly ferruginous, medium to coarse-grained, well rounded quartz sandstones which are characteristically very dark maroon colored as a result of the presence of hematite. Its thickness is between 30 and 40 m. The hematite occurs as cement, which coats the grains in thin layers, and as ooids usually containing a small quartz or fossil nucleus. Cross-

bedding is not common in the upper unit and bedding is mostly massive. Porosity in the Upper Hickory Sandstone ranges between 15 and 23% (El-Jard, 1982). The upper unit is friable, usually forms a gentle slope upon weathering, and forms a characteristic dark orange soil that is cultivated.

For mapping purposes, the upper contact of the Hickory Sandstone with the overlying Cap Mountain Limestone is placed above the last noncalcareous sandstone bed that is typically coincident with a topographic break. This contact is sometimes difficult to discern, presumably due to groundwater recharge leaching the calcitic cement of the Cap Mountain Limestone into the underlying Hickory Sandstone.

Cap Mountain Limestone. The Cap Mountain Limestone Member of the Riley Formation is primarily an impure limestone with calcareous-cemented quartz sandstones near the base grading upwards to a pure, granular limestone with quartzose sandstone interbeds. Regionally, the thickness ranges from about 52 m (170 feet) to 152 m (500 feet) with a southeastward thickening of the section (Barnes and Bell, 1977). The thickness of the Cap Mountain Limestone in the study area is estimated to be between 46 and 61 m (150 to 200 feet) (Wilson, 1957; Bridge and others, 1947).

In the Lower Comanche Creek area, the lower Cap Mountain Limestone consists of light reddish-brown to gray, fine to medium-grained, calcareous, quartz sandstone and interbedded limestone. Beds are commonly 10 to 20 cm thick. Porosity measurements of the lower calcareous sandstone unit range from 3.8 to 6.1%. Some glauconite is present, although not abundant. It is within this lower unit of the Cap Moun-

tain Limestone that deformation bands are typically found. The lower unit, other than the calcareous sandstone directly above the contact with the Hickory Sandstone, weathers to brown and gray ledges that produce alternating recessive zones that are usually well exposed.

The Cap Mountain Limestone gradually decreases in quartz and hematite content upsection. The upper part is primarily a calcarenite with minor amounts of glauconite. Bedding becomes thicker (up to 40 cm), and the weathered surface displays a "honeycomb" appearance (Wilson, 1957; Fuller, 1957).

The upper contact of the Cap Mountain Limestone with the Lion Mountain Sandstone is gradational and is arbitrarily placed below the first bed of trilobite coquinite containing an abundance of glauconite.

Lion Mountain Sandstone. The Lion Mountain Sandstone is the upper member of the Riley Formation. It ranges in thickness from 9 to 21 m (29 to 69 feet) (Barnes and Bell, 1977) and is estimated to be about 15 m (50 feet) thick in the study area.

The Lion Mountain Sandstone consists of highly glauconitic, calcareous sandstones and limestones. The quartzose sandstones are dark green to gray, medium to coarse-grained, rounded, and poorly sorted. Glauconite is a major fraction of the Lion Mountain Sandstone. Limestone beds are impure and contain phosphatic brachiopods (Barnes and Bell, 1977). The Lion Mountain Sandstone usually weathers to a gentle slope with an abundance of dark red to black ironstone nodules on the surface. The characteristic ironstone nodules are probably the result of the weathered glauconite.

The exposed portions of the upper contact between the Lion Moun-

tain Sandstone and the Welge Sandstone of the Wilberns Formation are sharp and represent a disconformity (Fuller, 1957; Barnes and Bell, 1977).

Wilberns Formation

Welge Sandstone. The Welge Sandstone is the lowest member of the Wilberns Formation, having a thickness between 3 and 9 m (11 to 30 feet) (Barnes and Bell, 1977). Within the Lower Comanche Creek area, the Welge Sandstone is well exposed in the western part and is about 6 m thick.

The Welge Sandstone is a distinctive, sparsely glauconitic, coarse-grained, dark yellow to pale orange, quartz sandstone. Beds are usually massive and rarely show cross-bedding. The Welge Sandstone is cemented primarily by silica but also by hematite, usually indurated, and resistant to weathering. Quartz overgrowths are common in the Welge Sandstone. It forms a distinctive ledge with an abundance of vegetation just below its upper contact. Porosities of the Welge Sandstone range from 17.4% in the friable, hematitic-cemented parts to 14.6% in the indurated, silica-cemented parts.

The contact with the overlying Morgan Creek Limestone Member is gradational and is placed at the first prominent dark-reddish colored, calcareous, quartz sandstone bed.

The primary differences between the Hickory Sandstone of the Riley Formation and the Welge Sandstone of the Wilberns Formation are the degree of sorting and the hematitic cement. The Welge Sandstone is a mature sandstone with well rounded, and well sorted, quartz grains

while the Hickory Sandstone, although well rounded, is usually poorly sorted. Also, the Hickory Sandstone is cemented primarily by hematite rendering it friable. In contrast, the Welge Sandstone is usually well indurated as a result of the silica cement.

Morgan Creek Limestone. The Morgan Creek Limestone of the Wilberns Formation consists of dark red, limey, quartz sandstones near the base and olive-gray, glauconitic limestones interbedded with shales further upsection. Bedding thickens upsection, and small, stromatolitic bioherm masses 0.3 to 1 m thick are found near the upper contact. The thickness of the Morgan Creek Limestone is approximately 30 m (100 feet) in the Lower Comanche Creek area.

The upper contact with the Point Peak Member is usually covered but can be identified by the presence of shale beds in the lower Point Peak which form a topographic and vegetational break.

Point Peak Member. The Point Peak Member of the Wilberns Formation consists primarily of greenish-gray, calcareous siltstones with interbedded, micritic limestones and intraformational conglomerates. Massive stromatolitic bioherms up to 7 m thick are present at the top of the incomplete section in the study area. The Point Peak is the stratigraphically highest unit mapped in the Lower Comanche Creek area. Bridge, et. al., (1947) report the thickness of the Point Peak to range between 7.5 and 82 m (25 and 270 feet) with an average thickness of approximately 49 m (160 feet). Approximately 30 m (100 feet) of section have been mapped in the study area.

CHAPTER III

FIELD OBSERVATIONS

The field investigation focuses on characterizing the large-displacement normal faults (macroscopic scale) and associated deformation bands (mesoscopic scale) in three Cambrian units of the Lower Comanche Creek area. Previous stratigraphic field studies in the Lower Comanche Creek area do not provide a sufficient characterization of the faulting, especially with respect to the location, orientation and morphology of the macroscopic and mesoscopic deformational features. This chapter describes the main faults, minor faults and deformation bands in order to better understand the tectonic development of the western Llano Uplift. The effects of lithologic and textural controls on the deformation bands at the mesoscopic scale also are addressed.

Macroscopic Structures

Deformation of the Paleozoics in the Llano Uplift probably occurred at shallow crustal conditions (<1.0 km). The Cambrian rocks at the base of the Cambrian section were buried by no more than 1000 m of overburden, which would give an effective pressure of nearly 13 MPa (130 bars) during deformation assuming a normal fluid pressure.

The macroscopic expression of cataclasis within the study area is manifest as large-displacement normal faults that trend roughly north-east. These normal faults are prominently displayed by vegetation lineations on aerial photographs. In addition, there are numerous minor faults that occur throughout the area but are not clearly visible as

vegetation lineations on aerial photographs.

The large-displacement and minor faults are identified in the Hickory and Welge Sandstones by the presence of abundant deformation bands typically concentrated along a narrow zone and/or local variations of bedding attitudes. The actual fault surfaces are rarely exposed; instead, the location of the faults often is delineated by an increased density of the deformation bands with proximity to the fault surface. The large faults identified in the field have normal offsets with throws up to about 100 m. Minor faults typically have throws ranging from less than 1 m to 5 m. Occasionally, a slip surface adjacent to a zone of deformation bands is exposed and displays offsets on the order of 1 m or less.

In the Cap Mountain Limestone, large faults are identified by the presence of deformation bands and fractures in concentrated zones. The juxtaposition of beds and increased dips of beds due to drag along the faults also are used to identify the location and amount of offset along the large faults.

Large-Fault Morphology. The large-displacement fault traces consist primarily of straight segments connected in a zig-zag pattern (Fig. 8 and Plate 1). Segment length is variable, but the change in orientation from one segment to the next is usually between 10 and 20 degrees. This zig-zag pattern of normal fault traces also was mapped north of the study area by Johnson (1983) and Becker (1985) in the lower part of the Paleozoic section.

Splay faults are common near the terminations of the large-displacement and minor faults, particularly in the Cap Mountain Lime-

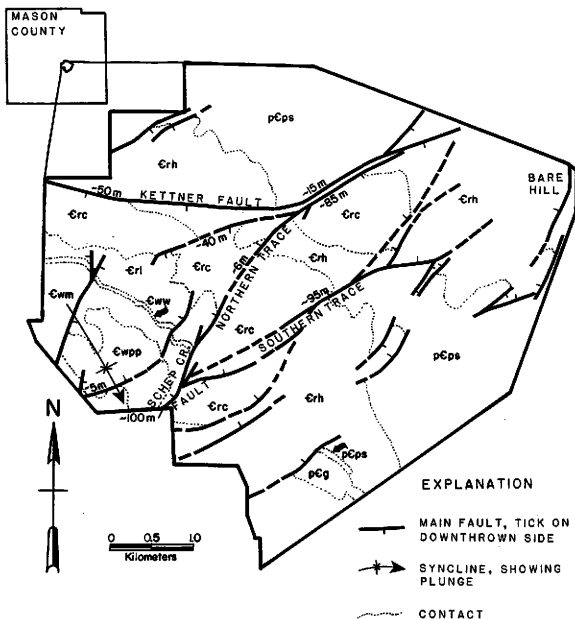


Figure 8. Large-displacement, macroscopic faults in the Lower Comanche Creek area. Note the linear, segmented character of the faults resulting in a slight zig-zag pattern. Also note the large lenticular fault block formed in the central part of the study area and bounded by the northern and southern traces of the Schep Creek Fault. Inferred normal displacement (in meters) along faults indicated by number. Units are as follows: pCps=Packsaddle Schist; pCg=younger granite; Crh=Hickory Sandstone; Crc=Cap Mountain Limestone; Crl=Lion Mountain Sandstone; Cww=Welge Sandstone; Cwm=Morgan Creek Limestone; and Cwpp=Point Peak Limestone.

stone (Fig. 8 and Plate 1). Typically, the main faults have one or two minor splays that intersect to make a small angle with the trend of the main fault. These splays vary in length between 25 and 400 m. Within the Hickory and Welge Sandstones, the splay faults consist of segmented zones of deformation bands. Apparently, the splay faults accommodate the displacement at the terminations of the large-displacement and minor faults.

Occasionally, slivers of fault-bounded material can be found along the faults. In the southwest part of the study area, a small sliver of Welge Sandstone occurs between the Point Peak Member of the Wilberns Formation and the Cap Mountain Limestone of the Riley Formation where they are in fault contact. The sliver is approximately 4 m wide, 10 m long, and lense-shaped. Within the fault sliver, the Welge Sandstone is replete with deformation bands and is very well cemented in the host rock areas between the deformation bands.

Oblique slip movements along the large-displacement faults were not identified in the field due to the lack of fault surface exposure. The presence of oblique slip on individual deformation bands adjacent to the faults possibly suggests fault interaction and the accommodation of three dimensional strain (Johnson, B., per. com.).

Although the large-scale normal faults rarely show drag, the drag in the Lower Comanche Creek area is normal when present. Reverse drag similar to that found along the Kothman fault west of Mason, Texas (Johnson, 1983) is not found along any of the large faults in the study area. Absence of reverse drag does not preclude its existence; it may be present but not exposed. Where seen, reverse drag extends much

farther from the associated fault than normal drag, which is usually restricted to about 10 m adjacent to the fault (Johnson, B., per. com.). Along the Schep Creek Fault in the southwest corner of the study area, the dip of bedding in the Cap Mountain Limestone indicates normal drag and increases from about 4 to 44 degrees in a distance approximately 4 m from the fault. Normal drag is not readily observed along faults in the Hickory Sandstone.

Faults that trend into the Packsaddle Schist and younger-aged granite are often difficult to distinguish from the numerous fracture traces in these units. However, the fractures in the Precambrian units are usually coincident in attitude with the mappable faults in the overlying sedimentary rocks. The Precambrian fractures typically increase in density where a fault can be traced from the Paleozoic strata into the underlying Precambrian rocks.

In summary, the large faults in the Lower Commanche Creek area typically have normal displacements and normal drag, are segmented, display splayed terminations, contain fault slivers in fault zones and typically display similar orientations to structural features such as fractures in the underlying Precambrian sequence.

Main Faults. There are two main faults that trend through the study area and are delineated by vegetation lineations on aerial photographs, namely the Kettner Fault and the Schep Creek Fault. In the northern section, the Kettner Fault runs roughly east-west for much of its exposure and then either makes an abrupt northerly bend to trend about N60E or intersects a northeast trending fault (Fig. 8, p. 34 and Plate 1). It is downthrown to the south and southeast along its entire

length. The Kettner Fault places Hickory Sandstone against Cap Mountain Limestone along its western section and Hickory against Hickory in the central, east-west section. To the northeast, the Packsaddle Schist is in the footwall with Lower Hickory Sandstone in the hanging wall. The throw along the Kettner Fault is greatest in the western area (up to 50 m) and decreases toward the northeast. Deformation bands are numerous in sandstones adjacent to the trace of the Kettner Fault with the dominant set of bands dipping to the south roughly 75 degrees.

The second main fault, the Schep Creek Fault (Sliger, 1957; Wilson, 1957; Fuller, 1957), trends northeast through the middle part of the study area (Fig. 8, p. 34 and Plate 1). It is well exposed at the southern end of the hills located in the western part of the area where it dips northwest and brings the Point Peak into contact with the Cap Mountain Limestone. At this point in the southwest corner of the study area, the fault trace bifurcates into two primary fault traces, informally referred to here as the northern trace and the southern trace of the Schep Creek Fault.

The northern trace is oriented about N26E and dips to the northwest, while the southern trace further bifurcates into splay faults that are oriented roughly N60-70E and also dip primarily to the northwest. The southern trace has a similar orientation (N65E) to the Schep Creek Fault prior to its point of bifurcation. Both the northern and southern fault traces appear to result from the intersection of two or more segmented faults.

Offsets along the Schep Creek Fault range from about 100 m (in the

southwestern section prior to the bifurcation) to about 95 m (in the southern trace). The northern trace decreases in throw to the northeast; however, this decrease in displacement may be accommodated by another closely oriented fault that dips to the southeast and runs parallel to the Kettner Fault along part of its length (see Fig. 8, p. 34 and Plate 1). The throw along this parallel fault is roughly the same as that of the southern trace of the Schep Creek Fault (about 85 m). It is possible that the displacement is being transferred from the Kettner Fault to this parallel fault as the Kettner Fault also decreases in throw to the northeast.

On the macroscopic scale, the faulting displays systematic relative changes in orientation resulting in a system of lense-shaped fault blocks. A large lenticular fault block extends northeasterly through the center of the Lower Comanche Creek area (Fig. 8, p. 34 and Plate 1). This block is about 1.0 km wide at the center and is about 4.5 km long. The boundary faults, except the northern trace of the Schep Creek Fault, dip toward the fault block. These bounding faults are segmented with two principal orientations, approximately N30-40E and N60-70E.

This lenticular fault-block geometry appears to be common in other areas of the Llano Uplift on the macroscopic scale. In the Riley Mountains of Llano County east of the study area, this pattern is very common. Also, the large-displacement faults west and northeast of Mason form the boundaries of lenticular blocks. Becker (1985) noted that faulting lower in the stratigraphic section gives rise to lense-shaped fault blocks, whereas further up in the section, faults inter-

sect less, are straight and exhibit an en échelon pattern.

Although large-displacement faults are the primary macroscopic structure, one large-scale, low amplitude fold is identified along the western edge of the study area (Fig. 8, p. 34 and Plate 1). The fold is a very open syncline defined by the outcrop expression and the very slight inclination of bedding (4 to 8 degrees) around its periphery. Small-scale folds or other minor structures are not found in the syncline hinge area, probably due to the open structure of the fold. The syncline plunges very slightly to the southeast. The axial plane is northwest trending at approximately N40W. The axial plane is colinear with the alignment of the loci of the maximum large-displacement fault throws south and southwest of Mascn (see Fig. 6, p. 18). The northwest strike orientation of the axial plane of the syncline possibly indicates basement control on the faulting and resultant macrostructure.

Minor Faults. Numerous faults with displacements as small as 0.5 m also were mapped and included on Plate 1. These smaller faults are commonly not noticeable on aerial photographs, and only close field examination reveals their presence. Within the Hickory Sandstone, these small faults are manifest by slip surfaces that have formed adjacent to a zone of deformation bands. Figure 9 shows three typical small faults that occur on the northwest side of Bare Hill (NE corner of Plate 1) within the middle unit of the Hickory Sandstone.

In addition to the dominant northeast-trending faults, there are a number of small-displacement faults that are oriented northwestward. These faults are located in the southeastern corner of the study area primarily adjacent to the younger Precambrian granitic body (Plate 1).



Figure 9. Three minor faults formed in the Middle Hickory Sandstone on the northwest side of Bare Hill (northeast corner of Plate 1). The faults consist of thick zones of anastomosing deformation bands each with a slip surface developed along one side of the zone. Offsets along the faults vary between 0.15 and 0.4 meters.

This is the only site where northwest-trending faults are located in the Lower Comanche Creek area. The faults are found mainly at the Precambrian/Hickory contact and in the lower part of the Hickory Sandstone. One northwest fault trends parallel to the granite/Packsaddle Schist contact at about N45-50W. The other northwest-trending faults are more northerly oriented, about N25-30W. The location and orientation of these northwest-trending faults may be a manifestation of the northwest-trending structures in the Precambrian basement and the resultant influence on the faulting in the Paleozoic section.

Strike Rosettes. Rosettes of fault strike were constructed to determine systematic orientations of the large-displacement and minor-displacement faults (Fig. 10). The strike rosettes display the percentage of total fault length as a function of fault strike. These plots were constructed by measuring the length and orientation of linear faults or linear segments of faults. For curved sections of faults, either a best-fit line was measured or the curve was represented by a number of linear segments and then the length and orientation were measured. Inferred faults (dashed on Plate 1) were not considered in the construction of the rosettes due to their estimated orientations. The fault-segment lengths were normalized relative to total fault length.

The large-displacement and minor faults are separated into three distinct areas based on a visual inspection of the fault orientations depicted on Plate 1. The three areas are not considered as structural domains since they do not actually represent statistically homogenous areas, but they are separated in order to avoid overprinting visually

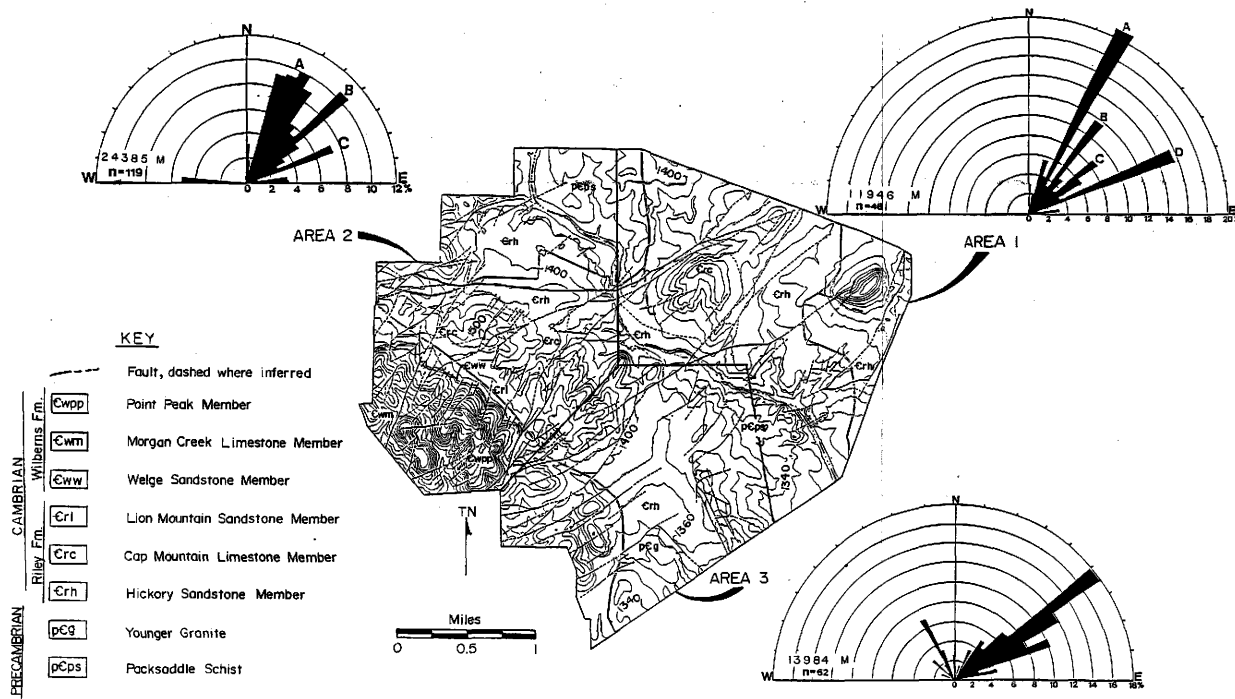


Figure 10. Strike rosettes constructed for the large-displacement and minor faults in three areas of the Lower Comanche Creek area. Fault segment lengths are normalized with respect to total fault length. M = total fault length in meters; n = number of fault segments measured in each area.

distinct fault orientations of one area on another. The strike rosettes for each area and their locations with respect to the geologic map of the Lower Comanche Creek area are shown in Figure 10.

The faults from Area 1 (Fig. 10, p. 42), located in the northeast section of the study area, display a number of concentrations that are oriented primarily between N25E and N70E. Four concentrations (A,B,C,D) can be delineated, specifically oriented at A:N25-30E, B:N35-40E, C:N50-60E, and D:N65-70E. Concentrations A and D dominate in Area 1, while concentrations B and C are less strong. No northwest-trending, large-scale faults are present in Area 1; however, a small percentage of the fault lengths are oriented N0-5E and N80-85E.

Area 2, located in the northwest corner of the study area, displays more dispersion of faults, yet concentrations are similarly oriented to those in Area 1. Overall, a slightly more northerly trend of faulting is depicted. The primary concentrations in Area 2 are oriented at A:N15-35E, B:N45-50E, and C:N65-70E. Concentration A potentially could be composed of two or more concentrations. The concentrations oriented east-west are from the Kettner Fault which trends nearly east-west through Area 2.

Faults in the southern section of the Lower Comanche Creek area, Area 3 (Fig. 10, p. 42), show a more easterly overall orientation than those in Areas 1 and 2. The strong concentrations are oriented between N50E and N70E. The strongest concentration in Area 1, namely A:N25-30E, is only weakly represented in Area 3. Area 3 also contains the northwest-trending faults which are in close proximity to the granitic body in the southern part of the area (Plate 1). These faults are

represented by a relatively weak concentration (7%) oriented N25-30W.

In summary, the macroscopic expression of cataclasis is characterized by northeast-trending, large-scale and minor normal faults which typically exhibit segmented linear traces. In a given region, faults and fault segments have primarily three to four principal orientations as illustrated by the strike rosette diagrams.

Mesoscopic Structures

Cataclasis on the mesoscopic scale in the Lower Comanche Creek area occurs in thin (typically <0.5 cm), linear or curvilinear fault zones demonstrating a high degree of comminution of the host rock grains. In other studies, these fault zones have been called deformation bands (Aydin, 1977; Jamison, 1979). In this context, deformation bands are defined to be small faults that demonstrate offsets on the order of millimeters to centimeters with pronounced comminution along the fault.

Deformation bands are the primary manifestation of the mesoscopic cataclastic deformation developed in the Hickory and Welge Sandstones in the study area. In the Cap Mountain Limestone, deformation bands are present in the lower quartz sandstone dominated parts of the member but are rare throughout the majority of the member where fracturing appears to dominate as the primary mechanism of brittle deformation.

The following sections present field observations of the deformation bands as they occur in the Paleozoic units exposed in the Lower Comanche Creek area. The observations focus on their physical expression, morphology and displacement characteristics. Various similari-

ties and differences in their characteristics within the different lithologic units are noted. Also included in this chapter is a brief discussion of fractures in the Precambrian rocks immediately underlying the Hickory Sandstone.

Deformation Bands. Single deformation bands in the Lower Comanche Creek area typically occur on weathered outcrop surfaces as raised-relief, slightly sinuous bands (Fig. 11). The width of a single band typically varies between <0.1 and 8 mm, depending on the host rock textural and/or compositional characteristics.

The raised-relief character of the bands illustrates their greater resistance to weathering and erosion than the host rock. The single bands often develop into anastomosing zones or ordered networks. The presence of these zones and networks is usually indicative of a nearby larger-displacement fault. Furthermore, the density of single bands and zones increases with proximity to a fault surface. Particularly in the Hickory Sandstone, the deformation bands are ubiquitous in conjunction with the macroscopic faulting in the Lower Comanche Creek area. The color of the gouge zone is related to the host rock color. Typically, the bands are white to light gray in the lower and middle units of the Hickory Sandstone, the Cap Mountain Limestone and the Welge Sandstone. In the Upper Hickory Sandstone and select bedding horizons in the middle Hickory Sandstone that display a high degree of hematite, the deformation bands are dark maroon-colored. The deformation bands in these two units contain an abundance of hematite derived from the host rock material giving them the dark color. Hematite is noticeably absent in the deformation bands in the Lower Hickory and



Figure 11. Single deformation bands manifest as raised-relief, slightly sinuous, intersecting ridges on weathered outcrop surfaces in the Lower Hickory Sandstone. Bedding plane view. Pencil for scale is 12 cm long.

Welge Sandstones even though both of these units contain a small percentage of hematite.

Deformation bands apparently act as barriers to fluid movement as indicated by the presence of orange-brown hematitic-stained and light gray host rock on opposite sides of a band or zone of bands. This observation is particularly noticeable in the Lower and Middle Hickory Sandstone units (Fig. 12). The intersection of deformation bands on bedding plane and cross-sectional views will often create isolated pods or rhombs of non-hematite-stained host rock.

Morphology of Deformation Bands. The deformation bands developed in the Lower Comanche Creek area occur as curvilinear to straight faults as seen on both bedding surfaces and cross-sectional views. The geometry of deformation bands is a function of the plane of observation relative to the slip vector. In planes roughly parallel to the slip vector, the bands typically display a straight character. In areas where strike-slip displacement occurs, the bands typically form a straight character on bedding surfaces. Conversely, deformation bands in cross-sectional views normal to the slip vector exhibit a curvilinear or anastomosing character. In a normal-slip dominated area, the anastomosing character primarily forms on bedding surfaces.

Along single deformation bands, small pods occasionally develop with dimensions typically about 3 to 7 cm long and 0.5 to 1 cm wide. These pods are frequently found in planes normal to the slip vector along the deformation band and have an internal structure of two to four bands in a crossing pattern.

Deformation bands more frequently occur as zones (i.e., closely

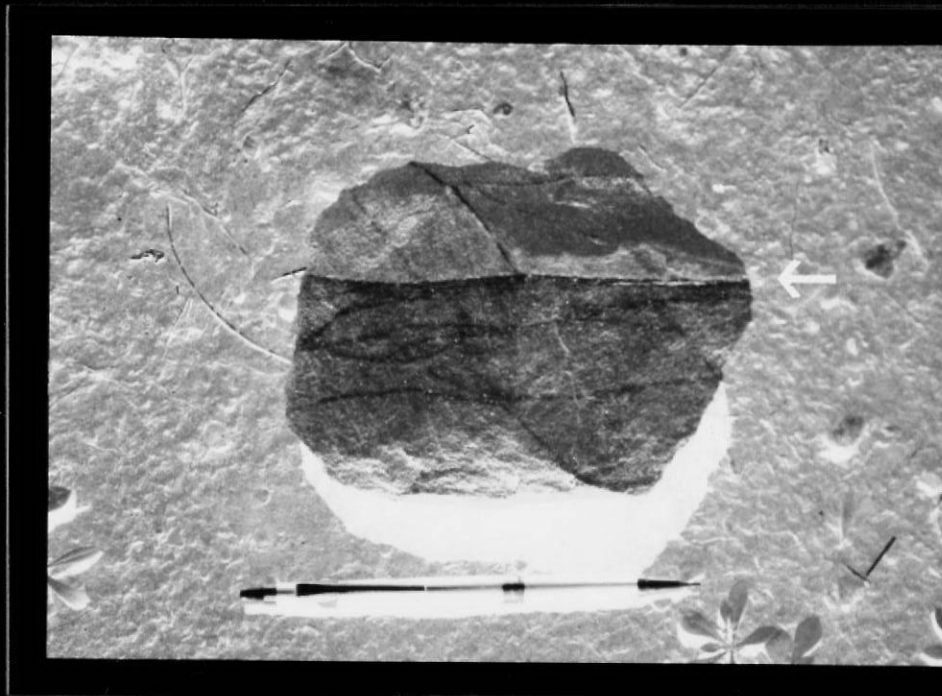


Figure 12. Small zone of deformation bands acting as a barrier to fluid movement as illustrated by the presence of orange-brown hematitic-stained (above arrow) and light-gray host rock (below arrow) on opposite sides of the zone. Sample is Lower Hickory Sandstone. Pencil is 15 cm long.

associated multiple deformation bands) consisting of two or more single bands with a common orientation. The deformation bands within these zones either anastomose into a braid-like character or form ordered networks (Fig. 13) where fault interaction occurs between two or more bands or zones resulting in displacement transfer between the small faults (Hedgcoxe and Johnson, 1986; Hedgcoxe, 1987). These ordered networks appear to be scale independent and occur on bedding planes in outcrops which have a dominant strike-slip component to the fault displacement. The ordered networks have been studied in detail and termed secondary fault zones (SFZ's) by Hedgcoxe and Johnson (1986). This term is derived from the fact that these ordered networks result from the interaction of two primary deformation bands, or more commonly, two primary sets of deformation bands.

In general, the predominant deformation bands have orientations similar to the large-displacement macroscopic faults. At any particular outcrop, typically at least two sets of deformation bands can be identified. The sets of bands commonly intersect on bedding surfaces with acute angles of 60 degrees or less and display offsetting relationships indicating their order of development (Fig. 14a). The bands also intersect in vertical planes and form rhombohedral-shaped blocks (Fig. 14b). At outcrops where the bedding plane and vertical face intersections occur together, the bands form with orthorhombic symmetry (Fig. 14c). The large-scale faults commonly have orientations parallel to intersecting sets of deformation bands, indicating that the deformation bands reflect the same deformation as the large-scale faults (or vice versa). In some cases, the deformation bands also

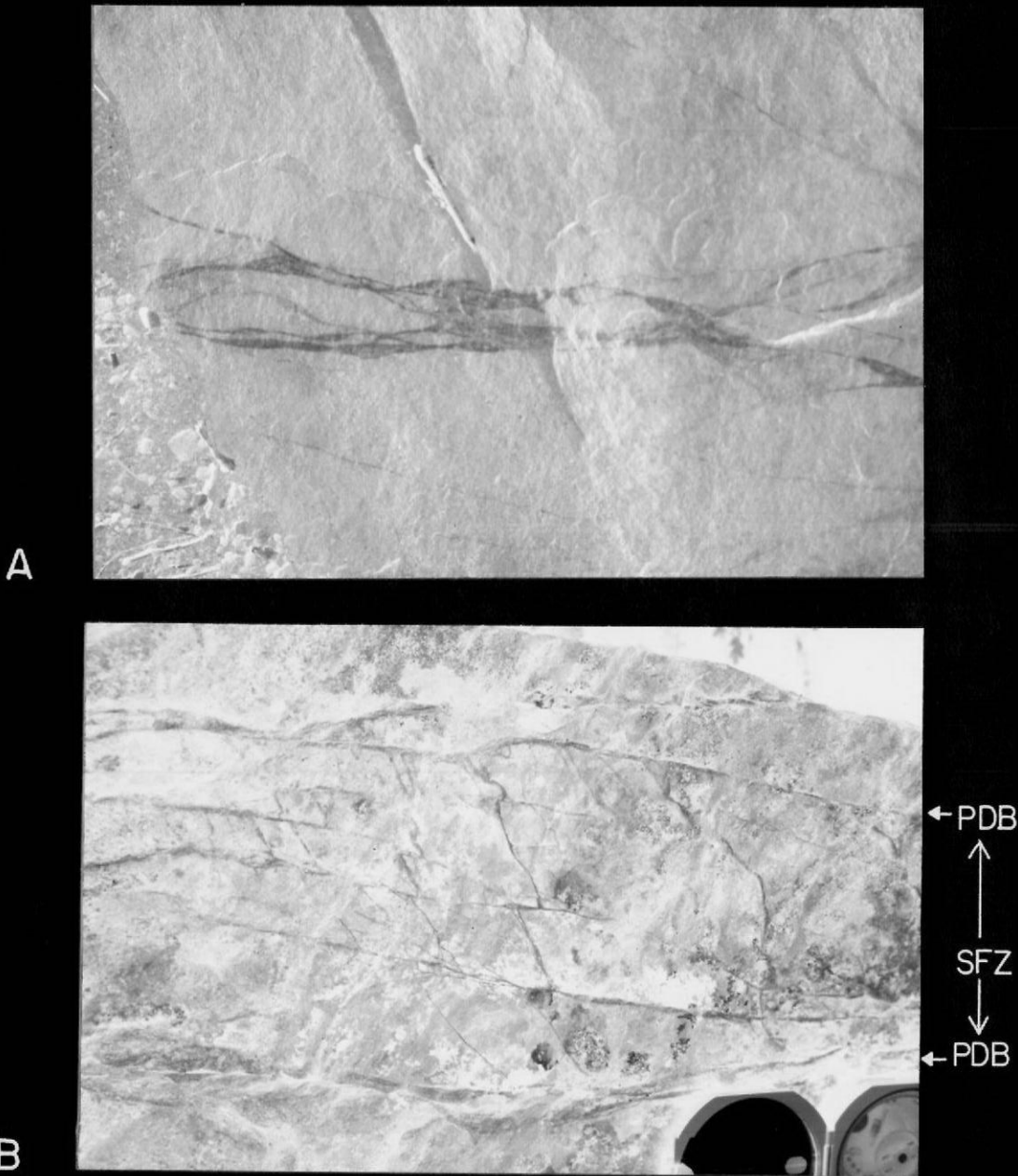


Figure 13. Zones of deformation bands consisting of multiple, closely associated deformation bands. (a) Zone formed by single bands anastomosing into a braided character. Vertical view of Lower Hickory Sandstone. Pencil is 12 cm long. (b) Ordered network of bands developed by the interaction of two primary deformation bands (PDB) that create an intervening secondary fault zone (SFZ) (discussed by Hedgcoxe, 1987). Sense of offset between primary deformation bands is right lateral. Brunton compass for scale.

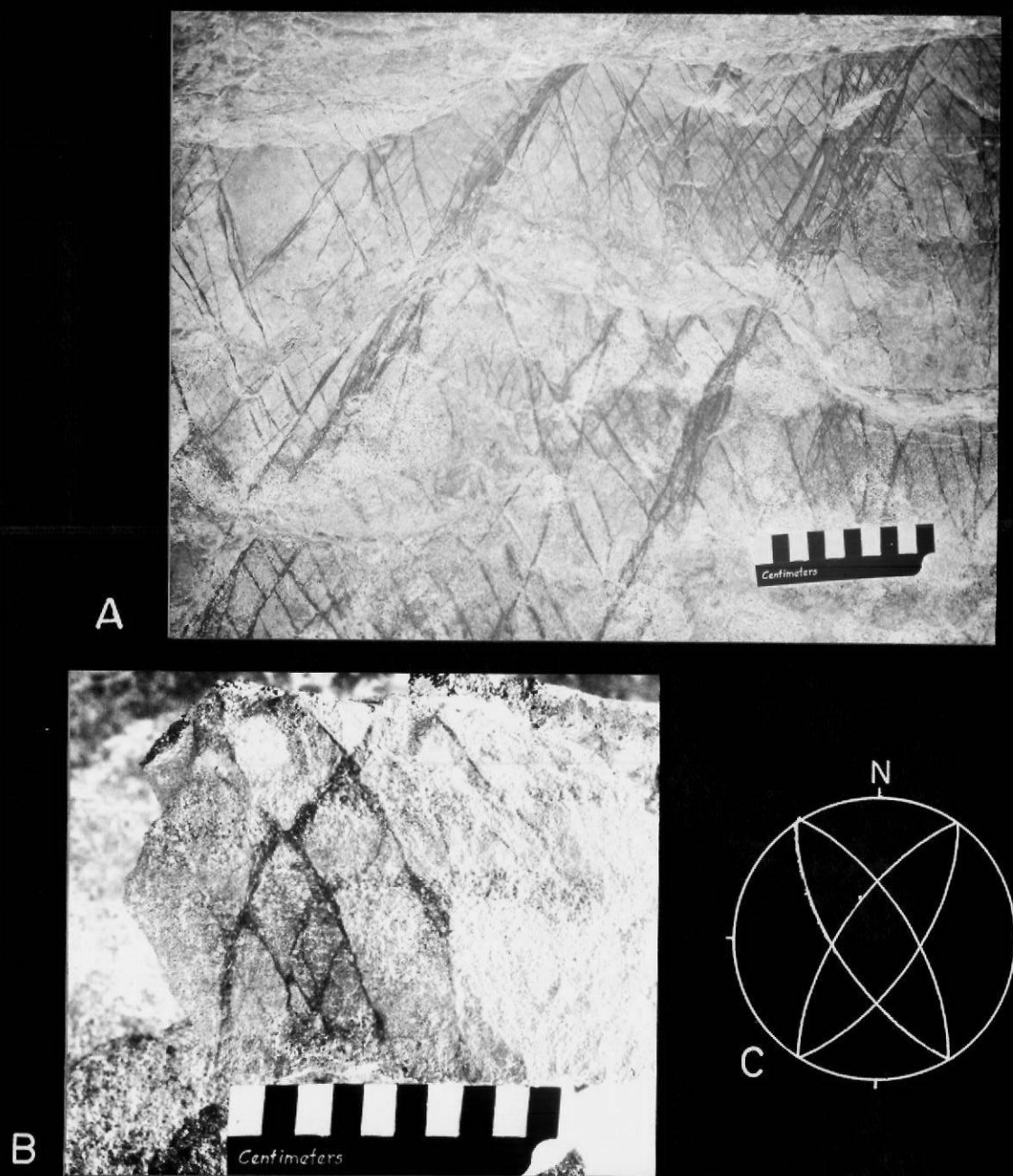


Figure 14. Intersecting sets of deformation bands typically with an acute angle < 60 degrees. (a) Predominant acute angle in Middle Hickory Sandstone outcrop in photo is 60 degrees. Bedding plane view. (b) two intersecting sets of deformation bands in cross-sectional view forming rhombohedral-shaped blocks bounded by bands. (c) Orthorhombic symmetry formed when deformation bands intersect on bedding plane and cross-sectional views at same outcrop. Thus, a total of four sets of faults shown (lower hemisphere projection; bedding=outer primitive circle).

reflect aspects of the deformation such as the dominant slip direction and large-fault attitude, often not reflected by the large-scale faults.

The thickness of the gouge zone of deformation bands varies between the three Lower Paleozoic units and depends primarily on the host rock textural and compositional characteristics. Within any one bedding horizon containing similar textural and compositional characteristics, the amount of displacement appears to have only a slight effect on band width. To examine this effect, eighty-one single deformation bands were measured for apparent offset and thickness in a plane roughly parallel to the slip vector where the dip-slip component dominated. Care was taken to measure these parameters within the same stratigraphic horizon to minimize the effects of compositional and textural variations.

In this horizon of the Middle Hickory, the deformation band widths exhibit a broad dispersion primarily between 0.2 and 2 mm (Fig. 15). Displacements along the single deformation bands also exhibit a high degree of dispersion but typically cluster between 0.5 and 4.0 mm. The largest measured displacement along a single band at this outcrop is 10 mm with a corresponding width of 4.0 mm. The plot of apparent offset versus deformation band thickness shows a significant variation, but it indicates that, on the average, the gouge zone thickness increases with displacement for displacements less than or equal to 10 mm. This is not necessarily true in a comparison between differing bedding horizons or other lithologic units.

The thickness of bands in the Lower Comanche Creek area typically

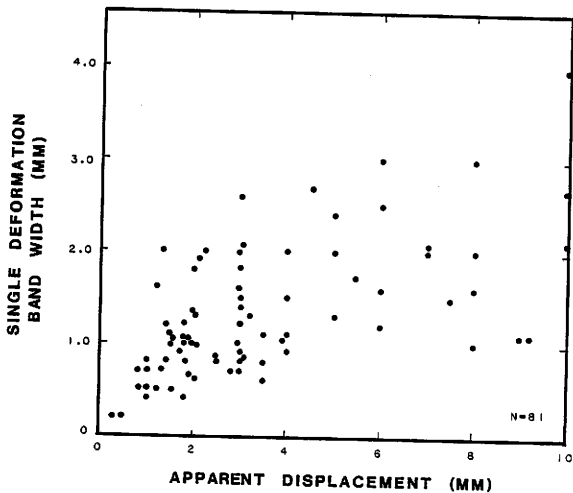


Figure 15. Gouge-zone thickness as a function of displacement for 81 single deformation bands in the Middle Hickory Sandstone. All measurements taken in one bedding horizon to minimize effects of variations in grain size, porosity, sorting and structural position. Measurements made at south end of Bare Hill.

ranges between 0.2 and 3.0 mm, although band width can reach up to 5.0 mm. In the coarse-grained beds of the Lower and Middle Hickory and Welge Sandstones, the individual deformation bands average 0.5 to >1.5 mm thick, whereas in the finer-grained beds in the Middle Hickory and Cap Mountain Limestone, single bands are generally <0.5 mm in width. This observation is most noticeable at outcrops where deformation bands transect alternating coarse and fine-grained beds or cross-bedded sequences. In the coarse-grained beds, individual deformation bands are thick (up to 2.0 mm) and commonly form pods consisting of two or three deformation bands. The thickness of the deformation bands greatly decreases (typically to <0.5 mm) in the fine-grained beds. Also, the deformation bands commonly decrease in density upon entering the fine-grained beds. Within subsequent coarse-grained beds, the thin bands frequently return to multiple, thick deformation bands similar in width to the bands in the previous, coarse-grained bed (Fig. 16).

Moreover, the deformation band changes character and thickness when it passes through a very fine siltstone or shale bed between two sandstone beds. Within the two sandstone beds, the single band consists of a comminuted zone of definable thickness. However, within the siltstone or shale layer, the band is manifest as a very thin, discrete small fault with detectable offset, yet does not display a detectable gouge zone of comminuted material.

Deformation bands within the conglomerate beds of the Middle Hickory Sandstone will often transect flat pebbles. Where this occurs, the bands will frequently be quite thick, possibly indicating dilation normal to the plane of the band, and yet display very little shear



Figure 16. Deformation bands in the Lower Hickory Sandstone traversing coarse and fine-grained beds. Note band thickness decrease, density decrease and color change in fine-grained bed in center of photo. Bands in coarse-grained bed also exhibit raised-relief character more than in the fine-grained bed. View is a vertical outcrop face.

displacement as evidenced by little offset of the pebbles. This observation perhaps suggests that the gouge zone material is slightly fluidized and, consequently, is somewhat mobile in the plane of the deformation band. If this is true, then the fabric development due to shearing motions may be altered or unrecognizable.

To assess the dependence of deformation band thickness on the host rock grain size, six samples of Hickory Sandstone were used to measure these parameters (Fig. 17). Measurements were made using a scaled pocket micrometer capable of measuring grains or band widths to 0.05 mm. A total of 165 to 301 grains were measured per sample and every deformation band within a sample was measured. The samples have a range of mean grain size from 0.14 to 0.47 mm and a range of mean deformation band thickness between 0.32 and 1.06 mm (Table 1). The plot of mean grain size versus mean deformation band thickness shows a slightly variable correlation, but a definite increase in deformation band width with increasing grain size.

Orientations. Nearly 500 deformation band orientations were measured and plotted on lower hemisphere, equal area stereonetts to ascertain spatial relationships of the mesoscopic structure. The bands were divided into the three areas defined previously in the macroscopic fault section to minimize overprinting of visually distinct band orientations from one area onto another.

Generally, all three areas demonstrate a strong northeast trend of the deformation bands with steep dips typically ranging between 70 and 90 degrees. The orientation diagrams each illustrate a girdle pattern with trends primarily between N10E and N70E. Northwest trending defor-

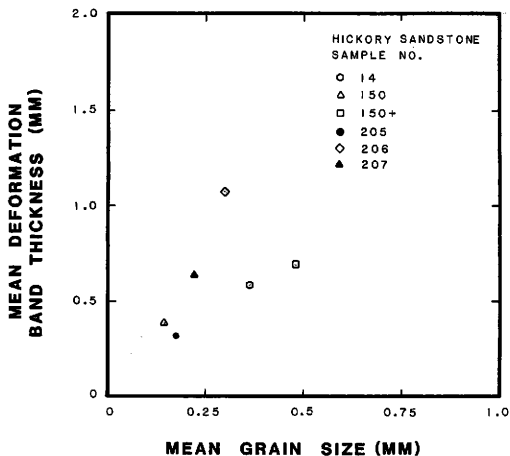


Figure 17. Deformation band thickness as a function of mean grain size for 6 hand samples. Measurements made using a pocket micrometer capable of measuring to 0.05 mm. See Table 1 for a summary of measurements. Total of 265 deformation band widths and 1410 grain diameters measured.

TABLE 1
Summary of
Grain Size/Deformation Band Width Measurements

Rock Type	Sample Number	Number of Deformation Bands Measured	Deformation Band Width (mm)			Number of Grains Measured	Grain Size (mm)		
			Mean	S.D.	Range		Mean	S.D.	Range
Hickory SS	205	47	0.32	0.12	0.15-0.7	301	0.17	0.07	0.05-0.4
Hickory SS	14	52	0.59	0.23	0.2-1.2	165	0.36	0.12	0.1-0.9
Bimodal Hickory SS	150+	15	0.67	0.23	0.4-0.9	181	0.47	0.32	0.05-1.8
Hickory SS	207	34	0.64	0.20	0.3-1.0	281	0.21	0.09	0.1-0.5
Hickory SS	206	36	1.06	0.32	0.6-2.0	281	0.28	0.11	0.1-0.8
Hickory SS	150X	81	0.37	0.12	0.15-0.8	201	0.14	0.05	0.05-0.3

mation bands are generally rare in the Lower Comanche Creek area except in localized areas. East-west trending bands can be common, although most bands measurements are either associated with the large east-west trending section of the Kettner Fault or with anthetic faults formed in secondary fault zones (SFZ's) (Hedgcoxe and Johnson, 1986; Hedgcoxe, 1987) developed along northeast-trending faults.

The preferred orientations of deformation bands in Area 1 form a girdle pattern primarily between N15E and N36E, with a mean concentration of about N18E (Fig. 18). Two additional concentrations are oriented approximately N64E and N27E. The mean concentration oriented about N18E is close to the large fault strike rosette concentration A:N25-30E (Fig. 10, p. 42). Also, the N64E preferred concentration roughly parallels the large-fault strike rosette concentration D:N65-70E (Fig. 10, p. 42). These two large-fault concentrations (A and D) dominate in Area 1, and it is not surprising that the deformation bands nearly parallel these orientations. However, both deformation-band strike orientations are slightly deviated from the dominant main fault orientations in Area 1.

Area 2 displays preferred orientations of deformation bands in a girdle pattern between N12E and N48E with a mean roughly at N30E (Fig. 19). This orientation correlates with a primary large-fault strike rosette concentration of N15E to N35E (A and B, respectively, Fig. 10, p. 42). A second concentration of deformation bands oriented about N60E could correlate to the large-fault concentration D:N60-70E. Also in Area 2, the east-west trending segment of the Kettner Fault is visible in both the large-fault strike rosette (Fig. 10, p. 42) and the

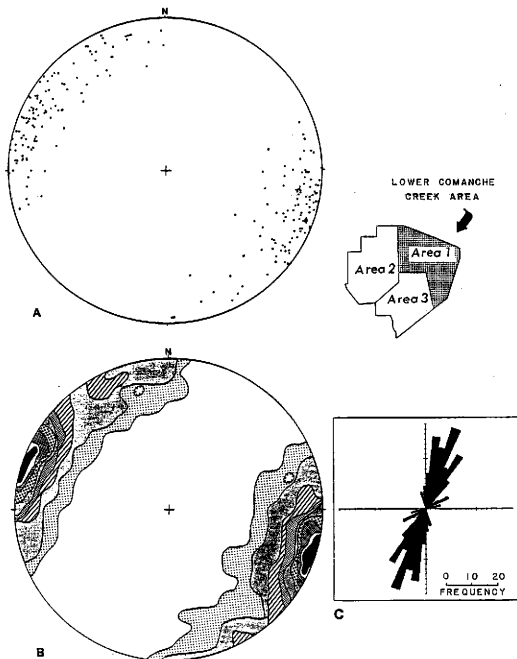


Figure 18. Scatter (18a), contour (18b), and rose (18c) diagrams illustrating preferred orientations of deformation bands in Area 1. Total of 218 points contoured on lower hemisphere, equal area projection. Contour intervals 1, 2, 3, 5, 7, 9, 11, 13, and >15% per 1% area. Rose diagram constructed for deformation band strike.

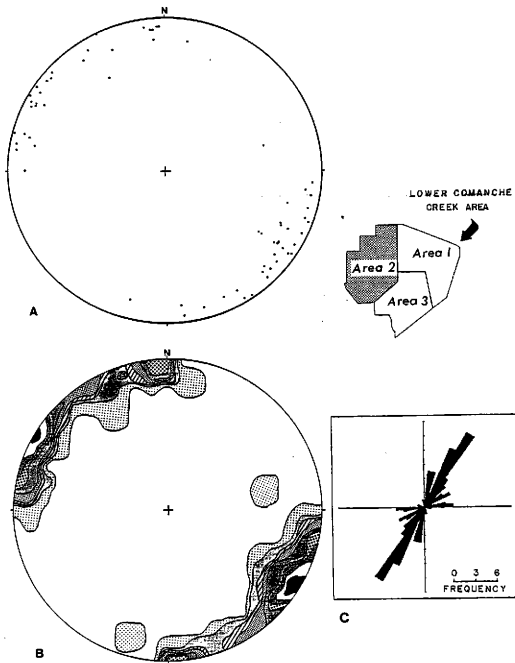


Figure 19. Scatter (19a), contour (19b), and rose (19c) diagrams illustrating preferred orientations of deformation bands in Area 2. Total of 64 points contoured on lower hemisphere, equal area projection. Contour intervals 1, 2, 3, 5, 7, 9, 11, 13, and >15% per 1% area. Rose diagram constructed for deformation band strike.

deformation band stereonet diagram (Fig. 19).

In contrast, preferred deformation band trends in Area 3 are oriented more easterly and occur in a smaller girdle pattern than those in Areas 1 and 2 (Fig. 20). The bands are oriented primarily between N26E and N60E with a mean at approximately N45E and N61E. These orientations agree closely with the large-fault strike rosette orientations between N50E and N70E (Fig. 10, p. 42). Also in Area 3, the northwest-trending deformation bands, associated with the macroscopic faulting in the southeast corner of the study area, are illustrated.

Deformation bands also were plotted for individual measurement stations around the Bare Hill area where Middle Hickory Sandstone crops out in particularly good exposures (Fig. 21). The individual pole diagrams illustrate the high variability in deformation band trends in a localized area. Measurement stations 1 through 3 illustrate similar trends in deformation band development. In contrast, station 4 illustrates a more easterly trend. Large faults near stations 1, 2, and 3 trend roughly N20E, whereas faults just east of station 4 are more easterly oriented.

Also, within a localized area, the deformation bands demonstrate slip directions similar to the large-displacement and minor faults. For example, at the south end of Bare Hill, the deformation bands predominantly display a down-to-the-southeast oblique slip direction. North of Bare Hill, the deformation bands predominantly display a down-to-the-northwest slip direction that correlates with the large-displacement fault northeast of Bare Hill (Fig. 21). This demonstrates the complexities associated with the macroscopic and mesoscopic

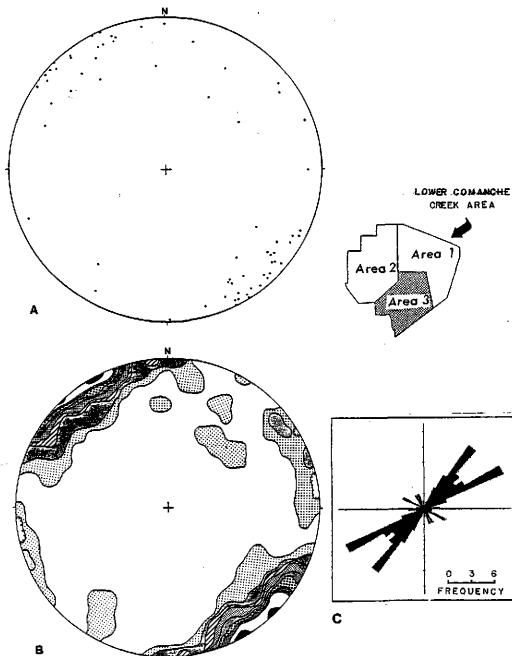


Figure 20. Scatter (20a), contour (20b), and rose (20c) diagrams illustrating preferred orientations of deformation bands in Area 3. Total of 66 points contoured on lower hemisphere, equal area projection. Contour intervals 1, 2, 3, 5, 7, 9, 11, 13, and $>15\%$ per 1 $\frac{1}{2}$ area. Rose diagram constructed for deformation band strike.

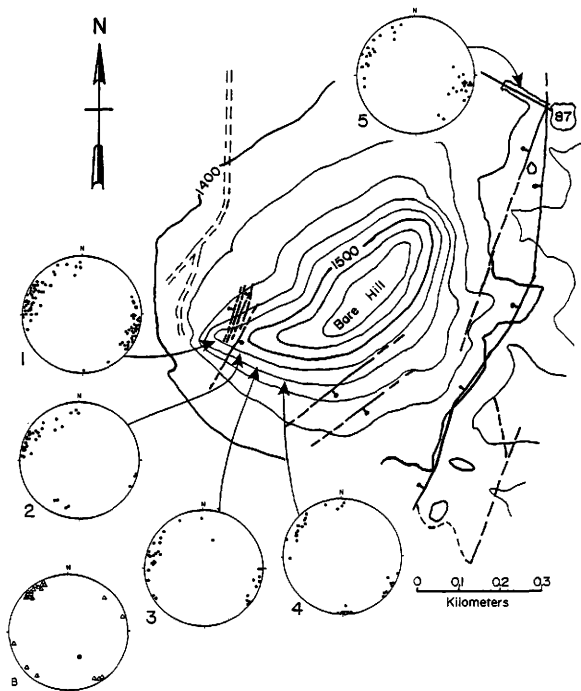


Figure 21. Scatter diagrams of deformation band orientations measured around the south and north ends of Bare Hill. Also, scatter diagram (b) of fractures measured south of the Bare Hill area in Packsaddle Schist. See Plate 1 for location of Bare Hill area in northeast corner of Lower Comanche Creek area.

faulting in a localized area.

Displacement Characteristics. Displacements along single deformation bands typically range between <1.0 mm to 1.0 cm depending on the host rock unit. Zones of deformation bands consisting of two or more single bands display a cumulative offset and commonly average around 0.5 to 2.0 cm of displacement. These offsets are not difficult to detect, although the amount and true sense of offset are not always discernable. In rare cross-sectional exposures of the Lower Hickory, bedding laminations and cross-bedding provide marker beds to help determine offset amount and orientation (Fig. 22 a). However, at most outcrops, intersecting deformation bands that offset each other provide the only means of measuring the relative sense of movement (Fig. 22 b). Generally, in finer-grained rocks, the displacements are slightly larger along bands than in coarser-grained rock units.

Within a single band, there typically appears to be no discrete slip surface developed, but rather the displacement is distributed across the entire width of the band. However, when slip surfaces are exposed, they usually occur along one band/host rock interface and contain slickenside grooves. These slickensided surfaces reveal the curvilinear nature of the deformation bands in three dimensions and exhibit the direction of slip. Since the displacements along the bands are generally small, the slickensides probably represent the entire displacement vector and not just the last recorded movement along the slip surface.

Displacement occurs in normal, reverse and strike slip directions although typically the displacement vector is a combination of these



Figure 22. Displacement associated with small faults manifest by: (a) offset bedding markers in cross-sectional view and (b) offset deformation bands in bedding plane (horizontal) view. Pencil in (a) is 12 cm long; centimeter scale in (b).

which results in oblique slip motions. Consequently, measurements of displacement on bedding plane or cross-sectional views are typically only apparent displacement and not a true measurement of the amount of slip. Measurements of slickensides at the southwestern end of Bare Hill indicate a dominant horizontal component to the slip vector (Fig. 23). In that particular cross-sectional view, all slickensides indicate right lateral oblique slip motions and have rake angles between 5 and 27 degrees from the horizontal.

Reverse slip motions are also present along many single deformation bands, particularly in the Lower and Middle Hickory Sandstone (Fig. 24 a). The apparent offset along many of these bands is on the order of a few millimeters or more. In nearly all cases, the deformation bands with reverse movements are associated with a larger zone of bands, which overall have normal or oblique slip motion. The bands with reverse slip are usually contained within certain stratigraphic horizons and form in an antithetic attitude to the large zone of bands displaying normal slip motions (Fig. 24 b). This orientation appears to alleviate "room problems" resulting from movement along the zone of normal slip.

Normal drag is occasionally present along deformation bands in the Lower and Middle Hickory. Figure 25 shows a small zone of deformation bands with about 4 cm of normal offset. Normal drag is developed on the downthrown side, and an antithetic zone of deformation bands has formed that also shows normal slip. Although difficult to see in this picture, there are abundant, very thin deformation bands present between the two larger zones of bands. The effect of the smaller deforma-

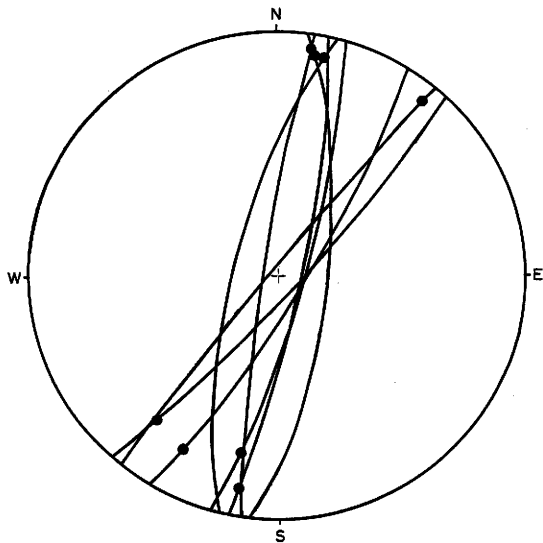


Figure 23. Slip vectors (black dots) manifest as slickensides on exposed deformation band surfaces at the south end of Bare Hill. Rake angles vary between 5 and 27 degrees from the horizontal and indicate oblique-slip with a strong component of horizontal displacement.

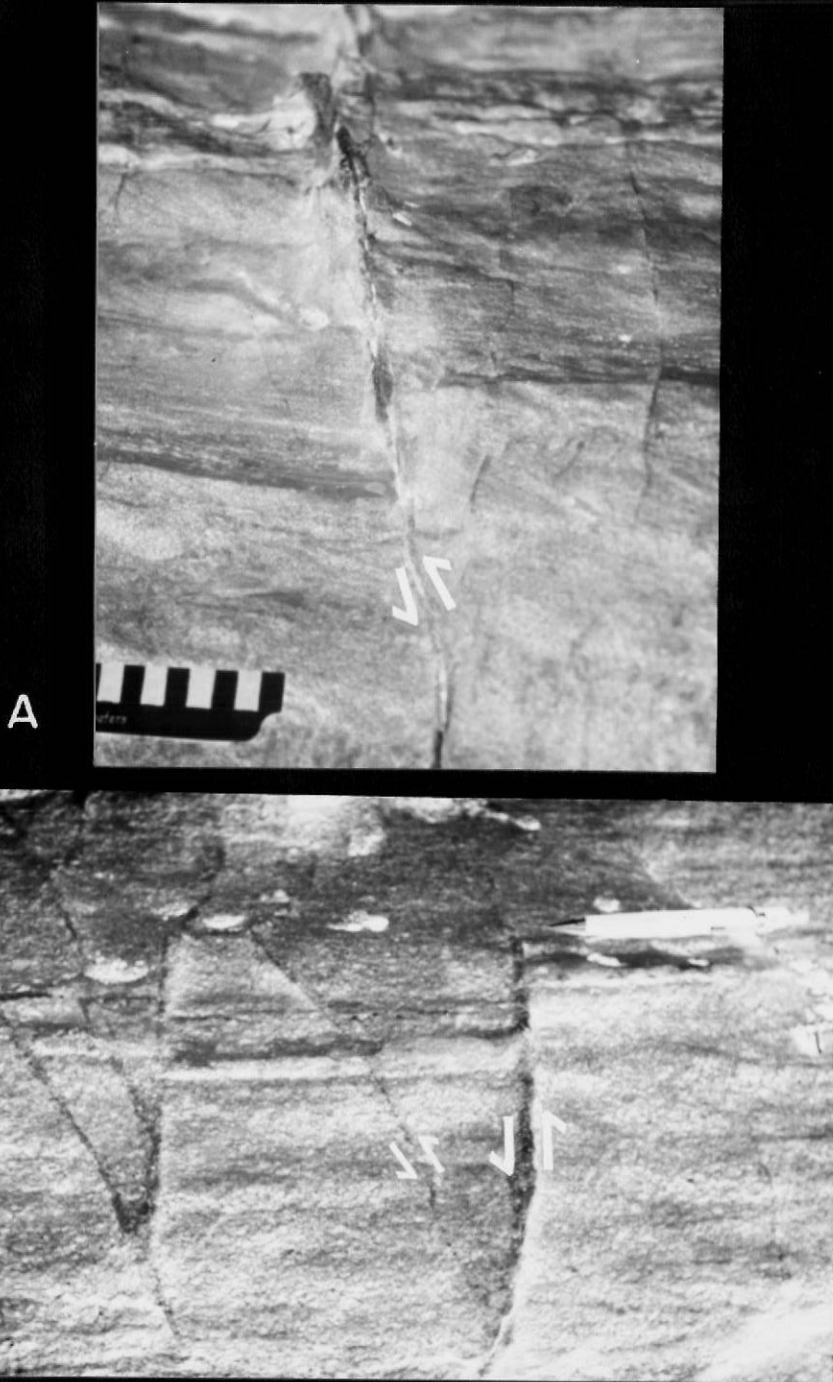


Figure 24. Deformation bands displaying reverse-slip displacements in the Middle Hickory Sandstone. (a) About 4 cm of displacement. Note small deformation bands to right of main band that exhibits normal-slip displacement. (b) Deformation bands with reverse-slip displacement formed in antithetic attitudes as a result of movement along the small (labeled) zone displaying normal-slip. Centimeter scale in (a); Pencil for scale in (b).

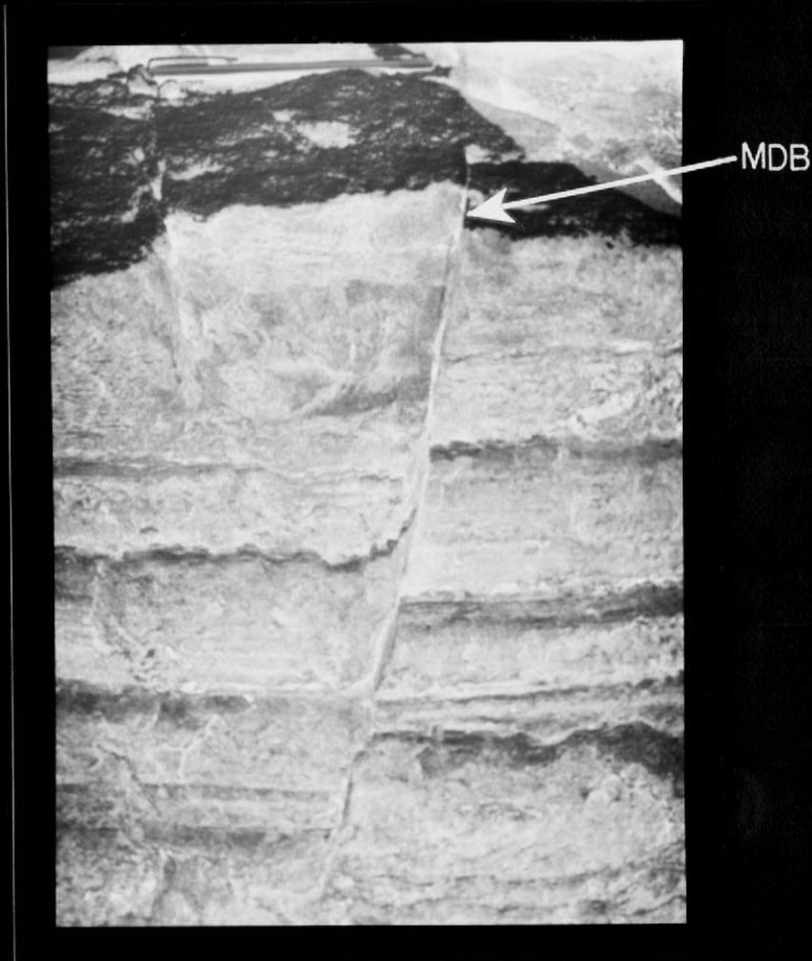


Figure 25. Normal drag formed as a result of normal-displacement along closely spaced deformation bands. About 3 cm of displacement along main deformation band (MDB) and 2 cm of cumulative displacement along smaller deformation bands for a total of about 5 cm of normal offset. View is a vertical face in the Middle Hickory Sandstone. Pointer for scale is 15 cm long.

tion bands is visible in the two lighter-colored layers in the middle of the photograph. In that area, the lighter-colored layers are small blocks which are broken along discrete surfaces and demonstrate rigid-body rotation. The numerous small deformation bands cumulatively account for the normal drag.

Fractures. Fractures are also a common brittle deformational structure occurring in the Paleozoic and Precambrian rocks in the Lower Comanche Creek area. Fracturing is more common in the Cap Mountain Limestone and the Precambrian rocks than in the Hickory and Welge Sandstones. This discussion of fractures is limited to observations made primarily in exposures of the Precambrian rocks. Becker (1985) gives a more detailed description of fracturing in the Paleozoic rocks in the Mason Fault area. He describes three general types of fractures: straight, segmented, and en échelon.

Fractures in the Precambrian rocks are characterized typically by regularly spaced, linear segments on outcrop surfaces that do not stand out in relief. Spacing between fractures in sets typically ranges between 10 and 30 cm. The exposed fracture planes commonly have smooth polished surfaces yet lack the trace of lineations on these surfaces. Dips measured for fracture planes are relatively steep and usually greater than 80 degrees. Offsets were not observed along fractures in the outcrops investigated. Fractures in an area south of Bare Hill have strike orientations that often parallel the primary set of deformation bands within the overlying Hickory Sandstone (see Fig. 21, p. 64).

Chapter IV

MICROSCOPIC OBSERVATIONS

The microscopic observations focus on the brittle deformation mechanisms operating at the grain scale. In particular, this chapter describes the characteristics of the deformation bands in thin section, the nature of the microfractures, the characteristics of the cementing materials, and the inferred effect of the cement on the grain-scale deformation.

Representative samples from the fine-grained section of the Lower Hickory Sandstone, the Cap Mountain Limestone and the Welge Sandstone were used to describe the host rock characteristics and deformation bands, as well as to map the associated microfracture spatial distributions. Microfracture orientations and lengths were measured for each sample described above. In addition, measurements along traverses parallel to the deformation bands were utilized for describing the grain-size reduction and microfracture density. A grain-boundary index was determined to represent the percentage of a single-grain boundary that is composed of a broken or fractured section.

In thin section, the Hickory Sandstone, Cap Mountain Limestone and Welge Sandstone are characterized by sub- to well-rounded host-rock quartz grains cemented primarily with hematite and calcite. In addition to detrital quartz, the compositions of the Hickory and Welge Sandstones contain feldspar and a discernable percentage of secondary quartz in the form of quartz overgrowths. In contrast, the quartz

sandstone of the lowermost Cap Mountain Limestone does not exhibit quartz overgrowths, but has about 6% carbonate grains and hematite coids. The porosity varies between 14 and 15.4% for the Hickory and Welge Sandstones and is somewhat less for the Cap Mountain Limestone at 7.7%. These values, determined from thin sections, are within the range of porosity values determined using a water saturation method. The host rock compositional and porosity characteristics are summarized in Table 2.

Deformation Band Characteristics

In thin section, deformation bands are characterized by a thin gouge zone (typically <0.5 mm) of fractured and highly comminuted grains (Fig. 26). The gouge-zone material typically has a strongly skewed grain-size distribution dominated by grains less than 0.05 mm in diameter (discussed subsequently). The gouge material is angular, and thin rims of hematite and/or overgrowths of quartz often surround the angular grains.

Within a typical gouge zone, a few large, relatively unfractured grains are intermixed and surrounded by the fine-grained gouge material. Most of the large grains display numerous intragranular microfractures, and they usually exhibit a broken grain boundary. However, some of the large grains in the zone are unfractured. In gouge zones associated with a large amount of shearing (displacements on the order of a centimeter), relative movement across intragranular microfractures gives these large grains a somewhat dilated and distorted form (Fig. 27). Occasionally, a slightly linear fabric is

TABLE 2
Host Rock Characteristics

Rock Type	Thin Section Number	Number of Grains Counted	Composition					Cement		Thin Section Porosity 2	Porosity Range (%) 3
			Detrital Quartz	Secondary Quartz 1	Feldspar	Rock Fragments	Carbonate/oids	Calcite	Hematite		
Hickory SS	202 S	350	54	11	11	3	0	0	7	14	8.2 to 17.4
Cap Mountain Limestone	184 BT	350	43	0	10.8	1.7	6	16.8	14	7.7	3.8 to 6.1
Welge SS	209 A	350	63	10.3	4	trace	0	0	7	15.4	14.6 to 17.4

- NOTES: 1. Secondary quartz as quartz overgrowths.
 2. Porosity determined by point count along linear traverses.
 3. Porosity range determined by water saturation method on cylindrical host rock blocks of each rock type. Reported range is for all samples of each rock type.

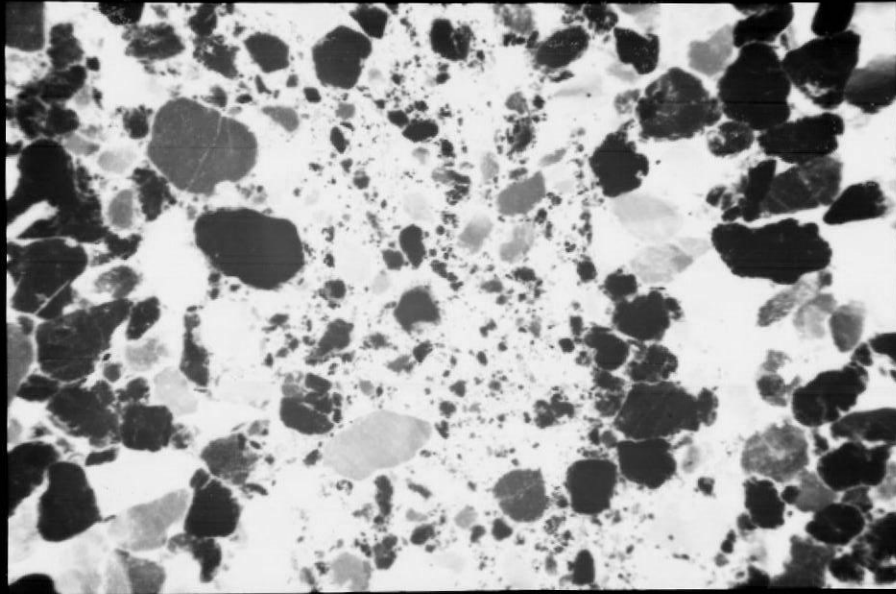


Figure 26. Typical deformation band in Hickory Sandstone thin section characterized by a thin gouge zone of fractured and highly comminuted grains. Gouge zone is 1.3 mm wide. Partially-polarized light; scale bar is 0.5 mm;

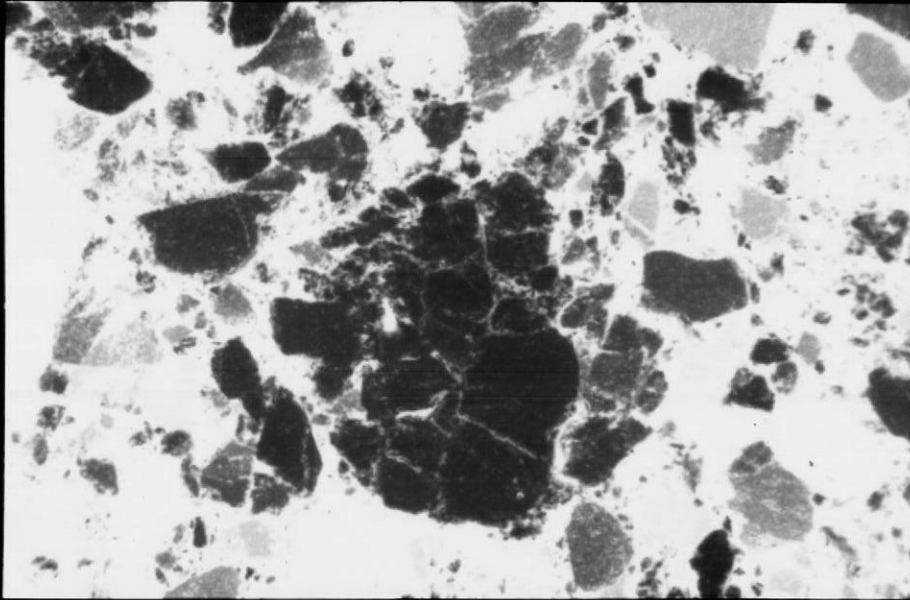


Figure 27. Large, microfractured grain in the gouge zone producing numerous fragments that have rotated, translated and become incorporated into the gouge material. The original grain boundary can still be distinguished. Hickory Sandstone. Partially-polarized light; scale bar is 0.5 mm.

developed roughly parallel to the plane of the gouge zone, reflecting the alignment of rod-shaped slivers of host rock grains produced by the large-grain microfracturing and intragranular movements (Fig. 28).

The contact between gouge material and host-rock grains is usually sharp. The edge of the deformation band can be delineated typically within one grain diameter. Along the band edge, there is often a very thin zone, typically one or two grain diameters thick, that exhibits a reduction in pore space (Fig. 29). Grain contacts in this thin zone are commonly tangential (i.e., point contacts), long or concavo-convex. Most concavo-convex and long contacts appear to result from pressure-solution at grain contact points. Also concentrated in this zone are intragranular microfractures that transect grains between the tangential, long and concavo-convex contacts.

In the Welge Sandstone thin sections, very fine-grained material resembling angular gouge zone material is present along one side of the pore spaces. This material is present up to 5 mm away from the deformation bands in the host rock. The consistent position of this material (i.e., polarity) plus its location away from the gouge zone is interpreted to reflect transport via pore fluid movement. This observation indicates the presence and movement of fluids within the host rock prior to a high degree of induration of the gouge zone material.

In the Cap Mountain Limestone, the gouge material consists almost entirely of comminuted quartz grains and hematite that are present in the host rock. In contrast with the adjacent host rock, very little calcite cement is found within the gouge zone.

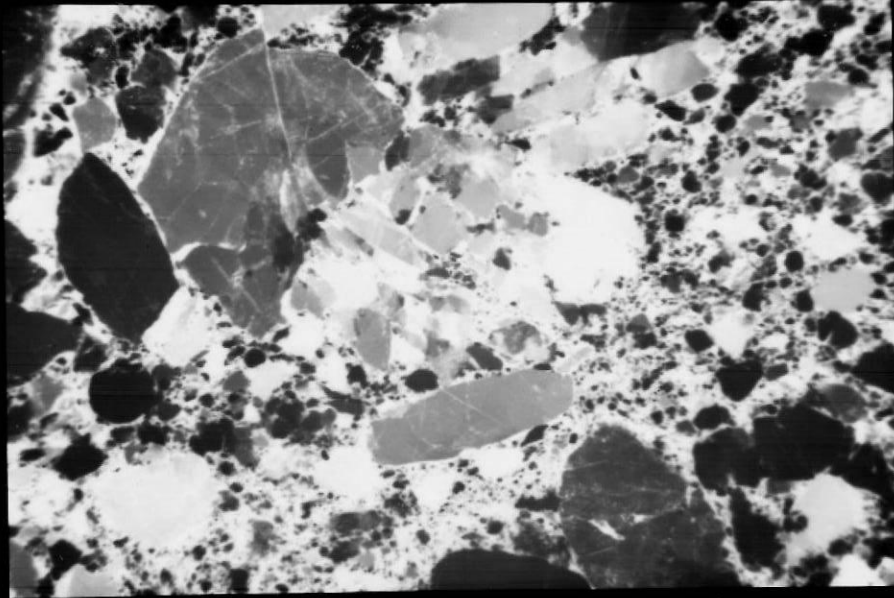


Figure 28. Elongated grain fragments produced by a concentration of microfractures in a quartz grain adjacent to a gouge zone. Elongated fragments can produce a linear fabric within a gouge zone upon alignment. Hickory Sandstone. Partially-polarized light; scale bar is 0.5 mm.

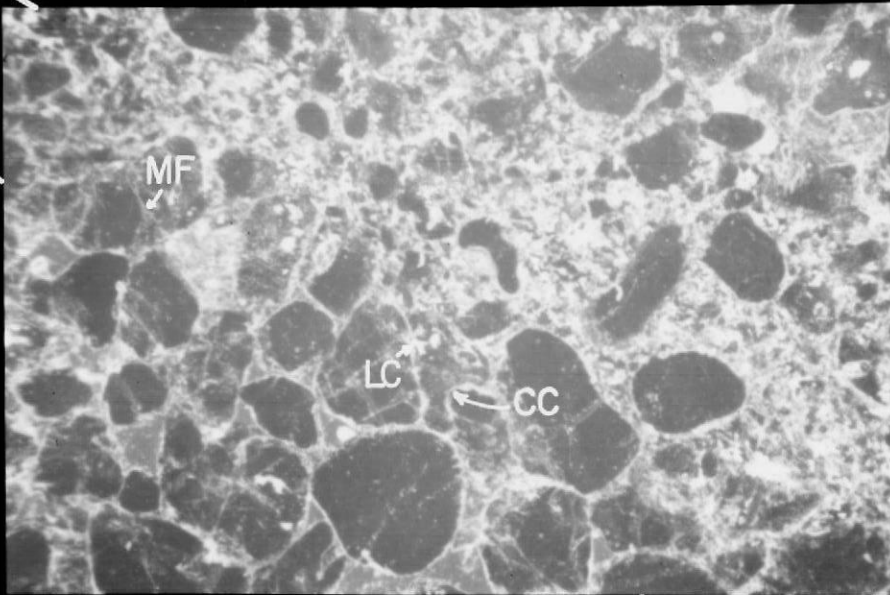


Figure 29. Thin zone immediately adjacent to a deformation band characterized by a reduction in pore space, an increase in concavo-convex (CC) and long (LC) contacts and by intragranular microfractures (MF). Hickory Sandstone. Plain light; scale bar is 0.5 mm.

Porosity within the gouge zone in the Hickory and Welge Sandstones is greatly reduced from that of the host rock. The porosity is estimated at less than 1%. The pores between the very small grains of the gouge material often appear to be filled with quartz overgrowths. In contrast, some samples within the Cap Mountain Limestone display a relatively high degree of porosity locally within the gouge zone.

The terminus of a deformation band was observed in a Welge Sandstone sample. At the termination, the gouge material abruptly ends within one grain diameter, and large pore spaces are present just beyond the terminus. Microfractures within the host rock and parallel to the gouge zone are present at this point although not in greater abundance than the bulk of the surrounding host rock material. Whether this represents a typical termination is not known since this is the only examined sample that contains a deformation-band termination.

Grain Size Reductions

Long axes of quartz grains were measured along parallel traverses within the deformation band gouge zone and at 2 and 4 mm away from the gouge zone boundary in order to determine grain-size reductions associated with the brittle deformation. Grain size within the gouge zone is typically less than 0.05 mm, although the histograms for the gouge zones indicate a skewed distribution toward even finer grain sizes (Fig. 30). In all samples, the smallest mean grain size occurs within the gouge zone. Additionally, the mean grain size at 2 mm from the gouge zone is less than that at 4 mm away, indicating increased grain breakage toward the deformation band (Fig. 31).

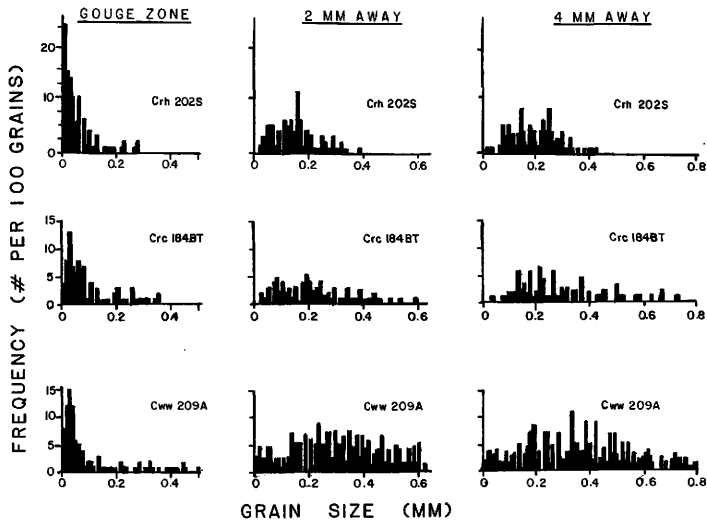


Figure 30. Histograms of grain size for traverses within and at 2 mm and 4 mm away from the gouge zone. Grain sizes determined by point count measurements of long axes for 100 grains in each traverse. Crh=Hickory Sandstone; Crc=Cap Mountain Limestone; Cww=Welge Sandstone.

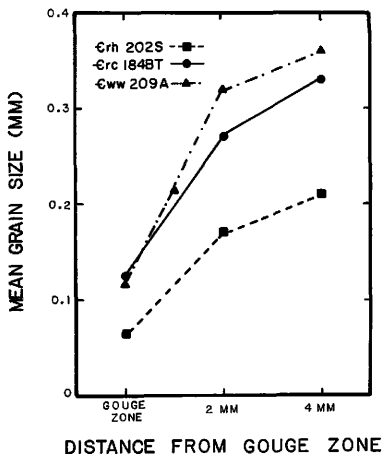


Figure 31. Mean grain size for the Hickory and Welge Sandstones and Cap Mountain Limestone as a function of distance from the center of the gouge zone. The decrease in grain size from 4 mm to 2 mm from the zone reflects the slightly lesser degree of grain breakage than that found closer to the gouge zone.

Grain Deformation

Brittle deformation on the grain-scale is caused primarily by the formation and subsequent linkage of intragranular microfractures connecting points of grain contacts (Fig. 32). The microfracturing occurs throughout the host rock with a relatively uniform density, but there is a concentration of microfractures localized adjacent to the deformation bands. Microfractures occur in all grain types including phosphatic and carbonate grains and hematite ooids. Furthermore, quartz overgrowths in the Hickory and Welge Sandstones are found both fractured and unfractured. There are three basic types of microfractures identified by morphology: through-going contact-contact fractures (Type-1); wedge-shaped fractures (Type-2); and microfractures that result in grain pulverization (Type-3). These three microfracture types are separated herein to facilitate discussion purposes. However, they may be related and represent a single type of microfracture that has developed to differing degrees.

Type-1 microfractures connect points of grain contact and predominate in each unit where the host rock exhibits a grain-supported texture. The microfractures often transect the entire grain. They typically have a frequency of one to three per grain, depending on the number of surrounding grain contacts (Fig. 33). These fractures can be linear or slightly curved and exhibit a discernable preferred orientation within the host rock (discussed subsequently). The through-going microfractures often link together to form a continuous microfracture three to four grain diameters in length.

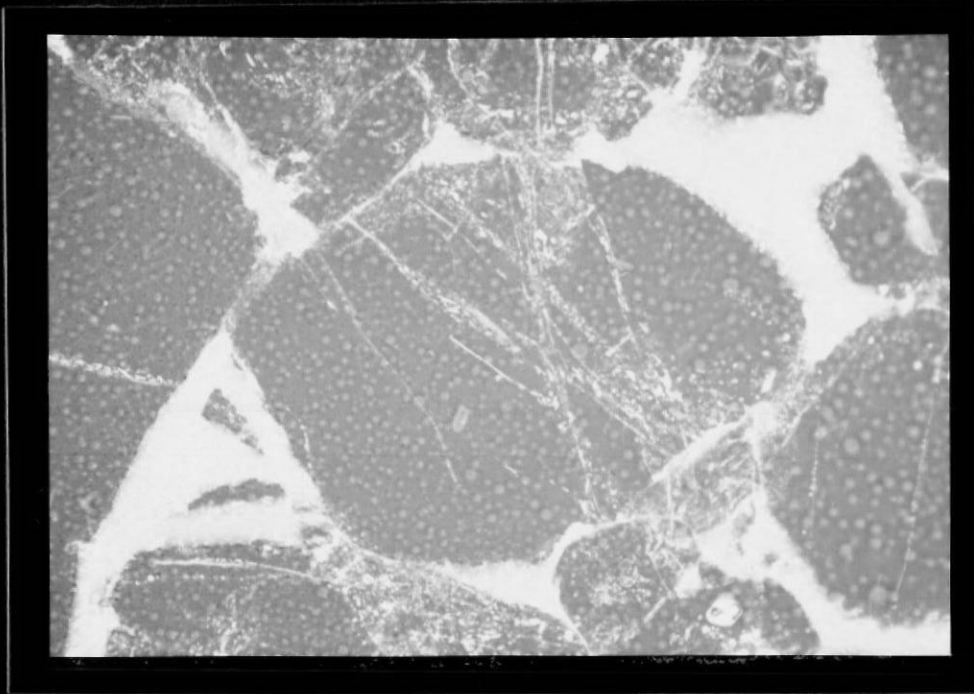


Figure 32. Intragranular microfractures connecting grain contacts in the Hickory Sandstone. Note the slight amount of translation of the grain fragments associated with movement along the microfractures. Hickory Sandstone. Partially-polarized light; scale bar is 0.1 mm.

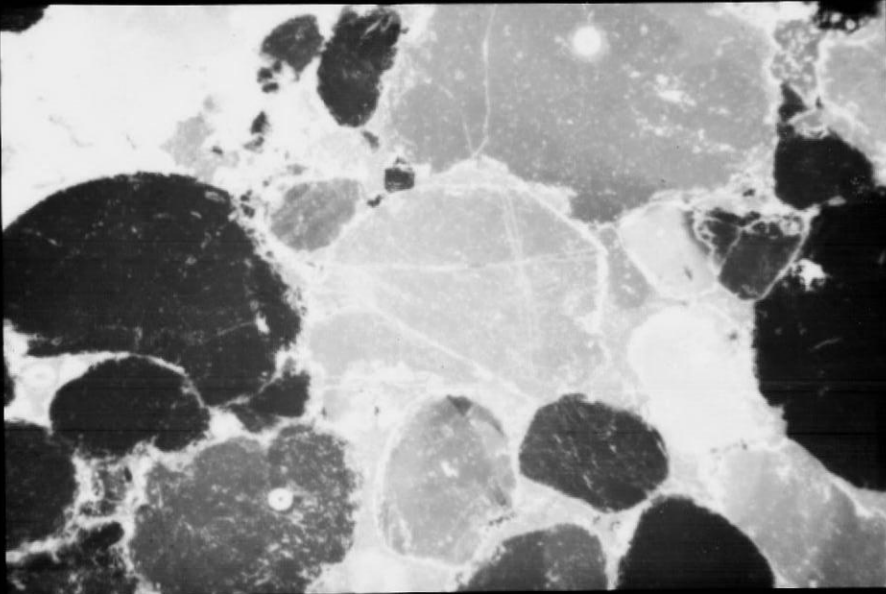


Figure 33. Type-1 microfractures in the Welge Sandstone that connect point contacts. Type-1 microfractures typically form with a frequency of one to three per grain separating the grain into two or more fragments. Partially-polarized light; scale bar is 0.5 mm.

The Type-1 microfractures are often healed, as evidenced by linear trains of bubbles that traverse grains between the contact points (Fig. 34). These bubble trails show varying degrees of healing along their length. The trails are roughly planar with the leading edge containing spherical bubbles. The spherical bubbles become elongated rods and "dog-bone shaped" along the healing fracture plane, presumably representing a lesser degree of healing (Smith and Evans, 1982).

Both bubble trails and microfractures occur in grains within and external to the deformation bands and can coexist within a single grain. Like the microfractures, the bubble lineations also display systematic orientations within the host rock. Infrequently, bubble lineations are also seen offsetting other bubble lineations at nearly right angles within a single grain (Fig. 35). The bubble lineations are interpreted to be healed microfractures. Their presence, together with cross-cutting relationships, may be indicative of multiple event brittle deformation, possibly with contemporaneous solution-related crack healing.

The second microfracture type (Type-2) is characterized by an arcuate shape and although they appear to originate at grain contacts, they do not fully penetrate the grain. They are typically wedge-shaped with the widest part located at the grain boundary (Fig. 36). The wedge-shaped fractures often are not healed as demonstrated by the lack of bubble trains formed in this orientation. Also, the wedge-shaped microfractures frequently have a thin hematite coating on the fracture surface in the Hickory and Welge Sandstones. In the Cap Mountain Limestone, the Type-2 microfractures may have a hematite or calcite

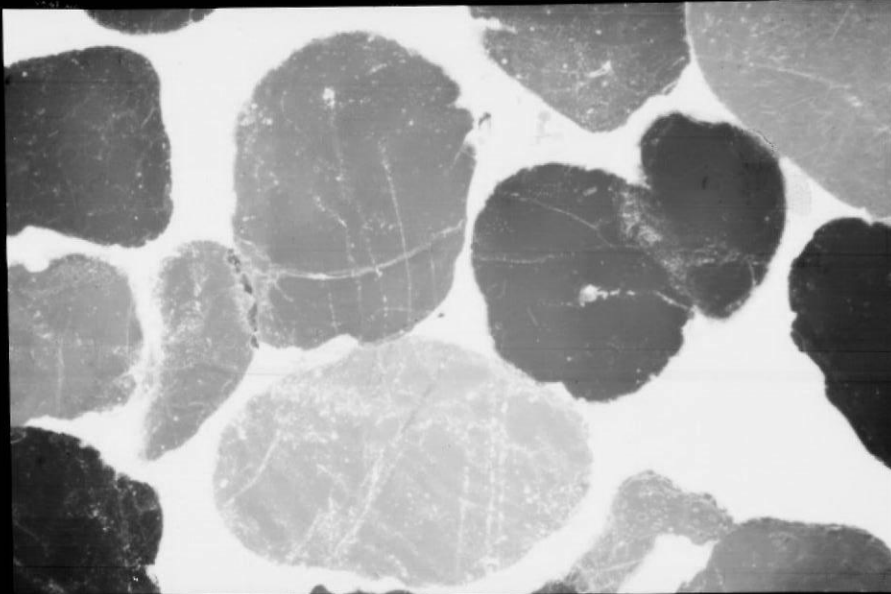


Figure 34. Healed Type-1 microfractures manifest as linear trails of fluid or bubble inclusions that traverse the grains between contact points. "Undeformed" Lower Hickory Sandstone sample. Partially-polarized light; scale bar is 0.5 mm.

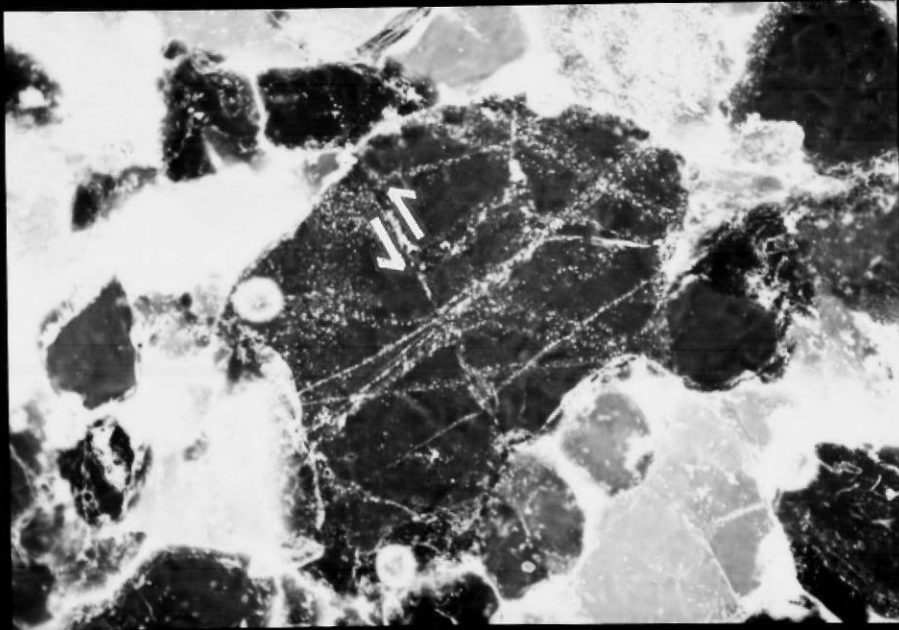


Figure 35. Offsetting bubble lineations at nearly right angles in Hickory Sandstone sample Crh 202T. Offset is left lateral. Partially-polarized light; scale bar is 0.5 mm.

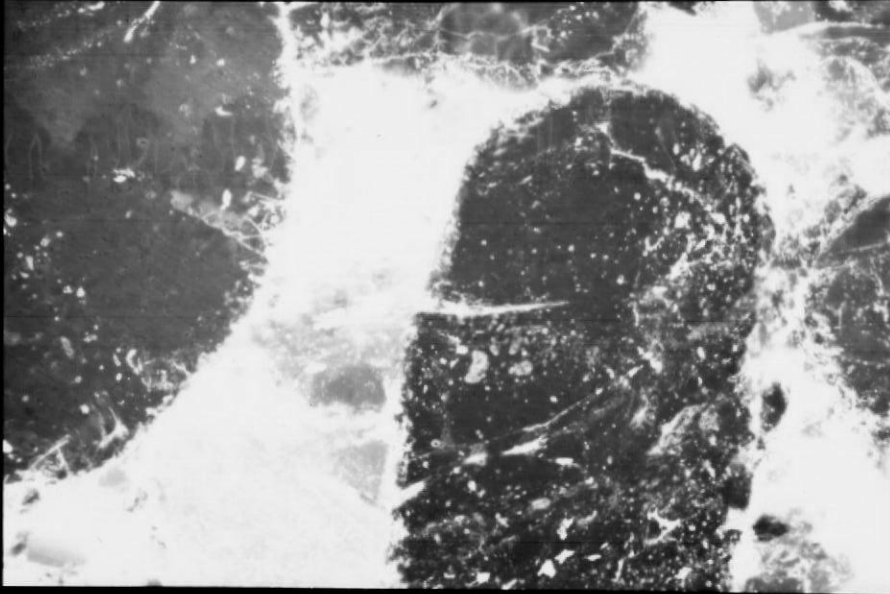


Figure 36. Type-2 wedge-shaped microfracture that partially penetrates the grain. The wedge-shaped microfractures are typically wider at the grain boundary and are usually not marked by healed planes of bubble lineations. Partially-polarized light; scale bar is 0.2 mm.

coating on the fracture surface.

Type-3 microfractures are characterized by a dense array of microfractures that result in full or partial pulverization of a grain (Fig. 37). They are common in grains contained in the thin zone of reduced porosity immediately adjacent to the deformation bands. This microfracture type, in many cases, represents Type-1 grain-contact fractures but to a greater density within a single grain. The Type-3 microfractures typically occur in grains where long and concavo-convex contacts occur with neighboring grains. The fracturing often displays a splay pattern that produces elongated, angular fragments. Small displacements are discernable along many of the Type-3 microfractures within a single grain. Relative displacement along the microfractures results in irregular-shaped grain boundaries (Fig. 38; also see Fig. 27, p. 76); although the original grain shape is usually roughly maintained. The grains with Type-3 microfractures often display a mosaic extinction pattern (Fig. 39). This mosaic extinction appears to be caused by brittle fracturing accompanied by rigid-body rotation and translation of the fragments that result in small crystallographic re-orientations.

Microfracture Orientation and Density

Microfracture maps were constructed in order to determine the spatial distribution and orientations of the microfractures. Rosettes of microfracture strike were constructed for each microfracture map to statistically analyze microfracture orientations. The strike rosettes were constructed from a random sampling of microfractures within the host-rock grains. A linear traverse point-count method was not used to

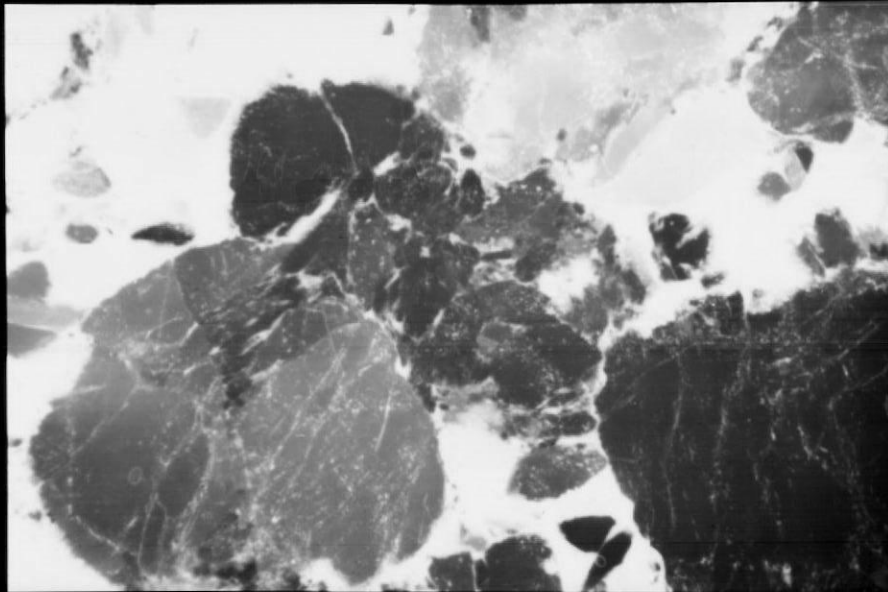


Figure 37. Type-3 microfractures manifest as a dense array of microfractures within a single grain that result in full or partial pulverization of the grain. Grain boundaries of these pulverized grains are typically concavo-convex or long. This type of fracturing is most prevalent immediately adjacent to the gouge zone. Note small grain fragments have rotated and translated. Adjacent grains display Type-3 microfracturing only in small sections. Partially-polarized light; scale bar is 0.5 mm.

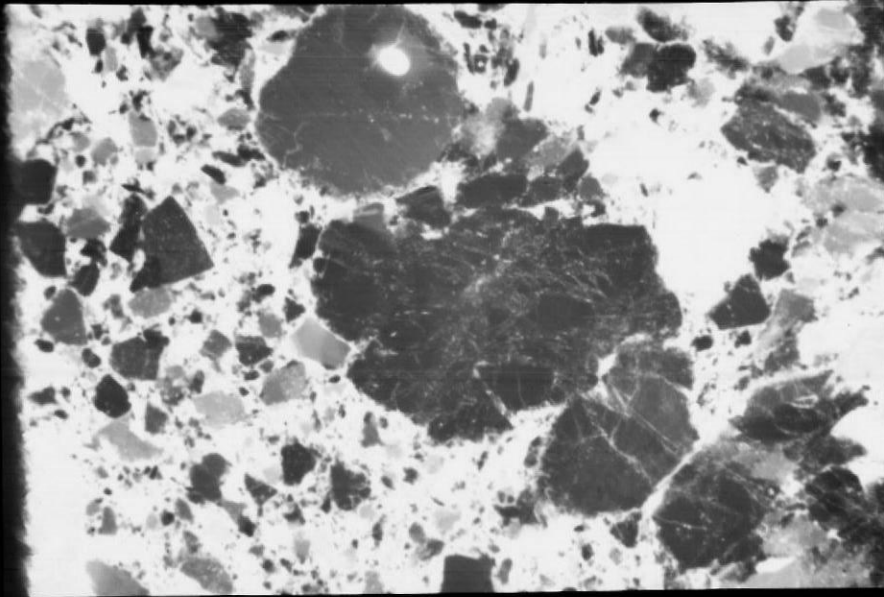


Figure 38. Intragranular movements resulting in translation and rotation of grain fragments and producing irregularly-shaped, but distinguishable grain boundaries. Hickory Sandstone. Partially-polarized light; scale bar is 0.5 mm.

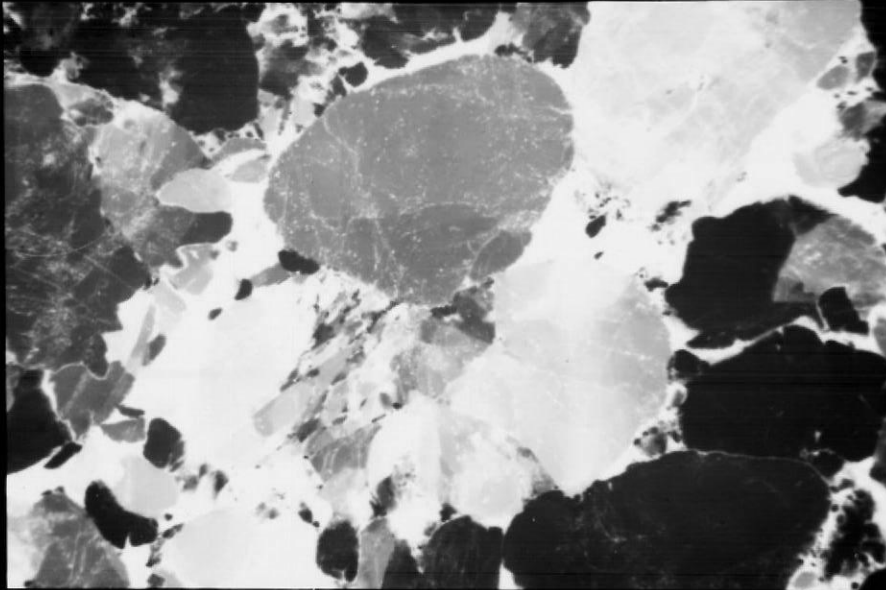


Figure 39. Mosaic extinction pattern manifest in a single grain by small crystallographic re-orientations due to rigid-body translation and rotation of the grain fragments. Hickory Sandstone sample Crh 164. Partially-polarized light; scale bar is 0.5 mm.

avoid a potential sampling bias introduced by not counting fractures that parallel the traverse direction, and thus do not cross the microscope cross-hairs. Within a single, randomly sampled grain, all single microfractures or microfracture sets were measured. Figures 40 through 43 illustrate microfracture maps for the Hickory Sandstone, Cap Mountain Limestone and Welge Sandstone, respectively. The strike rosettes for bubble lineations, microfractures and combined bubble train/microfracture orientations are also illustrated. The microfracture maps are views perpendicular to the plane of the deformation bands in either a horizontal (i.e., bedding plane) or vertical orientation. A common arbitrary reference direction is used for both the microfracture maps and the strike rosettes. For presentation purposes, this arbitrary reference direction is referred to as North.

The most distinctive feature of the microfracture maps is the pervasive distribution of the microfractures in each sample. Even in the host rock areas that appear mesoscopically undeformed, fractures and bubble lineations are prevalent. Linear densities of microfractures (i.e., average number per mm) that were determined along traverses parallel to the deformation bands, are greatest within and immediately adjacent to the bands (Table 3). At a distance of 2 and 4 mm away from the bands, the linear density of microfractures obtains a smaller, but constant, non-zero value (Table 3).

The rose diagrams of microfracture strike exhibit a relatively strong preferred orientation for both the bubble lineations and the microfractures. Generally, the strikes of both the bubble lineations and microfractures differ about 30 to 50 degrees from the strike of the

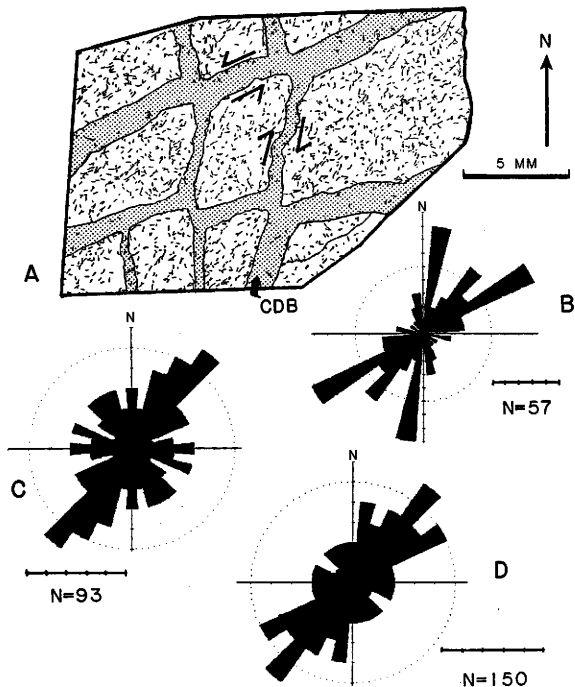


Figure 40. Microfracture map (a) and strike rosettes for Hickory Sandstone sample Crh 202T. Deformation bands on bedding plane view contain both left and right-lateral slip. This map is perpendicular to microfracture map Crh 202S (Fig. 41a) and shares a common deformation band to both maps, labelled "CDB". Scale bar of microfractures is 5 mm. Strike rosettes are separated into orientations of microfractures (b), bubble lineations (c), and combined (d). Strike rosettes plotted as a percentage of total measured; 5% scale bar indicated. n=total orientations measured.

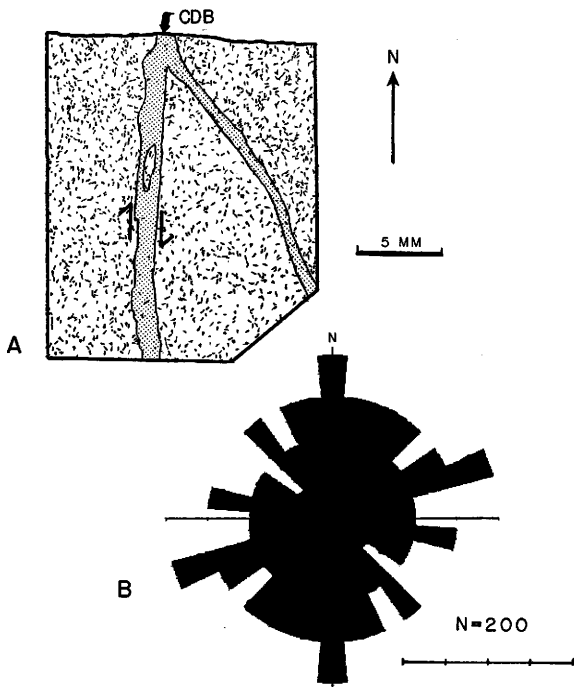


Figure 41. Microfracture map (a) and strike rosette for Hickory Sandstone sample Crh 202S. View is a vertical face with the predominant slip direction perpendicular to the plane of the map. A slight component of normal slip is visible in this map (arrows). Deformation band common to Fig. 40a labelled "CDB". Scale bar of microfracture map is 5 mm. Strike rosette (b) for both bubble lineations and microfractures. Strike rosette plotted as a percentage of total microfractures and bubble lineations measured; 5% scale bar indicated. n =total orientations measured.

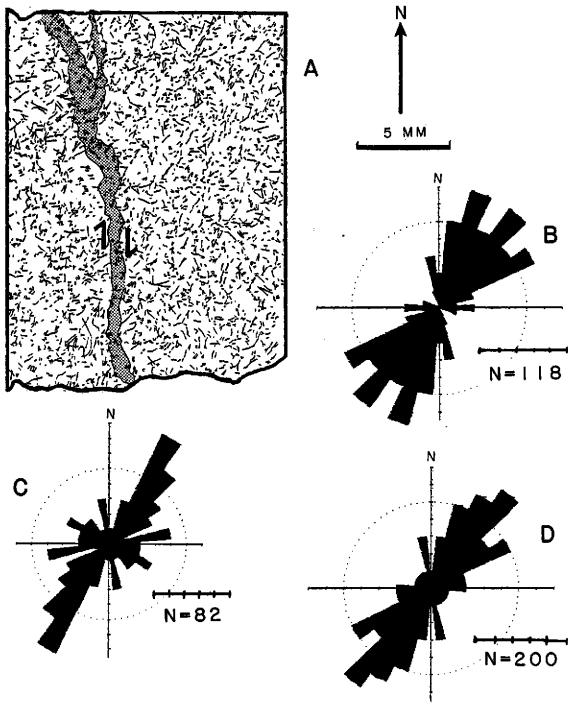


Figure 42. Microfracture map (a) and strike rosettes for Cap Mountain Limestone sample Crc 184BT. Map is a bedding plane view. Sense of offset postulated from microfracture and deformation band orientation data to be right lateral. Scale bar of microfracture map is 5 mm. Strike rosettes of microfractures (b), bubble lineations (c), and both combined (d). Strike rosette plotted as a percentage of total measured; 5% scale bar indicated. n=total orientations measured.

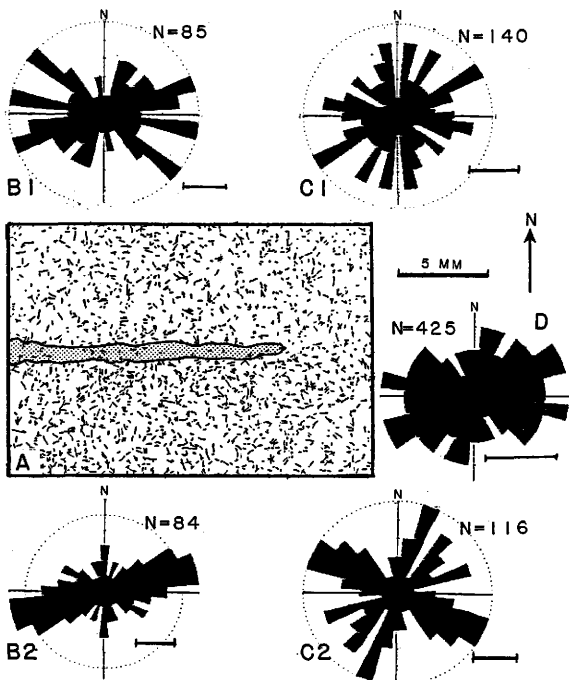


Figure 43. Microfracture map (a) and strike rosettes for Welge Sandstone sample Cwv 209A. Map is a bedding-plane view and sense and magnitude of displacement could not be determined. Scale bar microfracture map is 5 mm. Strike rosettes are separated into microfractures for the area above the deformation band (b1) and below the deformation band (b2), bubble lineations above (c1) and below (c2) the deformation band, and combined microfractures and bubble lineations (d) for the entire microfracture map. Strike rosettes plotted as a percentage of total number measured; 2.5% scale bar indicated. n =total orientations measured.

Table 3
 Microfracture Linear Density
 (microfractures/mm)

Sample Number	Gouge Zone		Edge of Gouge Zone		2 mm from Gouge Zone		4 mm from Gouge Zone	
	\bar{X}	S	\bar{X}	S	\bar{X}	S	\bar{X}	S
Ch 202S	7.6	2.5	8.5	1.7	6.2	1.4	6.0	1.8
Crc 184BT	11.5	2.2	9.7	2.1	6.2	1.9	6.1	1.6
Cw 209A	9.6	2.0	8.9	2.0	5.0	1.5	4.6	1.5

Note: Linear microfracture density calculated as the average number of fractures per millimeter for a two-centimeter traverse (\bar{X}); S = Standard deviation.

deformation band.

Two microfracture maps were constructed for Hickory Sandstone sample Crh 202 (Figs. 40 and 41). These two microfracture maps are oriented perpendicular to each other and share a common deformation band (labeled CDB on the maps). The first map (Fig. 40) is a bedding plane (i.e., horizontal) view and displays both left and right-lateral slip directions. The second map (Fig. 41) is a vertical view perpendicular to bedding and the plane of the deformation band and displays a small amount of right lateral offset.

The first Hickory Sandstone microfracture map (Fig. 40a, Sample Crh 202T) is oriented perpendicular to the deformation bands looking down on a horizontal bedding surface, and the main component of slip is parallel to the plane of the diagram. In this map, the magnitude of the displacement along the deformation bands varies between 0.68 and 1.13 mm. There also is a slight component of normal displacement (0.3 mm) into and out of the plane of the section along the band marked CDB. Both the bubble lineations and microfractures exhibit relatively strong preferred orientations. The bubble lineations are oriented primarily between N30E and N40E (Fig. 40b). However, microfracture orientations display concentrations oriented N10E and N60E with a lesser concentration about N40E (Fig. 40c). No prominent northwest trending microfractures are present. The combined bubble lineation/microfracture strike rosette displays a strong preferred northeasterly orientation (Fig. 40d). The northeasterly-trending orientations form an angle roughly 30 to 60 degrees with the set of deformation bands trending north-south and containing the greatest amount of slip.

The second microfracture map and associated strike rosette for Hickory Sandstone sample Crh 202S (Fig. 41a) shows a diffuse range of orientations. The bubble lineations and microfractures are not separated in the rose diagram (Fig. 41b). This figure is oriented as a vertical face roughly perpendicular to the plane of the band. In the plane of the thin section, the relative displacement along the main deformation band (CDB) is right lateral and totals about 0.3 mm. However, the component of displacement normal to the plane of the section predominates. This deformation band is common to the map of sample Crh 202 T (Fig. 40a). Two slightly preferred orientations occur, one roughly parallel to the deformation band and another concentration oriented about N70E. A diffuse fan concentration also exists between N25W and N45E.

Figure 42 presents the microfracture map and associated strike rosettes for Cap Mountain Limestone sample Crc 184BT. This map is a horizontal view with the dominant slip direction in the plane of the map. The bubble lineations display a strong preferred orientation of about N30-40E (Fig. 42b). The orientations of the microfractures exhibit a more diffuse character but preferentially strike north-easterly (Fig. 42c). The northeasterly-trending concentrations are oriented between N10E and N60E. Taken as a whole, the bubble-lineations and microfractures strike preferentially N30-40E, roughly at an angle of 35-45 degrees relative to the deformation band. Based on the microfracture and deformation band orientations, the sense of offset is postulated to be right lateral.

The microfracture map for the Welge Sandstone sample Cww 209A is a bedding plane view of the deformation band (Fig. 43a). The relative sense and amount of offset along the band could not be determined. The bubble lineations for the Welge Sandstone display primarily three preferred orientations (Fig. 43b), the strongest at N50-70W and slightly weaker concentrations at N20E and N60E. Microfractures also display three preferred orientations at N60-80E, N50W and N80W with the strongest concentration at N60-80E (Fig. 43c). The combined strike rosette displays a diffuse range of orientations 40 to 50 degrees to either side of the strike of the deformation band (Fig. 43d). Slight concentrations 10 to 30 degrees on either side of the deformation band strike also occur.

Microfracture Length

Lengths of 150 to 425 microfractures were measured along linear traverses in each thin section. Histograms of microfracture length are presented in Figure 44. The histograms display nearly normal distributions but are slightly skewed to the smaller fracture lengths. The mean microfracture length for each thin section is essentially equal to the mean grain size. This relationship between mean microfracture length and mean grain size is not surprising since most microfractures transect the grains between point contacts.

Grain Boundary Index

To qualitatively determine the degree of grain deformation in the host rock and gouge zone, a grain-boundary index was determined. The

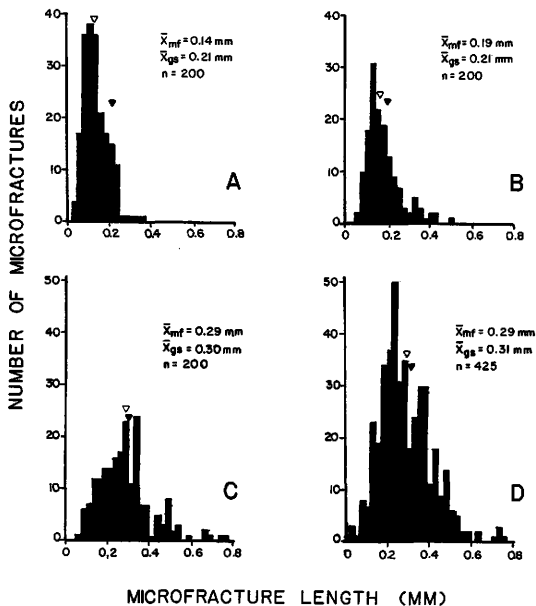


Figure 44. Histograms of microfracture length. Mean microfracture length and mean grain size for sample indicated by open and closed triangles, respectively. (A) Hickory Sandstone sample Crh 202S, (B) Hickory Sandstone sample Crh 202T, (C) Cap Mountain Limestone sample Crh 184BT, and (D) Wedge Sandstone sample CwW 209A. \bar{X}_{mf} =mean microfracture length; \bar{X}_{gs} =mean grain size; n=number of microfractures measured.

grain-boundary index is defined to be the percentage of a grain boundary that is comprised of a broken or fractured section. Traverses were made in each thin section within the gouge zone and at 2 and 4 mm away from the boundary of the gouge zone. Along each traverse, the boundaries of 100 grains were qualitatively classified into four categories representing the percentage of each grain boundary that is fractured. The categories include: (1) intact grain boundaries, (2) <30% of grain boundary is broken, (3) 30-60% of grain boundary is broken, and (4) >60% of grain boundary is broken.

The grain-boundary index for each sample is illustrated in Figure 45. For gouge zones, this index indicates that the majority of grains are >60% broken with only a small percentage of grains (<10%) totally intact. Numerous grains within the gouge zone fall in the intermediate group with 16-30% of the grains having an index of 3 (30-60% broken). Almost all of the large grains within the gouge zones display at least some breakage of the original grain boundary.

The greatest difference between intact (Index of 1) and >60% broken (Index of 4) occurs at 4 mm from the zone. Also, Figure 45 illustrates that grains at 2 mm from the zone have undergone some brittle deformation probably accompanied by dilational and distortional movements that result in a relatively large percentage of grains with indices of 2 and 3.

Cementing Material Observations

The effect of the cementing material within the host rock on the cataclasis and formation of deformation bands is not well understood.

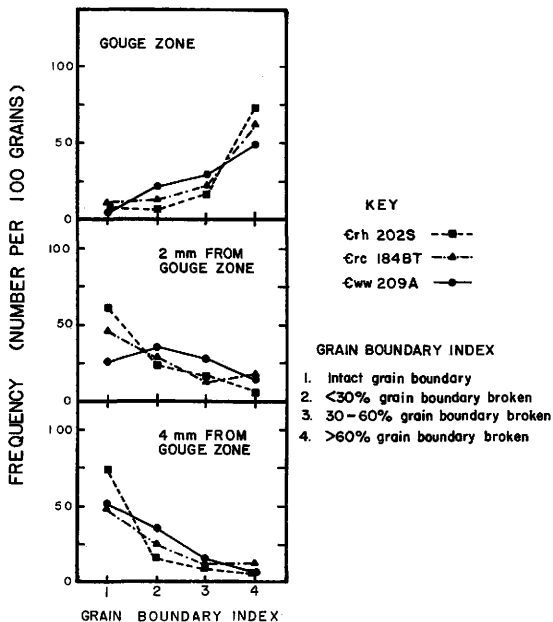


Figure 45. Grain boundary index as a function of distance from the gouge zone. The grain-boundary index is a qualitative determination of the grain breakage and represents the percentage of each grain boundary that is fractured. For example, a high grain-boundary index of 4 is assigned to grains with > 60% of their boundary broken.

Observations of the cements within the Hickory and Welge Sandstones and Cap Mountain Limestone were made to provide additional insight into the role of this parameter. The following observations focus on the hematite cement and secondary quartz overgrowths in the Hickory and Welge Sandstones and the calcite cement in the Cap Mountain Limestone.

The amount and nature of hematite cement within the Hickory and Welge Sandstones varies, but is most prominent in the Upper Hickory Sandstone. Hematite in the Upper Hickory Sandstone occurs both as ooids and as the primary cement. The ooids appear to behave mechanically both in a brittle and ductile manner. Occasionally, the ooids will contain microfractures and actually show a separation between the concentric layering. In contrast, many of the hematite ooids are highly deformed and appear to have "flowed" into the interstices between the quartz grains. In this case, the deformed hematite ooids have the shape of a multi-pointed star and form a pseudomatrix around the quartz grains (Fig. 46). Hematite cement occurs in the deformation bands and host rock as thin stringers and as small spherical shells that typically surround grains and fill wedge-shaped Type 2 microfractures. It also appears that hematite inhibits quartz overgrowth within the Upper Hickory Sandstone.

Quartz overgrowths occur quite commonly in both the Hickory and Welge Sandstones. The overgrowths are present primarily as scaly overgrowths surrounding small grains and sections of larger grains (Fig. 47). Quartz overgrowths also occur as euhedral crystal faces that extend into pore spaces (Fig. 48). The overgrowths are in optical continuity with the host grains and are typically separated from the



Figure 46. Deformation of concentric-layered hematite ooid into a multi-pointed star that appears to have "flowed" into the interstices between grains. Sample of Cap Mountain Limestone (Crc 184T). Scale bar is 0.2 mm.

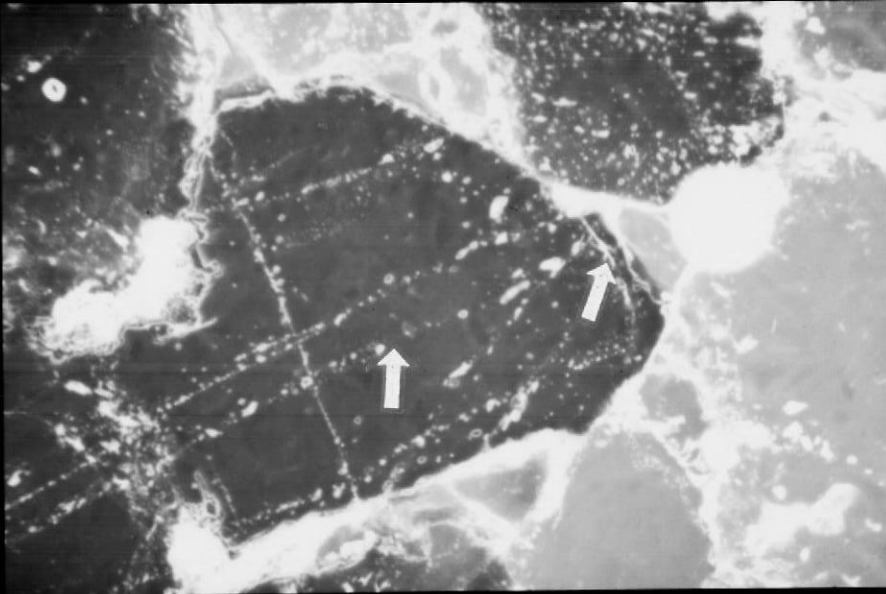


Figure 47. Scaly quartz overgrowths surrounding and optically continuous with a rounded quartz grain. The overgrowth has been fractured and healed as shown by the linear bubble trails traversing both the grain and overgrowth (arrows). Welge Sandstone sample. Partially-polarized light; scale bar is 0.1 mm.

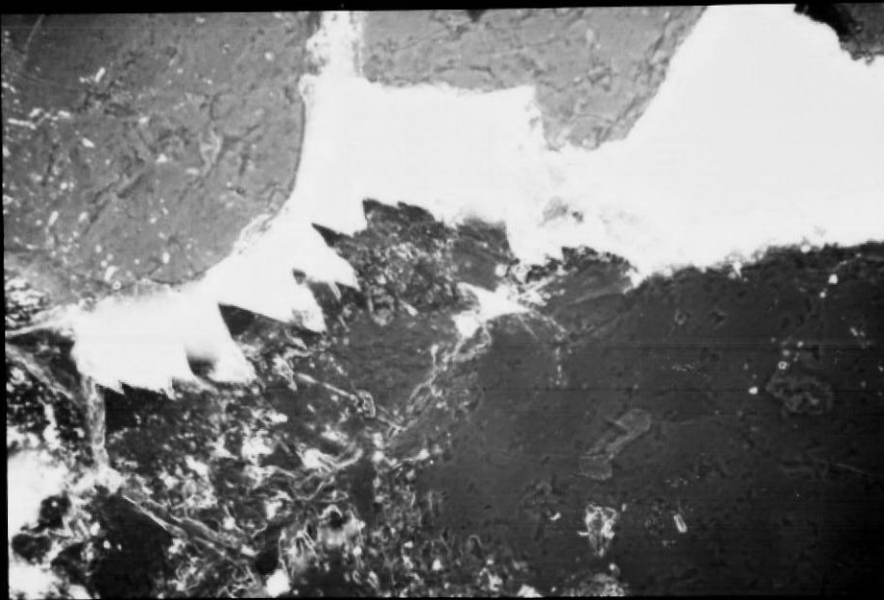


Figure 48. Euhedral-shaped quartz overgrowths that have grown into the pore spaces between grains. The euhedral overgrowths are not fractured. Hickory Sandstone sample. Partially-polarized light; scale bar is 0.1 mm.

host grain by a thin "dust" rim. Small overgrowths that surround numerous fine-grained fragments in the gouge zone are common throughout the Hickory and Welge Sandstones. The presence of the overgrowths in the gouge zones may suggest a mechanism for the high degree of induration and increased resistance to weathering of the deformation bands on outcrop surfaces.

Fractures within the host rock grains typically penetrate the overgrowths, indicating that the overgrowth formation precedes the microfracturing in this case (Fig. 47). However, occasional grain fractures that do not penetrate quartz overgrowths are also present, suggesting a post-fracturing time of formation.

The calcite cement in the Cap Mountain Limestone occurs as pore-filling cement and large poikilitic grains that encompass several quartz grains. The mechanical behavior of the calcite cement depends on whether the host rock is quartz grain-supported or matrix-supported. In the grain-supported sections of the Cap Mountain Limestone, the quartz grains exhibit point contacts, and the calcite cement fills the interstices between the quartz grains. In this case, the quartz grains contain Type-1 microfractures that typically transect the grains. The fractures in the quartz grains display dilational and distortional movements. Fluid inclusion trails in the grain-supported Cap Mountain Limestone quartz grains are common. The calcite cement typically is not twinned or fractured except on rare occasions where it is caught between two quartz grains. Twinning is also not common along the gouge zone boundary of the deformation bands in the grain-supported Cap Mountain.

In contrast, within matrix-supported Cap Mountain Limestone, the calcite surrounds the quartz grains, and as a result, point contacts are minimal. The calcite is typically twinned, and Type-1 microfractures are rare and occur only where two or more grains contact at points. The density of the twin planes is much greater than that encountered in the grain-supported Cap Mountain, and conversely, the quartz-grain fracture density is much less. Adjacent to the deformation band gouge zone, there is no noticeable increase in the density of the twin planes. Also, fluid inclusion trails that occur within the quartz grains are more sparsely distributed than in the grain-supported Cap Mountain Limestone.

Chapter V

DISCUSSION

As demonstrated in this study, brittle deformation of the lower Paleozoic sandstones and limestones on the southwestern flank of the Llano Uplift occurs on the macroscopic, mesoscopic and microscopic scales. Macroscopic deformation is manifest by the numerous large-displacement and minor faults; mesoscopic deformation by the localized deformation bands; and microscopic deformation by the microfracturing and cataclasis of individual grains. The brittle deformation is accompanied by mechanical twinning (calcite cement), dissolution and precipitation mechanisms (pressure solution).

This chapter discusses the mesoscopic-scale deformation bands, the relationships between the mesoscopic-scale deformation bands and the large-scale faults, implications of basement-fault control and the characteristics of the controlling textural/mineralogic parameters. Characteristics of the microscopic deformation are also discussed in relation to other deformational features and observations of previous studies. In addition, a chronology of grain-scale deformation leading to the development of the deformation bands is presented.

Deformation Bands and Large-Displacement Faults

Deformation bands provide a unique tool in determining the large-displacement fault characteristics in areas where fault exposure and outcrop is limited. In the Llano Uplift, deformation bands occur in close association with faults in the Paleozoic sandstones and typically

exhibit the greatest concentration near large-displacement faults. Often the large-displacement fault surface is not visible in outcrop, but its location can be estimated by an increase in density of deformation bands in a localized area. Therefore, these structural features should be utilized when field mapping other structural elements.

Deformation bands also provide some indication of fault attitude. Typically, the dip and strike of the dominant set of deformation bands adjacent to a large-displacement fault parallels that of the fault. In the Lower Comanche Creek area, the deformation bands roughly parallel the faults and display relatively steep dips that generally vary between 80 and 90 degrees. Exposed large-displacement faults in this area usually have similar spatial attitudes.

In addition, deformation bands provide some indication of the localized strain field by providing markers, such as slickensided surfaces and offset intersecting bands that indicate the sense of movement. The deformation bands also form in systematic networks that provide information on fault-fault interactions (Hedgcoxe, 1987; Hedgcoxe and Johnson, 1986).

Aydin (1977) and Aydin and Johnson (1983) found that single deformation bands precede the development of zones of deformation bands and that zones precede the formation of discrete slip surfaces (macroscopic faults). Thus, they concluded that deformation bands are primary structural features that represent the initiation of faulting and deformation of an area. However, based on observations during this investigation, deformation bands can also occur as secondary features that form as a result of movement along the large-displacement and

minor faults. This is suggested by deformation band formation in antithetic attitudes to other small faults (Fig. 24, p. 69) and by the development of ordered networks of deformation bands in the overlap region of two interacting faults forming a secondary fault zone (Fig. 13, p. 50).

The formation of deformation bands in antithetic attitudes possibly results from movements along nearby faults that create localized secondary deformation fields in the adjacent host rock. Also, antithetic faults form due to closely spaced, primary fault-fault interactions. The antithetic-oriented deformation bands display small displacements in response to these secondary deformation fields. As a consequence of the antithetic fault formation, displacement can be transferred from one primary fault to another.

In a localized area on the northeast side of Bare Hill, deformation bands parallel to the main fault in this area (oriented about N20E) are found to offset and be offset by another set of deformation bands (oriented about N70E). The offsetting relationships of the two sets of deformation bands may indicate that their formation is closely spaced in time. The orientation of the large-displacement fault also may reflect preferential development with respect to one of the deformation band sets. In addition, the presence of oblique slip on many of these deformation bands may be an indication that the local strain field is not plane strain but is three-dimensional.

Basement Fault Control

Faults within the overlying Paleozoic rocks in the Llano Uplift

differ in detail over granitic versus metamorphic basement terrains (Becker, 1985). Becker noted that faults located in the Paleozoic sedimentary rocks over granitic basement typically have larger throws and hence are more pronounced than faults over metamorphic basement. He suggested that faults in the granitic rocks are localized and contain larger throws, whereas faults in the metamorphic rocks appear to have smaller throws and are more pervasively distributed.

Most of the Precambrian rocks underlying the Lower Comanche Creek area are Packsaddle Schist, except possibly in the south and extreme western part of the area. As previously noted, the location of the axial plane of the syncline in the western section is coincident with the maximum throws along the main large-displacement faults (Fig. 6, p. 18). This northwest-trending zone of maximum throw along faults is presumably colinear with the granitic-metamorphic contact (Becker, 1985).

Since most of the study area is underlain by Packsaddle Schist, differences between the faults and deformation bands in the Paleozoic rocks overlying different Precambrian basement types were not studied. However, the extreme abundance of deformation bands in the Hickory Sandstone perhaps reflects the relative degree of basement deformation in the area.

If the Hickory Sandstone is mimicking pervasively distributed deformation in the Packsaddle Schist, then one would expect to see widely distributed deformation bands. Qualitatively, this is the case in the study area as deformation bands are ubiquitous in the Hickory Sandstone where obvious deformation has occurred. Also, orientations

of deformation bands are nearly colinear with measured fracture trends in the underlying Packsaddle Schist (Fig. 21, p. 64). Since the Hickory Sandstone appears pervasively deformed, it probably dampens some of the deformation resulting from movement along numerous faults in the Packsaddle Schist. Consequently, upsection from the Hickory Sandstone, the deformation would be concentrated along more discrete zones that are coincident with basement faults exhibiting larger displacements.

Northwest of the present study area, Becker (1985) noted differences in the character of the faulting as a function of vertical position in the stratigraphic section. In the lower Paleozoics, he found that faults intersect often, have a wide range of orientations, and splay faults are common. Further up in the stratigraphic section within the Pennsylvanian rocks, the faults have an en echelon geometry, do not intersect or splay as often, and have a greater regularity of spacing and orientation.

Thus, the overall orientation and distribution of faults in the Lower Comanche Creek area are probably influenced by basement faulting and vertical stratigraphic position.

Parameters Controlling Deformation Band Development

The parameters most often cited as controlling the width of the gouge zone of small faults include: displacement (e.g. Engelder, 1974), porosity (Young, 1982), and normal stress (Handin, 1972). This section gives a general assessment of the effects of displacement and porosity parameters in addition to the potential effect of grain size as yet

another parameter controlling deformation band thickness.

In the Lower Comanche Creek area, displacement along deformation bands is found to exhibit a weak direct relationship with deformation band thickness (Fig. 15, p. 53). This coincides with observations of prior studies where the relationship between gouge zone thickness and displacement is not well established. For example, Young (1982) observed a slight increase in thickness of deformation bands with increasing displacement. Similarly, Robertson (1983) determined a linear relationship between gouge zone width and displacement along breccia zones. In contrast, Jamison (1979) and Blenkinsop and Rutter (1985) did not find a definite correlation between gouge zone thickness and displacement. Engelder (1974) also noted the lack of a clear relationship between thickness and displacement in the naturally occurring deformation bands but suggested a linear relationship exists for experimentally-formed gouge zones in Coconino Sandstone.

Although Young (1982) observed a slight increase in thickness of deformation bands with increasing displacement, he determined a more significant change in gouge zone thickness as a function of porosity. Dunn and others (1973) showed that small-fault gouge zones in experimentally deformed sandstones are thicker in the higher porosity sandstones. In contrast, the gouge zones in the Lower Comanche Creek area are characteristically wider in the slightly lower porosity, coarse-grained sandstones than in the higher porosity, fine-grained sandstone. Moreover, a single deformation band will increase in width when crossing from a fine-grained sandstone bed to a coarse-grained bed. This dissimilarity of results is most likely attributed to the possible

effect of grain size on deformation band thickness. Measurements shown on Figure 17 (p. 57) indicate an increase in deformation band thickness with increasing mean grain size for various samples of the Hickory Sandstone.

In previous studies, differences in deformation band thickness have not been correlated with grain size. However, Borg and others (1960) determined that for experimentally deformed specimens of uniform grain size, the coarsest-grained sand exhibited more fracturing than finer-grained sands (under equivalent stress conditions). An accrual of fracturing would lead to a high degree of grain comminution as grains rotate and translate and point contacts become more abundant. The increased grain comminution may result in the greater thickness of deformation bands in the coarse-grained sandstones.

In addition, Gallagher (1976) tested quartz grains in diametral compression and found that the tensile strength of the quartz grains increases with decreasing grain size. If grain breakage and subsequent gouge generation is a function of grain size, then it can be surmised that less gouge, and thus thinner gouge zones, should be produced during grain breakage in the finer-grained quartz sandstones.

Hence, the development of deformation bands is controlled by the interaction of environmental and intrinsic parameters including, but not limited to, displacement, porosity and host-rock grain size.

Microfractures

Brittle deformation of the Hickory and Welge Sandstones and Cap Mountain Limestone is manifest on the microscopic-scale by grain micro-

fracturing with subsequent rotation and translation of the grain fragments. The microfractures occur as open, filled and healed surfaces that connect grain contacts. Coalescence and linkage of microfractures occurs, but it is unclear whether this is the mechanism that forms the localized, extremely fine-grained gouge zones (i.e., deformation bands).

In this study, microfracturing in the host rock appears to be pervasively distributed but is enhanced within and immediately adjacent to the deformation bands. This is indicated by the ubiquitous occurrence of microfractures on the microfracture maps and the measured linear fracture densities. Moreover, samples collected from the Hickory Sandstone, Welge Sandstone and Cap Mountain Limestone units that do not contain deformation bands also exhibit grain microfracturing that is controlled by grain contact geometry. Qualitatively, the microfracture density in these samples appears less than that found for the samples containing deformation bands.

Pervasive microfracturing in sandstones containing deformation bands has not been recognized in past studies. Aydin (1977) indicated that deformation in the Entrada and Navajo Sandstones was restricted to a thin zone about 0.25 mm on either side of the deformation bands. Jamison (1979) found that virtually all microfracturing in the Wingate Sandstone occurred within or immediately adjacent to the deformation bands. He also speculated that crystal-plastic deformation mechanisms, manifest as different types of grain extinction, occurred adjacent to the deformation bands. From these and other observations, he concluded that the Wingate was not pervasively deformed, but that deformation was

localized almost entirely along the discrete deformation bands. Similarly, Young (1982) indicated that microfracturing in five different sandstones containing deformation bands in both faulted and folded environments was not pervasively distributed throughout the host rock. In the units he studied, grain microfracturing was limited to within two or three grain diameters from the deformation bands.

More recently, Blenkinsop (1986) studied small faults developed in a quartzite within the Moine thrust zone. He determined that at the time of deformation, the host rock was not highly cemented and that it deformed like a granular medium. He utilized cathodoluminescence to delineate the microfractures and determined that many bubble lineations were actually healed microfractures. In an undeformed section of an antiform, he noted that extension microfractures occurred, accompanied by pressure solution and porosity reduction. Although not stating that the microfracturing was pervasive, he noted a homogenous distribution of extension microfractures formed at the impingement points of grain contacts within the more deformed region of the fold hinge.

The microfractures observed in the Hickory and Welge Sandstones and grain-supported Cap Mountain limestone are associated primarily with grain contacts. Microfractures form primarily between grain contacts and separate the grains into two or more fragments. However, the microfractures between the fragments often are not open, but instead are healed. Linear bubble trails mark their position. This association of microfractures with grain contacts has been recognized by many investigators in rocks that are grain-supported and primarily deform like a loose (not well-cemented), granular medium (Borg and Maxwell,

1956; Bory and others, 1960; Gallagher, 1974; Engelder, 1974). Experimentally, grain-contact microfracture geometry has been suggested to be extension fractures that propagate parallel to the maximum compressive stress trajectories (Brace and Bombolakis, 1963; Friedman and Logan, 1970; Gallagher, 1974; Krantz, 1983). This grain-contact control of microfracturing would occur in rocks displaying a lack of cement, high porosity, and in cemented aggregates where grain contacts prevail, but the mechanical strength between the cement and grains is different.

Therefore, this type of fracturing is dependent on the initial microstructure of the host rock at the time of deformation. The presence of this fracture type suggests that the Hickory and Welge Sandstones and grain-supported sections of the Cap Mountain Limestone deformed as if they were essentially a granular medium. Sections of the Hickory and Welge that now appear to be quartzitic and very well cemented with quartz overgrowths probably became well cemented after the deformational event and perhaps as a result of the deformation.

The preferred orientations of the microfractures within the host rock indicates that although the grain fractures are controlled by grain contact geometry and hence the local stresses on the grain-scale, the regularity of orientations indicates that the microfractures are related to the orientation of the principal stresses at the mesoscopic scale. If the microfractures parallel the maximum principal stress direction, then the localization of the deformation band would be expected at an angle around 30 to 40 degrees to the microfractures. The microfractures mapped for the three Lower Paleozoic units typically

form an angle with the deformation bands between 20 and 50 degrees. Consequently, the microfractures and bubble lineations may be utilized to indicate the maximum compressive stress orientation, at least on the local (mesoscopic) scale.

For sections of the Cap Mountain Limestone that are dominated by calcite and only have rounded quartz and feldspar grains "floating" between the calcite grains, microfractures form only where two quartz grains are in contact. Fractures in the calcite matrix are rare, although twinning is more common than in the grain-supported section. Twin planes are rather evenly distributed throughout the host rock, although there does not appear to be an increase in the twinning adjacent to the deformation bands. The fractures in the detrital grains, although controlled by grain-contact geometry, do not have a strong "axial" orientation (i.e., parallel to the maximum principal stress) as found by Friedman (1963) in experimentally deformed calcite-cemented sandstones.

Since the Cap Mountain Limestone stratigraphically lies between the Hickory and Welge Sandstones that exhibit pervasive microfracturing, it is assumed that the Cap Mountain Limestone was subjected to relatively the same level of tectonic stress. It appears that sufficient stresses are being transmitted through the host rock to fracture the quartz grains, but the calcite matrix is deforming via crystal twinning (and possibly gliding) mechanisms.

Mesoscopic fracturing of the Cap Mountain Limestone is visible in outcrop, and although not studied in detail, is likely to be the deformation mechanism that is dominant in the more calcite-dominated sec-

tions. Whether the mesoscopic fracturing is more prevalent in the matrix-supported Cap Mountain Limestone versus the grain-supported Cap Mountain Limestone has not been investigated. However, the paucity of mesoscopic fractures in the grain-supported Hickory and Welge Sandstones suggests that mesoscopic fracturing may also be less prevalent in the grain-supported Cap Mountain Limestone.

Bubble Lineations

Many bubble lineations within the Hickory and Welge Sandstones and Cap Mountain Limestone are healed microfractures. This is evidenced by their ubiquitous occurrence in the host rock grains, their systematic orientations and their presence along lines connecting grain contacts. To my knowledge, these bubble lineations have not been recognized previously as healed microfractures within these lower Paleozoic rocks of the Llano Uplift.

The occurrence of fluid inclusions have long been recognized as the product of healed microfractures. For example, Tuttle (1949) investigated the systematic orientations of fluid inclusion planes in a large regional area in the Washington D.C. area. Regionally, the fluid inclusions have a non-random orientation throughout the metamorphic rocks. Maxwell (1960) noted that fluid inclusions in Oriskany Sandstone represented healed microfractures. Recently, Lespinnasse and Pecher (1986) investigated fluid inclusions in a granite massif in France. They noticed a correlation between the fluid inclusion trails and the mesoscopic fractures and paleostress fields. The fluid inclusions were oriented parallel to the paleostress directions and were

separated into different stress fields by microthermometric methods. In studies relative to deformation bands, fluid inclusions that potentially represent healed microfractures were recognized by Jamison (1979); however, he did not study the fluid inclusions systematically.

The observations of bubble lineation orientations made during this study, particularly with respect to the deformation bands, indicate that the systematic development of the bubble lineations is related to the deformation of the host rock. Similar to the open microfractures, the bubble lineations may represent a response of the rock mass to the local mesoscopic stress field. Thus, in future work, they may be used to determine paleostress directions.

Intersecting and offsetting relationships of bubble lineations within a single grain (Fig. 35, p. 88) may indicate a re-orientation of the local stress in the grain, assuming that the bubble trails are extension microfractures. This re-orientation of the local stresses on the grain scale may be due to closely-spaced, superimposed episodic deformation periods that re-orient the regional (and/or mesoscopic) stresses. This also indicates that the healing process of the microfractures possibly restores the mechanical continuity of the grain prior to the next increment of deformation, a result also found by Iespinasse et.al (1986). Sprunt and Nur (1979) have shown, using cathodoluminescence, that this restoration of mechanical continuity is demonstrated by the microfracturing and healing of granite. Similarly, Ramsey (1980) described crack-seal type microfractures shown by the repeated parallel, but distinct, fractures in crystals.

An alternative interpretation of the intersecting and offsetting

relationships of bubble lineations may include grain breakage that results in a local change in grain contacts due to offsets along microfractures or rotation of grains. New grain contacts may result in a re-orientation of the local grain-scale stress orientations. Consequently, stress concentrations may arise at the new contact points and result in grain fractures that intersect at high angles to and offset previously formed microfractures.

The offsetting relationships of bubble lineations in single grains also provides some insight into the relative timing of the failure chronology. In sample Crh 202T, for example, intersecting bubble lineations in a single grain (Fig. 35, p. 88) demonstrate very small left-lateral offsets indicative of some shearing accompanying the extension microfracturing. Figure 35 also illustrates that the bubble lineations oriented about N60W (relative to arbitrary N direction) precede the bubble lineations oriented roughly N46E. This same left-lateral relationship is found in the deformation bands visible in the microfracture map (Fig. 40, p. 95), although the orientations of the bands with respect to north are different.

From the intersecting observations, it appears that the relative timing of the second set of bubble lineations occurred sufficiently long after the first set that the microfractures in the grains had time to heal. Smith and Evans (1984) have indicated that microfracture healing can be a relatively rapid process if the temperature is high. In experimentally cracked quartz crystals, microfracture healing occurred within one to two days for cracks at temperatures as low as 400 degrees centigrade. The healing was determined to be a function of the

temperature, time, crack dimensions and initial silica concentration in the pore fluid. Favorable conditions for crack healing were obviously present during the deformation of the Paleozoic rocks even though the temperature probably was less than 100 degrees centigrade (Johnson, B., per. comm.).

Thus the bubble lineations found in the host rock grains in the Lower Paleozoic units appear to indicate that: (1) they are healed microfractures, (2) they developed in response to the mesoscopic stress state in the rock mass, and (3) the relationships within a single grain may reflect a re-orientation of the mesoscopic or grain-scale stresses in addition to providing some indication of the relative timing of the deformation.

Chronology of Deformation

Observations on the mesoscopic and microscopic scales during this investigation suggest a chronology of deformation events leading to the development of the deformation bands. This chronology can be separated into four overlapping phases: (1) pore collapse/pressure solution, (2) grain microfracturing and comminution, (3) localization and fracture concentration and (4) subsequent displacement along the localized zone. During all phases, solution/precipitation mechanisms activate that promote healing and cementation of microfractures and resultant gouge zones.

During the first phase, a slight amount of pore collapse and pressure solution occurs. It is uncertain whether this is diagenetically or tectonically induced. Point contacts and stresses increase

enough to create concavo-convex and long grain contacts. This phase probably continues throughout the deformational history of the host rock.

During the second phase, stresses within the grains become high enough to initiate grain microfracturing. This fracturing is probably extensional in nature and consequently follows the maximum compressive stress trajectories in individual grains (Gallagher, 1974). As fracturing increases, the resultant grain fragments rotate, translate and create additional point contacts. Alternatively, an increase in the differential stress due to a change in the mesoscopic stress field (e.g., a lateral stress reduction) would also initiate grain microfracturing by creating larger differential loads on point contacts. Stresses at the new contact points are large enough that grain comminution continues producing numerous very small fragments. Formation of these small grain fragments is the beginning of the fault localization phase.

Although the mechanism by which localization occurs is uncertain, more grains become fractured and comminuted during the localization phase. Probably a critical microfracture density is achieved (Krantz and Sholtz, 1977), at least in a localized area. This is suggested by the increased linear fracture density in the host rock immediately adjacent to the gouge zone. Linkage and coalescence of microfractures and grain boundary cracks probably also occurs, although it is unclear if this leads to localization of the gouge zone. Accompanying the localization is a volume reduction and an increase in the bulk density within the zone of comminuted grains.

After or simultaneously with the development of a localized gouge zone, shearing along this zone is initiated. This shearing possibly results in additional grain fracturing and incorporation of grains at the gouge zone/host rock boundary into the gouge zone. The amount of displacement may be limited by a strengthening of the gouge material as densification occurs or as overgrowths form contemporaneous with the deformation.

Simultaneous with grain comminution and cataclasis associated with shearing, microfracture healing and cementation by secondary overgrowths of quartz occurs. The healing of the microfractures is manifest by the bubble lineations. The intersecting relationships of the bubble lineations possibly suggest polyepisodic deformation events, probably rather closely spaced in time. Smith and Evans (1984) have indicated that microfracture healing can be a relatively rapid process, particularly with respect to geologic time. The fact that all microfractures are not healed suggests that the healing process is closely related to the deformation event. Also, the presence of overgrowths that are both fractured and unfractured implies their formation occurs both before and after the deformation. It is not unreasonable to assume that overgrowths were also forming, fracturing and subsequently healing during the deformation phases.

The presence of the small gouge particles along one side of the pore spaces and away from the bands suggests that at the initial stages of gouge development, the gouge was uncemented and therefore mobile. These small gouge particles have subsequently been cemented in place. This observation may indicate that the gouge material did not become

surrounded by quartz overgrowths until after the deformation period.

In a related study, Heald (1956) noted that secondary quartz overgrowths were more common in the deformation bands than the host rock. Overgrowths probably preferentially nucleate within the gouge zone as result of a silica source by pressure solution and the large surface area created due to the comminution of the host rock grains. It is believed that this subsequent cementation of the gouge zones results in the deformation bands displaying a resistance to weathering and consequently standing up as small ridges on weathered outcrop surfaces. Perhaps a detailed study of the overgrowths in the gouge zone and host rock using electron microscopy would reveal more information on their source, significance and occurrence within the framework of the deformational event.

Chapter VI

SUMMARY AND CONCLUSIONS

An investigation of the brittle deformation of the Lower Comanche Creek area on the southwest flank of the Llano Uplift was conducted. Under shallow crustal deformation conditions ($P < 13$ MPa and $T < 100$ C) and with rock types including quartz sandstone and calcite-cemented quartz sandstone, the following observations and conclusions are warranted:

1. Brittle deformation of the Lower Paleozoic in the Lower Comanche Creek area occurs on the macroscopic, mesoscopic and microscopic scales. Macroscopic deformation is manifest by large-displacement (up to 100 m) and minor faults (typically 1 to 5 m displacement); mesoscopic deformation by deformation bands (small faults); and microscopic deformation primarily by intragranular microfractures that appear pervasively distributed throughout the investigated units.
2. The macroscopic structure of the study area is dominated by northeast-trending, large-scale faults with displacements up to 100 m. The large-displacement faults are characterized by linear fault segments connected in a zig-zag pattern. Large, lenticular, fault-bounded blocks form due to the intersections of the macroscopic faults. Two main faults traverse through the Lower Comanche Creek area: the Schep Creek Fault and the Kettner Fault. The Schep Creek Fault bifurcates in the southwest corner of the study area to form two segments: a northern and southern trace. The Kettner Fault trends nearly east-west through

the central part of the study area and then makes a northerly bend to trend northeasterly. The displacements on both of these main faults decrease to the east and northeast. Numerous minor faults with displacements on the order of a few meters or less also occur in the study area and are often not visible on aerial photographs.

3. A large, open syncline is present in the western part of the Lower Comanche Creek area. The axial plane of the syncline is colinear with a northwest-trending zone marked by the loci of maximum throw of the large-displacement faults. This northwest-trending zone extends from the Lower Comanche Creek area to northwest of Mason, Texas and is approximately coincident with the granitic-metamorphic basement contact.

4. Mesoscopic deformation of the Hickory and Welge Sandstones and Cap Mountain Limestone in the Lower Comanche Creek area is manifest primarily by deformation bands. The deformation bands are characterized by curvilinear, intersecting, primarily light-colored gouge zones that appear in raised relief on weathered outcrop surfaces. The width of the gouge zones typically varies between <0.1 and 8.0 mm. Displacement associated with single deformation bands is typically on the order of a few millimeters or less. The single deformation bands often develop into anastomosing zones or ordered networks of deformation bands. The presence of these zones and networks is usually indicative of a nearby large-displacement fault. The density of single bands and zones increases with proximity to a large-displacement fault. As a result, the deformation bands are ubiquitous in conjunction with the macroscopic faulting in the sandstones of the Lower Paleozoic units.

5. The geometry of deformation bands is a function of the plane of observation relative to the slip vector. In planes roughly parallel to the slip vector, the bands will typically display a straight character. In areas where strike-slip displacement occurs, the bands form as linear segments on bedding surfaces. Conversely, deformation bands in cross-sectional views normal to the slip vector exhibit a curvilinear or anastomosing character. In normal-slip dominated areas, the anastomosing character forms primarily on bedding surfaces.
6. Deformation band thickness depends primarily on the host rock textural and compositional characteristics. Also, there exists a slight positive correlation between displacement and gouge zone thickness. Mean thickness of the gouge zones is observed to vary with host rock grain size.
7. Orientations of deformation bands vary spatially in the study area. Generally, the deformation bands form a girdle-pattern on contour diagrams with concentrations indicating a dominant northeast orientation. Three to four orientations can be identified within three regional subareas of the Lower Comanche Creek study area. Dip angles on the deformation bands are typically greater than 75 degrees. Within a local area, deformation band orientations also vary spatially and appear to reflect influences of nearby large-displacement faults. The separation of deformation band orientations into structural domains is therefore difficult and should be limited to extremely localized areas such as single outcrops.
8. Deformation bands commonly display normal, reverse, oblique and strike-slip movements in the same outcrop. Reverse-slip movements are

typically associated with small secondary deformation fields developed due to slip on adjacent faults. Oblique slip is manifest by slickensides on exhumed deformation band slip surfaces. Normal drag is frequently present along deformation bands in the Lower and Middle Hickory Sandstones. The combination of movements probably represents an accommodation of the localized three-dimensional strain.

9. Deformation bands provide a unique tool in determining the large-displacement fault characteristics and hence should be utilized when field mapping structural elements. Deformation bands provide some indication of the large-fault locations and attitudes. In addition, deformation bands provide an indication of the localized strain field by providing markers such as slickensided surfaces and offset intersecting bands that indicate the sense of displacement in a localized area.

10. Microscopic deformation is manifest primarily by intragranular microfractures associated with the host rock deformation and development of the deformation band gouge zones. In thin section, the gouge zones are characterized by a thin zone (typically <0.5 mm) of fractured and highly comminuted grains. The gouge material is angular and has a grain size typically less than 0.05 mm. Microfractures connect grain contacts and commonly transect the entire grain. Where grain contacts are long or concavo-convex, the microfractures can be replete within a grain and create numerous grain fragments. Small translational and rotational movements of these fragments result in a mosaic extinction pattern within the grain. The mosaic pattern does not appear to result

from crystal-plastic re-orientations but rather from brittle mechanisms involving cataclasis.

11. Microfractures are preferentially oriented with respect to the deformation bands and typically form at angles between 20 and 50 degrees to the band. The microfractures may parallel the maximum principal stress direction and may be used to infer orientations of the local and possibly the regional stress fields.
12. Microfractures are frequently healed as indicated by numerous trails of bubble or fluid inclusions. These bubble lineations typically transect the grains and form between grain contact points. Like the microfractures, the bubble lineations are preferentially oriented with respect to the deformation band gouge zones. Offsetting and intersecting bubble lineations at nearly right angles within single grains possibly indicates a re-orientation of the mesoscopic stress state or the local stress state within a grain.
13. Microfracturing, manifest either by open microfractures or bubble lineations, appears to be ubiquitous within the Lower Paleozoic sandstones in the Lower Comanche Creek area. Pervasive microfracturing associated with deformation bands has not been recognized in previous studies.
14. Observations on the mesoscopic and microscopic scales suggest a chronology of deformation leading to the development of deformation bands. This chronology can be separated into four overlapping phases: (1) pore collapse/pressure solution, (2) grain microfracturing and comminution, (3) localization and fracture concentration and (4) subsequent or simultaneous displacement along the localized gouge zone.

During all phases, solution/precipitation mechanisms activate that promote healing and cementation of microfractures and resultant gouge zones.

REFERENCES

- Aydin, A., 1977, Faulting in sandstone (Ph.D. thesis): Palo Alto, California, Stanford University, 246 p.
- Aydin, A., 1978, Small faults formed as deformation bands in sandstone: *Pure Applied Geophysics*, v. 116, p. 913-930.
- Aydin, A., and Johnson, A.M., 1978, Development of faults as zones of deformation bands and as slip surfaces in sandstones: *Pure Applied Geophysics*, v. 116, p. 931-942.
- Aydin, A., and Johnson, A. M., 1983, Analysis of faulting in porous sandstones: *Journal of Structural Geology*, v. 5, p. 19-31.
- Aydin, A., and Reches, A., 1982, Number and orientation of fault sets in the field and in experiments: *Geology*, v. 10, p. 107-112.
- Barnes, V. E., 1981, *Geologic Atlas of Texas, Llano Sheet*, Virgil E. Barnes Edition: Bureau of Economic Geology, University of Texas, Austin, Texas.
- Barnes, V. E., and Bell, W.C., 1977, *The Moore Hollow Group of Central Texas*, Bureau of Economic Geology, University of Texas, Austin, Texas, 169 p.
- Barnes, V. E., and Parkinson, G.A., 1940, *Dreikanterers from the basal Hickory Sandstone of Central Texas*: University of Texas, Austin, Publication 3945 p. 655-670.
- Becker, J. E., 1985, *Structural analysis of the western Llano Uplift with emphasis on the Mason Fault* (M.S. thesis): College Station, Texas, Texas A&M University, 203 p.
- Becker, J. E., and Johnson, B., 1985, *Structural analysis of the western Llano Uplift with emphasis on the Mason Fault*: *Transactions, American Geophysical Union*, v. 66, no. 46, p. 1089.
- Blenkinsop, T. G., and Rutter, E. H., 1986, *Cataclastic deformation of quartzite in the Moine thrust zone*: *Journal of Structural Geology*, v. 8, no. 6, p. 669-681.
- Brace, W. F., and Bombolakis, E. G., 1963, *A note on brittle crack growth in compression*: *Journal Geophysical Research*, v. 68, p. 3709-3713.
- Bridge, J., Barnes, V.E., and Cloud, P.E., 1947, *Stratigraphy of the Upper Cambrian, Llano Uplift, Texas*: *Geological Society of America Bulletin*, v. 58, p. 109-124.

- Borg, I. Y., and Maxwell, J.C., 1956, Interpretation of fabrics of experimentally deformed sands: *American Journal of Science*, v. 254, p. 71-81.
- Borg, I. Y., Friedman, M., Handin, J., and Higgs, D.V., 1960, Experimental Deformation of St. Peter Sand: A study of cataclastic flow: in *Rock Deformation*, D. Griggs and J. Handin, eds., Geological Society of America Memoir 79, p. 133-191.
- Cheny, M. G., and Goss, L. F., 1952, Tectonics of Central Texas: *American Association of Petroleum Geologists Bulletin*, v. 36, p. 2237-2265.
- Cloud, P. E., Jr., and Barnes, V. E., 1948, The Ellenburger Group of Central Texas: University of Texas, Austin, Publication 4621, 473 p.
- Coughran, T., 1959, Geology of the Doss-North Area, Mason and Gillespie Counties, Texas (M.S. Thesis): College Station, Texas, Texas A&M University, 111 p.
- Daugherty, T. D., 1960, A petrographic and mineralogical analysis of the Lion Mountain and Welge Sandstones of southern Mason County, Texas (M.S. Thesis): College Station, Texas, Texas A&M University, 87 p.
- Dekker, F. E., 1966, Sedimentology of the Upper Cambrian Lion Mountain and Welge Sandstones, Central Texas (M.S. Thesis): Austin, Texas, University of Texas, 79 p.
- Dunn, D. E., LaFountain, L. J., and Jackson, R. E., 1973, Porosity dependence and mechanism of brittle fracture in sandstones: *Journal of Geophysical Research*, v. 78, no. 14, p. 2403-2417.
- Dyer, R., 1983, Jointing in sandstones: Arches National Park, Utah (Ph.D. thesis): Palo Alto, California, Stanford University, 224 p.
- El-Jard, M. R., 1982, Diagenesis of the Hickory Sandstone (Cambrian), McCulloch and Mason Counties, Central Texas (M.S. thesis): Austin, Texas, University of Texas, 179 p.
- Engelder, J. T., 1974, Cataclasis and the generation of fault gouge: *Geological Society of America Bulletin*, v. 85, p. 1515-1522.
- Friedman, M., and Logan, J. M., 1973, Luder's bands in experimentally deformed sandstones and limestones: *Geological Society of America Bulletin*, v. 84, p. 1465-1476.
- Fritz, J., 1954, Geology of an area between Bluff and Honey Creeks, Mason County, Texas (M.S. thesis): College Station, Texas, Texas A&M University, 111 p.

- Fuller, R. L., 1957, Geology of the Grossville School area, Mason County, Texas (M.S. Thesis): College Station, Texas, Texas A&M University, 114 p.
- Gallagher, J. J., 1976, Fracturing of quartz sand grains: Proceedings, 17th U.S. Symposium on Rock Mechanics, Snow Bird, Utah, p. 2A4-1-2A4-8.
- Gallagher, J. J., Friedman, M., Handin, J., and Sowers, G. M., 1974, Experimental studies relating to microfracture in sandstone: Tectonophysics, v. 21, p. 203-247.
- Goolsby, J., 1957, A study of the Hickory Sandstone (M.S. Thesis): College Station, Texas, Texas A&M University, 91 p.
- Guzzetta, G., 1966, A rapid procedure for the preparation of density diagrams using the Lambert equal-area projection according to the Schmidt's grid method: Geological Society of Italy Bulletin, v. 85, p. 671-674.
- Handin, J., Friedman, M., Logan, J. M., Pattison, L. J., and Swolfs, H. S., 1972, Experimental folding of rocks under confining pressure. I. Bucking of single-layer rock beams: in Flow and Fracture of Rocks, The Griggs Volume, American Geophysical Union Monograph, v. 16, p. 1-28.
- Heald, M. T., 1956, Cementation of Simpson and St. Peter Sandstones in parts of Oklahoma, Arkansas, and Missouri: American Association of Petroleum Geologists Bulletin, v. 57, p. 16-30.
- Hedgcoxe, H. R., 1987, Development of secondary faults between en-echelon oblique slip faults: Examples from basement controlled small-fault systems in the Llano Uplift of Central Texas (M.S. Thesis: College Station, Texas, Texas A&M University, 110 p.
- Hedgcoxe, H. R., and Johnson, B., 1986, Interaction between en-echelon faults and formation of displacement transfer zones: Examples from small fault systems in the Llano Uplift of Central Texas: Geological Society of America Bulletin, Abstracts with Programs, v. 18, p. 633.
- Hobbs, B. E., Means, W. D., and Williams, P. F., 1976, An outline of structural geology: New York, John Wiley and Sons, Inc., 571 p.
- Hooks, D., 1961, Petrographic and mineralogical analysis of the Welge Sandstone, Central Mineral Region, Texas (M.S. Thesis): College Station, Texas, Texas A&M University, 99 p.
- Jamison, W. R., 1979, Laramide deformation of the Wingate Sandstone, Colorado National Monument: A study of cataclastic flow (Ph.D. Thesis): College Station, Texas, Texas A&M University, 170 p.

- Johnson, B., 1983, Anatomy of a normal fault in the Llano Uplift: Geological Society of America Bulletin, Abstracts with Programs, v. 15, p. 38-39.
- Johnson, B., and Becker, J. E., 1986, Normal fault development in the western Llano Uplift of Central Texas: Geological Society of America Bulletin, Abstracts with Programs, v. 18, no. 6, p. 646.
- Krantz, R. L., 1983, Microcracks in rocks: a review: Tectonophysics, v. 100, p. 449-480.
- Krantz, R. L., and Scholtz, C. H., 1977, Critical dilatant volume of rocks at the onset of tertiary creep: Journal of Geophysical Research, v. 82, p. 4893-4897.
- Lespinasse, M., and Pecher, A., 1986, Microfracturing and regional stress field: A study of the preferred orientations of fluid-inclusion planes in a granite from the Massif Central, France: Journal of Structural Geology, v. 8, no. 2, p. 169-180.
- Peng, S., and Johnson, A. M., 1972, Crack growth and faulting in a cylindrical sample of Chelmsford Granite: International Journal of Rock Mechanics and Mining Science, v. 9, p. 37-86.
- Peterson, D. H., 1959, Geology of the Middle Beaver Creek area, Mason and Gillespie Counties, Texas (M.S. Thesis): College Station, Texas, Texas A&M University, 99 p.
- Pittman, E. D., 1981, Effect of fault-related granulation on porosity and permeability of quartz sandstones, Simpson Group (Ordovician), Oklahoma: American Association of Petroleum Geologists Bulletin, v. 65, p. 2381-2387.
- Ramsey, J. G., 1980, The crack-seal mechanism of rock deformation: Nature, London, v. 284, p. 137-139.
- Reches, Z., 1978, Analysis of faulting in three-dimensional strain field: Tectonophysics, v. 47, p. 109-129.
- Reches, Z., 1983, Faulting of rocks in three-dimensional strain fields: II. Theoretical analysis: Tectonophysics, v. 95, p. 133-156.
- Robertson, E. C., 1983, Relationship of fault displacement to gouge and breccia thickness: Mining Engineering, v. 35, p. 1426-1432.
- Rudnicki, J. W., and Rice, J. R., 1975, Conditions for the localization of deformation in pressure-sensitive dilatant materials: Journal of Mechanics and Physical Solids, v. 23, p. 371-394.
- Sliger, K. L., 1957, Geology of the Lower James River area, Mason County, Texas (M.S. Thesis): College Station, Texas, Texas A&M University, 94 p.

- Smith, D. L., and Evans, B., 1984, Diffusional crack healing in quartz: *Journal of Geophysical Research*, v. 89, no. B6, p. 4125-4135.
- Sprunt, E. S., and Nur, A., 1979, Microcracking and healing in granites: new evidence from cathodoluminescence: *Science*, Washington, v. 205, p. 495-497.
- Tapponier, P., and Brace, W. F., 1976, Development of stress induced microcracks in Westerly Granite: *International Journal of Rock Mechanics and Mining Science*, v. 13, p. 103-112.
- Tchalenko, J. S., 1968, The evolution of kink bands and the development of compression textures in sheared clay: *Tectonophysics*, v. 6, p. 159-174.
- Tuttle, O. F., 1949, Structural petrology of planes of liquid inclusions: *Journal of Geology*, v. 57, p. 331-356.
- Wermund, E. G., and Jenkins, W. A., 1970, Recognition of deltas by fitting trend surfaces to upper Pennsylvanian sandstones in north-central Texas: in Morgan, J. P., *Deltaic sedimentation, modern and ancient: Society of Economic Paleontologists and Mineralogists Special Publication no. 15*, p. 256-269.
- Wilson, G. J., Jr., 1957, *Geology of the Big Bend of the Llano River area, Mason County, Texas (M.S. Thesis): College Station, Texas, Texas A&M University, 101 p.*
- Wilson, W. F., 1962, *Sedimentary petrology and sedimentary structures of the Cambrian Hickory Sandstone Member, Central Texas (M.A. Thesis): Austin, Texas, University of Texas, 127 p.*
- Young, S. R., 1982, *Characterization of and parameters controlling small faults in naturally deformed porous sandstones (M.S. Thesis): College Station, Texas, Texas A&M University, 117 p.*

VITA

John Mark Schmittle

- Personal:** Born June 8, 1960 in Erie, Pennsylvania.
Married to Lori Pollock Schmittle.
Parents: Reverend S. James and Louise J. Schmittle
- Education:** B.S. in Geology, Allegheny College, Meadville, PA,
1982.
- Professional
Experience:** Hydrogeologist, ERM-Southwest, Inc., Houston, TX.
June 1985 - present.
- Teaching and Research Assistant, Center for
Tectonophysics and Department of Geology, Texas
A&M University, 1983 - 1985.
- Teaching and Research Assistant, Department of
Geology, Allegheny College, 1979 - 1982.
- Permanent
Address:** 2702 Droxford
Houston, Texas 77008
- Business
Address:** 16000 Memorial Drive
Suite 200
Houston, Texas 77079